Scale and Parity Symmetry Breaking in Graphene: Universality, Discrete Scale Invariance and Vacuum charge

Omrie Ovdat

Scale and Parity Symmetry Breaking in Graphene: Universality, Discrete Scale Invariance and Vacuum charge

Research thesis

In Partial Fulfillment of The Requirements for the Degree of Doctor of Philosophy

Omrie Ovdat

Submitted to the Senate of the Technion - Israel Institute of Technology

Shebat, 5779, Haifa, January, 2019

The Research Thesis was done under the supervision of Professor Eric Akkermans in the Department of Physics.

The generous financial help of the Technion is gratefully acknowledged

Publications:

1. O. Ovdat, J. Mao, Y. Jiang, E. Andrei, E. Akkermans, "Observing a scale anomaly and a universal quantum phase transition in graphene", Nature Communications 8, Article number: 507 (2017).

2. D. Brattan, O. Ovdat, E. Akkermans, "Scale anomaly of a Lifshitz scalar: a universal quantum phase transition to discrete scale invariance", Physical Review D, Rapid Communications, 97, 6 (2018)

3. D. Brattan, O. Ovdat, E. Akkermans, "On the landscape of scale invariance in quantum mechanics", J. Phys. A: Math. Theor. 51 435401 (2018)

Contents

List of Figures

Abstract

One of the most interesting predictions resulting from quantum physics is the violation of classical symmetries, collectively referred to as anomalies. A remarkable class of anomalies occurs when the continuous scale symmetry of a scale-free quantum system is broken into a discrete scale symmetry for a critical value of a control parameter. This is an example of a (zero temperature) quantum phase transition. Such an anomaly takes place for the quantum inverse square potential known to describe 'Efimov physics'.

The first part of this thesis is dedicated to the study this transition in the framework of a general scale invariant system. We explore its universal features, ingredients and realizations in other relevant cases. Specifically, we demonstrate the existence and universality of this quantum phase transition for a massless fermion in an attractive Coulomb potential and present convincing experimental evidence of it as realized around a charged vacancy in graphene. Furthermore, we consider an infinite class of scale invariant hamiltonians allowing for anisotropic scaling between space and time. We show that the transition to discrete scale invariance is realized as a generic feature in the landscape of these hamiltonians. We formulate a renormalization group picture and demonstrate that close to the critical point, the discrete scale invariant phase is characterized by an isolated, closed, attracting trajectory in renormalization group space (a limit cycle). Moving in appropriate directions in the parameter space of couplings this picture is altered to one controlled by a quasi periodic attracting trajectory (a limit torus) or fixed points. We identify a direct relation between the critical point, the renormalization group picture and the power laws characterizing the

zero energy wave functions.

An additional type of anomaly occurs when the parity symmetry of the ground state of a massless Dirac system is broken in the presence of a magnetic flux. In this case, the flux induces zero energy bound states and a fractional vacuum charge with abnormal parity. As a result, the Index of the corresponding Dirac operator acquires non-zero values proportional to the flux as well as to the vacuum charge.

The second part of this thesis is devoted to the study of neutral vacancies in graphene and their relation to the aforementioned physics of gauge field induced vacuum charge. A single vacancy induces a localized stable charge of order unity interacting with other charges of the conductor through an unscreened Coulomb potential. It also breaks the symmetry between the two triangular graphene sub-lattices hence inducing zero energy states at the Dirac point. Here we show the fractional and pseudo-scalar nature of this vacancy charge. A continuous Dirac model is presented which relates zero modes to vacuum fractional charge and to a parity anomaly. This relation constitutes an Index theorem and is achieved by using particular chiral boundary conditions, which map the vacancy problem onto edge state physics. Vacancies in graphene thus allow to realize prominent features of $2 + 1$ quantum electrodynamics but without coupling to a gauge field. This essential difference makes vacancy physics relatively easy to implement and an interesting playground for topological charge switching.

Nomenclature

CSI Continuous scale invariance

DSI Discrete scale invariance

α_G Effective fine structure constant in graphene $\alpha_G \equiv e^2/\hbar v_F$

QED Quantum electrodynamics

RG Renormalization group

β Coupling parameter of $1/r$ potential in H_D

H_D Dirac hamiltonian $H_D = -i\gamma^0\gamma^j\partial_j - \beta/r$

H_L Lifshitz hamiltonian $H_L = (-\nabla^2)^N - \lambda_N/x^{2N}$

H_N Lifshitz hamiltonian with a general scale invariant potential term

H_S Schrödinger hamiltonian $H_S = -\nabla^2/2\mu - \xi/r^2$

j Total angular momentum quantum number

λ_N Coupling parameter of $1/x^{2N}$ potential in H_L

N_A, N_B Number of vacancies on sublattice A, B respectively

v_F Fermi velocity in graphene $v_F \simeq 10^6\,\mathrm{m/s}$

1 Introduction

Continuous scale invariance (CSI) – a common property of physical systems – expresses the invariance of a physical quantity $f(x)$ (e.g., the mass) when changing a control parameter x (e.g., the length). This property is expressed by a simple scaling relation, $f(ax) = b\, f(x)$, satisfied $\forall a > 0$ and corresponding $b(a)$, whose general solution is the power law $f(x) = C\, x^{\alpha}$ with $\alpha = \ln b / \ln a$. Other physical systems possess the weaker discrete scale invariance (DSI) expressed by the same aforementioned scaling relation but now satisfied for fixed values (a, b) and whose solution becomes $f(x) = x^{\alpha}\, G\left(\ln x / \ln a\right)$, where $G(u+1) = G(u)$ is a periodic function. Since $G\left(u\right)$ is a periodic function, one can expand it in Fourier series $G\left(u\right) = \sum c_n e^{2\pi i n u}$, thus, $f\left(x\right) = \sum_{n=-\infty}^{\infty} c_n x^{\alpha + i\frac{2\pi n}{\log a}}$. If $f\left(x\right)$ would require to obey CSI, $G\left(x\right)$ would be constraint to fulfill the relation $G\left(x\right) = G\left(x+a\right)\ \forall a \in \mathbb{R}$. In this case, $G\left(x\right)$ can only be a constant function, that is, $c_n = 0$ for all $n \neq 0$ eliminating all terms with complex exponents. Therefore, real exponents are a signature of CSI and complex exponents are signature of DSI. Physical systems having DSI are also known as self-similar fractals [1] (Fig. 1.1). Is it possible to observe the breaking of CSI into DSI at the quantum level? Yes, a result which constitutes the basis of a special kind of scale anomaly.

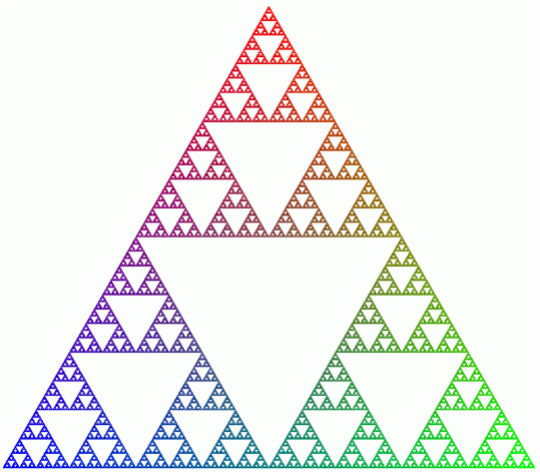

Figure 1.1: Sierpinski gasket as typical geometric picture featuring such iterative fractal structures.

Classical symmetries broken at the quantum level are termed anomalies. Since their discovery [2, 3], anomalies have become a very active field of research in physics. One class of anomalies describes the breaking of CSI. In the generic case, quantization of a classically scale invariant hamiltonian is ill-defined and necessitates the introduction of a regularization scale [4] which breaks CSI altogether. However, there are particular instances where a residual DSI remains after regularization.

A well studied example is provided by the problem of a particle of mass μ in an attractive inverse square potential [5, 6] which plays a role in various systems [7–10] and more importantly in Efimov physics [11–13]. Although well defined classically, the quantum mechanics of the scale – and conformal [14] – invariant hamiltonian ($\hbar = 1$)

$$H_S = -\nabla^2/2\mu - \xi/r^2 \tag{1.1}$$

has an interesting yet disturbing property – the power law form of the corresponding

potential matches the order of the kinetic term. As a result, the Schrödinger equation $H_S\psi = E\psi$ is dependent on a single dimensionless parameter $\zeta \equiv 2\mu\xi$ which raises the question of existence of a characteristic energy scale to express the eigenvalues E_n. This absence of characteristic scale displays the invariance of $H_S\psi = E\psi$ under the scale transformation $x^i \to ax^i$, $E \to a^{-2}E$ [14] which implies that if there is one negative energy bound state then there is an unbounded continuum of bound states which render the Hamiltonian nonphysical and mathematically not self-adjoint [15, 16]. The eigenstates of H_S can be solved in terms of Bessel functions which confirms these assertions in more detail. Particularly, for $E < 0$ and lowest orbital angular momentum subspace $l = 0$, the most general decaying solution is described by the radial function

$$\psi_0(r) \approx r^{-\frac{d-2}{2}}\left((kr)^{-\sqrt{\zeta_c-\zeta}}\left(1+\mathcal{O}(kr)^2\right)+(kr)^{\sqrt{\zeta_c-\zeta}}\left(1+\mathcal{O}(kr)^2\right)\right) \tag{1.2}$$

where $k \equiv \sqrt{-2\mu E}$ and $\zeta_c \equiv (d-2)^2/4$ [1]. As seen in (1.2), for $\zeta > \zeta_c - 1$, $\psi_0(r)$ is normalizable $\forall\, \mathrm{Re}(E) < 0$ which constitute a continuum of complex valued bound states of H_S. Thus, for $\zeta > \zeta_c - 1$, H_S is no longer self-adjoint, a property that originates from the strong singularity of the potential and is characteristic of a general class of potentials with high order of singularity [5].

A simple, physically instructive procedure to deal with the absence of self-adjointness is to remove the singular $r = 0$ point by introducing a short distance cutoff L and apply a boundary condition at $r = L$ [17–23]. The most general boundary condition

[1] For higher angular momentum channels ζ_c is larger and given by $(d-2)^2/4 + l(l+d-2)$

is the mixed condition

$$L\frac{\psi'(L)}{\psi(L)} = g, \tag{1.3}$$

$g \in \mathbb{R}$, for which there is an infinite number of choices each describing different short range physics. As a result, the spectrum of H_S, now well defined on the interval $L < r < \infty$ with condition (1.3), exhibits two distinct pictures in the low energy $kL \ll 1$ regime. For $\zeta < \zeta_c \equiv (d-2)^2/4$, the spectrum contains no bound states close to $E = 0$, however, as ζ goes above ζ_c, an infinite series of bound states appears. Moreover, in this "over-critical" regime, the states arrange themselves in a geometric series

$$k_n = \frac{1}{L^2} k_0(g,\zeta) \exp\left(-\pi n/\sqrt{\zeta-\zeta_c}\right), \tag{1.4}$$

$n \in 0, 1\ldots$, accumulating at $E = 0$. The absence of any states for $\zeta < \zeta_c$ is a signature of CSI while the geometric structure of (1.4) for $\zeta > \zeta_c$ is a signature of DSI since $\{E_n\} \to \left\{\exp\left(-2\pi/\sqrt{\zeta-\zeta_c}\right) E_n\right\}$. Accordingly, as seen explicitly in (1.2), the characteristic behavior of the eigenstates for $kr \ll 1$ manifest an abrupt transition from real to complex valued exponents as ζ exceeds ζ_c. Thus, H_S exhibits a quantum phase transition (QPT) at ζ_c between a CSI phase and a DSI phase. The characteristics of this transition are independent of the values of L, g which enter only into the overall factor k_0 in (1.4). The functional dependence of k_n on $\sqrt{\zeta-\zeta_c}$ is characteristic of Berezinskii-Kosterlitz-Thouless (BKT) transitions as was identified in [9, 24–26]. Finally, the breaking of CSI to DSI in the $\zeta > \zeta_c$ regime constitutes a special type of scale anomaly since a residual symmetry remains even after regularization (see table 1).

Table 1: **Quantum phase transition, discrete scale invariance and scale anomaly.** Schematic description of the essential phenomenon exhibited by the Hamiltonian H_S. The same essential physics occurs for H_D, H_L, H_N as explained in the text and in [27–29].

$\zeta < \zeta_c$		$\zeta > \zeta_c$
CSI	Formal Hamiltonian	CSI
$H = H^\dagger$	Self-adjointness	$H \neq H^\dagger$
Redundant	Regularization with L	Essential
CSI	Quantum solution space	DSI

Scale anomaly $\Downarrow$

Quantum Phase Transition $\Longrightarrow$

The inverse square hamiltonian (1.1), a simple system exhibiting a remarkably rich set of phenomena, inspires studying the ingredients which lead to the aforementioned QPT and whether they are found in other systems. One such candidate system is described by a massless Dirac fermion in an attractive Coulomb potential with the scale invariant hamiltonian

$$H_D = -i\gamma^0\gamma^j\partial_j - \beta/r. \tag{1.5}$$

Based on the previous example, it may be anticipated that, like H_S, H_D will exhibit a sharp spectral transition at some critical β in which the singularity of the potential will ruin self-adjointness. In [27], we rigorously verified this assertion and emphasized the universality of this transition between H_S, H_D. We show the discrete scale invariant structure in the density of states of H_D and discuss its connection to parity symmetry breaking, which present new structure appearing only in H_D and not

H_S.

The similarities between H_S, H_D motivates the study of whether a transition of this sort is possible for a generic scale invariant system. Since these different operators share the property that the power law form of the corresponding potential matches the order of the kinetic term, it would be interesting to examine whether this property is a sufficient ingredient by considering a generalized class of one dimensional hamiltonians

$$H_L = \left(-\nabla^2\right)^N - \frac{\lambda_N}{x^{2N}}, \tag{1.6}$$

where N is an integer and λ_N a real coupling. Hamiltonian (1.6) describes a system with non-quadratic anisotropic scaling between space and time for $N > 1$. This "Lifshitz scaling symmetry" [30], manifest in (1.6), can be seen for example at the finite temperature multicritical points of certain materials [31, 32] or in strongly correlated electron systems [33–35]. It may also have applications in particle physics [30], cosmology [36] and quantum gravity [37–39]. The non-interacting mode ($\lambda_N = 0$) can also appear very generically, for example in non-relativistic systems with spontaneous symmetry breaking [40]. In [28], we studied the system H_L as a function of λ_N and its relation to the universal features exhibited by H_S, H_D.

An alternative useful tool in the characterization of the QPT from continuous to discrete scaling is the renormalization group (RG). For the case of $H_{S,D,L}$, it consists of introducing an initial short distance scale L and defining model dependent parameters such as the potential coupling and the boundary conditions, according to physical information. At low energies with respect to the cut-off L, a RG formalism allows one to determine the dependence of these parameters on L and thus how physical

and regularization independent information can be extracted from a scheme dependent result. For example, an attractive fixed point represents a class of parameters describing the same low energy predictions, characterized by the effective hamiltonian corresponding to the fixed point. In that sense, the fixed point hamiltonian describes universal[2] physics. However, termination at a fixed point is not the only possible outcome of a RG flow. In principle, there are three other distinct behaviors that one can find: limit cycles, limit tori and strange attractors [41]; all of which are rare in applications of RG.

The study of H_S and H_D using RG [9, 19, 20, 24, 42, 43] shows that the quantum critical phase transition is characterized by two fixed points (UV and IR) which combine and annihilate at a critical point representing a sufficiently strong attracting potential. In this, over-critical regime, all the flows are log-periodic in the cut-off and therefore exhibit DSI, independent of the choice of initial boundary condition and scale. As a result, there is an infinite equivalent set of scales described by a geometric ladder. This is manifested in (1.4) as it implies $E_{n+k+1}/E_{n+k} = E_{n+1}/E_n$ for all $n, k \in \mathbb{Z}$. Remarkably, even in the absence of fixed points, there is universal information in this regime represented by the geometric series factor E_{n+1}/E_n.

Hamiltonians $H_{S,D,L}$ share the property of scaling uniformly under $r \mapsto a\, r$. This suggests widening our perspective even further and consider all possible radial hamil-

[2]Note that we refer to two types of universal properties of the QPT from CSI to DSI. One type of universal property allow the appearance of the transition in different systems such as those described by $H_{S,D,L}$. The second type of universal property allow the appearance of the transition independent of the details of the short distance physics of the specific system.

tonians with CSI and spherical symmetry. Such hamiltonians are given by

$$H_N = p^{2N} + \sum_{i=1}^{2N} \frac{\lambda_i}{r^i} d_r^{2N-i}, \tag{1.7}$$
$$p^2 = -d_r^2 - \frac{d-1}{r} d_r + \frac{\ell(\ell+d-2)}{r^2}$$

where $N > 0$ is an integer, $\lambda_i \in \mathbb{R}$, $d_r \equiv \frac{d}{dr}$, ℓ is the orbital angular momentum quantum number and d is the number of spatial dimensions. In [29] we studied, using a RG approach, the systems described by (1.7). We classified the RG space corresponding to (1.7), discussed the connection to the universal features exhibited by $H_{S,D,L}$ and presented new structure appearing only in H_N.

A particularly interesting condensed matter system where $H_D = -i\gamma^0\gamma^j\partial_j - \beta/r$ in (1.5) seem to be relevant is graphene in the presence of implanted Coulomb charges in conveniently created vacancies [44]. It is indeed known that low energy excitations in graphene behave as a massless Dirac fermion field with a linear dispersion $\epsilon = \pm v_F|p|$ and a Fermi velocity $v_F \simeq 10^6\,\mathrm{m/s}$. These characteristics have been extensively exploited to make graphene a very useful platform to emulate specific features of quantum field theory, topology and especially QED [45–48], since an effective fine structure constant $\alpha_G \equiv e^2/\hbar v_F$ of order unity is obtained by replacing the velocity of light c by v_F.

It has been recently shown that single-atom vacancies in graphene can stably host local charge [44]. Density functional theory calculations have shown that when a carbon atom is removed from the honeycomb lattice, the atoms around the vacancy site rearrange into a lower energy configuration [49]. The resulting lattice reconstruction

causes a charge redistribution which in the ground state has an effective local charge of ≈ 1. Vacancies are generated by sputtering graphene with He^+ ions [50, 51]. Charge is modified and measured at the vacancy site by means of scanning tunneling spectroscopy and Landau level spectroscopy as detailed in [44]. Applying multiple pulses allows for a gradual increase in the vacancy charge, which in turn acts as an effective tunable Coulomb source. In [27], we use this method to obtain convincing experimental evidence of the CSI to DSI transition corresponding to a massless Dirac particle in an attractive Coulomb potential. This work, done in collaboration with the experimental group of Prof. Eva Andrei, is one of the main parts of this thesis. Our contribution was to propose observing the aforementioned quantum phase transition in graphene, interpret and solve the theoretical model, analyze the experimental data and make contact with the theory.

Utilization of local charge is one of several recent experimental and theoretical studies of vacancies [27, 44, 49, 52–65]. Notably, vacancies induce other effects on the physics of graphene such as zero energy modes and sub-lattice symmetry breaking. In the presence of $N_A + N_B$ vacancies, where N_A (N_B) is the number of vacancies corresponding to the two triangular sublattices, the tight binding hamiltonian has $|N_A - N_B|$ zero energy eigenvalues with vanishing wave function on the minority sub-lattice [52–55, 66]. For $N_A \neq N_B$, sub-lattice symmetry is broken and so is parity in the continuum limit. For a single vacancy, the degeneracy lifting between the two lowest angular momentum channels $j = \pm 1/2$, a clear indication of parity symmetry breaking, has been indeed observed [27].

The combined appearance of local charge, zero energy modes and parity breaking

associated with vacancies in graphene bears much resemblance with the Dirac physics of charge fractionalization and the parity anomaly [67–83]. In a simple realization of the later [76], consider a $2+1$ dimensional massless Dirac particle in the presence of a vector gauge field $\vec{A}$ which induces a finite quantized magnetic flux Φ around the origin such that $\vec{A}\,(r \to \infty) = \Phi/r\,\hat{\theta}$. For this system, the resulting Hamiltonian eigenspace is characterized by a set of $e\Phi$ zero energy eigenstates. In addition, the charge of the ground state is given by $Q = e\left\langle \hat{N} \right\rangle = \Phi\, e/2$, which is proportional to Φ, the number of zero modes and can acquire half integer values. Since Φ is a pseudo scalar, the vacuum state breaks parity ($Q \to -Q$) even though the Hamiltonian is invariant.

Motivated by the resemblance between vacancy physics and the features of the parity anomaly, we present in [84] a continuous Dirac model of graphene, valid at low energy and applicable to an arbitrary configuration of isolated vacancies. This model describes the physics of vacancies detailed above and accurately interprets it as a realization of parity anomaly physics with the role of the flux now replaced by holes in the plane with a special type of boundary.

2 Methods

2.1 Observing a scale anomaly and a universal quantum phase transition in graphene

Theory: We use standard analytic methods to solve the Dirac Coulomb system using special functions. The positions of the quasi-bound states as a function of the Coulomb strength β is obtained using two different methods. The first is the method of Gamow [85] from which the analytic expression (supplementary eq. 17) is dervied. In the second, using symbolic and numerical computer software [86], we obtained an expression for $\mathrm{d}\eta\left(E\right)/\mathrm{d}E$ (see plots in Fig. 2a, Fig. 3, top of Fig. 4) and located the energy position of the maxima as a function of β (see curves in Fig. 5 and Fig. 6).

(The experimental part detailed below was performed by Jinhai Mao, Yuhang Jian and Professor Eva Andrei from Rutgers university)

Experiment: Our sample is stacked two layers of graphene on top of a thin BN flake (see Fig. 1f). The standard dry transfer procedure is followed to get this heterostructure. A large twisted angle between the two layers of graphene is selected in order to weaken the coupling. The free-standing feature for the top layer is checked by Landau level spectroscopy. To achieve the diluted single vacancies, the sample is exposed to the helium ion beam for a short time ($100\,\mathrm{eV}$ for $5\,\mathrm{s}$) followed by high temperature annealing. The experiment is performed at $4.2\,\mathrm{K}$ with a home-built STM. The $\mathrm{d}I/\mathrm{d}V$ (I is the current, V is the bias) is

recorded by the standard lock-in technique, with a small AC modulation $2\,\mathrm{mV}$ at $473.1\,\mathrm{Hz}$ added on the DC bias. To tune the effective charge on the vacancy, we apply the voltage pulse $(-2\,\mathrm{V},\ 100\,\mathrm{ms})$ with the STM tip directly located on top of the vacancy.

2.2 Scale anomaly of a Lifshitz scalar: a universal quantum phase transition to discrete scale invariance

We use standard analytic methods to solve the wave equation of the Lifshitz scalar using special functions. Using symbolic and numeric computer software [86] we obtain the spectrum for various choices of boundary conditions (Figs. 2,3)

2.3 On the landscape of scale invariance in quantum mechanics

Using numeric computer software [86] we solve the RG equations (11) as a set of dynamical equations and obtain the plots presented in Figs. 2,3,4. The position of the fixed points presented in Figs. 1,2 is extracted from eq. (11) using algebraic Riccati equation theory [87].

2.4 Vacancies in Graphene: Dirac Physics and Fractional Vacuum Charges

We use standard analytic methods to solve the Green's function of Dirac system on a punctured plane with a chiral boundary condition in terms special functions. In the

multi-vacancy configuration we apply the zero range approximation [88] to obtain the expression for the zero energy wave function (eq. 13).

Figs. 1a,2a,3 are obtained from the diagonalization of the tight binding Hamiltonian

$$H_{\mathsf{TB}} = -t \sum_{\langle i,j \rangle} \left(c_i^\dagger c_j + \text{H.c.} \right) + M \sum_i s_i c_i^\dagger c_i \tag{2.1}$$

in the one particle subspace and position space basis. In (2.1), the label i represents the lattice sites and $c_i^\dagger, c_j$ are creation and annihilation operators. The first term contains a sum over nearest neighbor sites and in the second term $s_i = \pm 1$ when i corresponds to a site from sub-lattice A, B respectively. Parameters t, M are kinetic energy and mass terms. Our lattice consists of 1302 sites with $M/t = 10^{-9}$.

The presence of the mass term shifts the zero modes and its goal is to remove the ambiguity of $\text{sign } 0$ in the expression for the vacuum charge density

$$\rho(\boldsymbol{r}) = \frac{e}{2} \sum_n \text{sign}(E_n) \, \psi_n^\dagger(\boldsymbol{r}) \, \psi_n(\boldsymbol{r}) \, . \tag{2.2}$$

The ambiguity associated with $E = 0$ results from the necessity to determine whether or not $E = E_F = 0$ states are occupied or not. The introduction of a small mass term is one way to regularize this ambiguity. The mass term shifts the zero modes to $\text{sign}(N_A - N_B) M$, which depending on its sign, discriminates between occupying the zero modes or not. For that reason, the sign of M (along with $\text{sign}(N_A - N_B)$) determines the sign of $\rho(\boldsymbol{r})$. The physical meaning of the mass term is to associate a different constant potential energy to A, B sublattices and thereby differentiate between them. Such a term can arise by placing a graphene sheet above a Boron-Nitrite

substrate (as in [27, 44] for example). Boron-Nitrite has the same in-plane hexagonal lattice structure composed out of two different triangular sub-lattices of Boron and Nitrite. When placed below a graphene sheet with no angular or linear displacement between the hexagonal lattices the Boron and Nitrite atoms induce different on-site potentials V_A, V_B on the graphene sub-lattices. As a result, the tight binding Hamiltonian in the $\psi = \begin{pmatrix} \psi_A & \psi_B \end{pmatrix}^T$ basis is modified to

$$H = \begin{pmatrix} V_A & H_{AB} \\ H_{BA} & V_B \end{pmatrix} \tag{2.3}$$

where $H_{AB} = H_{BA}^{\dagger}$ are the tight binding hopping terms and the diagonal terms described the on site potentials induced by the substrate. A shift of H by an unimportant constant energy $-(V_A + V_B)/2$ yields

$$H \to H = \begin{pmatrix} 0 & H_{AB} \\ H_{BA} & 0 \end{pmatrix} + \frac{V_A - V_B}{2}\sigma_3. \tag{2.4}$$

Defining $M \equiv \frac{V_A - V_B}{2}$ gives the form of Hamiltonian (2.1).

3 Articles

1. Observing a scale anomaly and a universal quantum phase transition in graphene, (2017, Nature Communications 8, Article number: 507)

2. Scale anomaly of a Lifshitz scalar: a universal quantum phase transition to discrete scale invariance, (2018, Physical Review D, Rapid Communications, 97, 6)

3. On the landscape of scale invariance in quantum mechanics, (2018, J. Phys. A: Math. Theor. 51 435401)

nature COMMUNICATIONS

ARTICLE

DOI: 10.1038/s41467-017-00591-8 OPEN

Observing a scale anomaly and a universal quantum phase transition in graphene

O. Ovdat[1], Jinhai Mao[2], Yuhang Jiang[2], E.Y. Andrei[2] & E. Akkermans[1]

One of the most interesting predictions resulting from quantum physics, is the violation of classical symmetries, collectively referred to as anomalies. A remarkable class of anomalies occurs when the continuous scale symmetry of a scale-free quantum system is broken into a discrete scale symmetry for a critical value of a control parameter. This is an example of a (zero temperature) quantum phase transition. Such an anomaly takes place for the quantum inverse square potential known to describe 'Efimov physics'. Broken continuous scale symmetry into discrete scale symmetry also appears for a charged and massless Dirac fermion in an attractive $1/r$ Coulomb potential. The purpose of this article is to demonstrate the universality of this quantum phase transition and to present convincing experimental evidence of its existence for a charged and massless fermion in an attractive Coulomb potential as realized in graphene.

[1] Department of Physics, Technion, Israel Institute of Technology, Haifa 3200003, Israel. [2] Department of Physics and Astronomy, Rutgers University, Piscataway, NJ 08854, USA. O. Ovdat and Jinhai Mao contributed equally to this work. Correspondence and requests for materials should be addressed to E.A. (email: eric@physics.technion.ac.il)

Continuous scale symmetry (CS)—a common property of physical systems—expresses the invariance of a physical quantity $f(x)$ (e.g., the mass) when changing a control parameter x (e.g., the length). This property is expressed by a simple scaling relation, $f(ax) = bf(x)$, satisfied $\forall a > 0$ and corresponding $b(a)$, whose general solution is the power law $f(x) = Cx^{\alpha}$ with $\alpha = \ln b/\ln a$. Other physical systems possess the weaker discrete scale symmetry (DS) expressed by the same aforementioned scaling relation but now satisfied for fixed values (a, b) and whose solution becomes $f(x) = x^{\alpha}G(\ln x/\ln a)$, where $G(u+1) = G(u)$ is a periodic function. Physical systems having a DS are also known as self-similar fractals[1] (Fig. 1a). It is possible to break CS into DS at the quantum level, a result which constitutes the basis of a special kind of scale anomaly[2, 3].

A well-studied example is provided by the problem of a particle of mass μ in an attractive inverse square potential[4, 5], which plays a role in various systems[6–9] and more importantly in Efimov physics[10, 11]. Although well defined classically, the quantum mechanics of the scale—and conformal[12]—invariant Hamiltonian $H = -\Delta/2\mu - \xi/r^2$ (with $\hbar = 1$) is well posed, but for large enough values of ξ, H is no longer self-adjoint[13, 14]. The corresponding Schrödinger equation for a normalisable wave function $\psi(r)$ of energy $k^2 = -2\mu E$ is,

$$\psi''(r) + \frac{d-1}{r}\psi'(r) + \frac{\zeta}{r^2}\psi(r) = k^2\psi(r), \qquad (1)$$

where $\zeta \equiv 2\mu\xi - l(l+d-2)$ is a dimensionless parameter, d the space dimensionality and l the orbital angular momentum. Equation (1) is invariant under the transformation $r \to \lambda r$ and $k \to k/\lambda$, $\forall\lambda$ (CS), namely to every normalisable wave function of energy k^2 corresponds a continuous family of states with energies $(\lambda k)^2$, so that the bound spectrum is a continuum unbounded from below. Various ways exist to cure this problem, based on cutoff regularisation and renormalisation group[15–21], and all lead for the low-energy spectrum to a quantum phase transition (QPT) monitored by ζ, between a single bound state for $\zeta < \zeta_c$ to an infinite and discrete energy spectrum for $\zeta > \zeta_c$, independent of the regularisation procedure and given by

$$k_n(\zeta) = \epsilon_0\, e^{-\frac{\pi n}{\sqrt{\zeta-\zeta_c}}},\ n \in \mathbb{Z}, \qquad (2)$$

which clearly displays DS. The critical value $\zeta_c = (d-2)^2/4$ depends on the space dimensionality only, and ϵ_0 is a regularization dependent energy scale. In the overcritical phase $\zeta > \zeta_c$, the corresponding renormalization group solution provides a rare example of a limit cycle[15, 16, 22]. Building on the previous example, it can be anticipated that the problem of a massless Dirac fermion in an attractive Coulomb potential[23–25], $-Z\alpha/r$, is also scale invariant (CS) and that the spectrum of resonant quasi-bound states presents similar features and a corresponding QPT.

In this work, we demonstrate the existence of such a universal QPT for arbitrary space dimension $d \geq 2$ and independently of the short distance regularisation. We obtain an explicit formula for the low-energy fractal spectrum in the overcritical regime. In contrast to the Schrödinger case equation (1), the massless Dirac Hamiltonian displays an additional parity symmetry which may be broken by the regularisation. In that case, the degeneracy of the overcritical fractal spectrum is removed and two intertwined geometric ladders of quasi-bound states appear in the s-wave channel. All these features are experimentally demonstrated using a charged vacancy in graphene. We observe the overcritical spectrum and we obtain an experimental value for the universal geometric ladder factor in full agreement with the theoretical prediction. We also explain the observation of two intertwined ladders of quasi-bound states as resulting from the breaking of parity symmetry. Finally, we relate our findings to Efimov physics as measured in cold atomic gases.

Results

The Dirac model. The Dirac equation of a massless fermion in the presence of a $-Z\alpha/r$ potential is obtained from the Hamiltonian (with $\hbar = c = 1$),

$$H = -i\gamma^0\gamma^j\partial_j - \frac{\beta}{r}, \qquad (3)$$

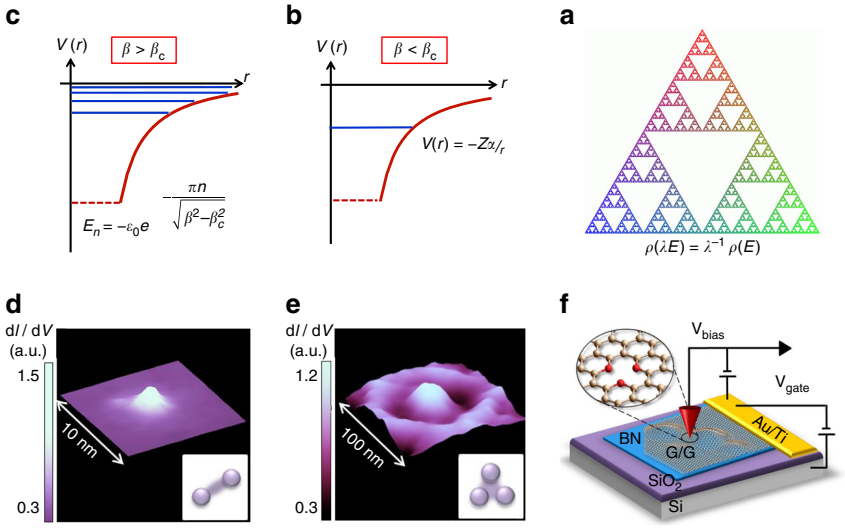

Fig. 1 Schematic visualization of the purpose and main results of this paper. **a** Sierpinski gasket as typical featuring of such iterative fractal structures. This QPT is realized experimentally by creating single-atom vacancies in graphene. The function $\rho(E)$ is the density of states and obeys a scaling relation characterising the existence of discrete scale symmetry. **b**, **c** Illustration of the universal quantum phase transition (QPT) obtained by varying the dimensionless parameter $\beta \equiv Z\alpha$ (see text for precise definitions) in the low-energy spectrum of a massless fermion in a Coulomb potential $V = -Z\alpha/r$ created by a charge Z. **b** For low values, $\beta < \beta_c$, there is a single quasi-bound state close to zero energy. **c** For overcritical values, $\beta > \beta_c$, the low-energy spectrum is a ladder E_n characterized by a discrete scale symmetry $\{E_n\} = \{\lambda E_n\}$ for $\lambda = \exp(\pi/\sqrt{\beta^2 - \beta_c^2})$. **d**, **e** Experimental dI/dV maps of charged vacancy for fixed $\beta < \beta_c$ (**d**) and $\beta > \beta_c$ (**e**). The images illustrate the characteristic probability density of the resonances in (**b**, **c**). **f** Scanning tunnelling microscopy (*STM*) setup. Local charge Z is accumulated at the single vacancy in graphene by applying voltage pulses to the STM tip

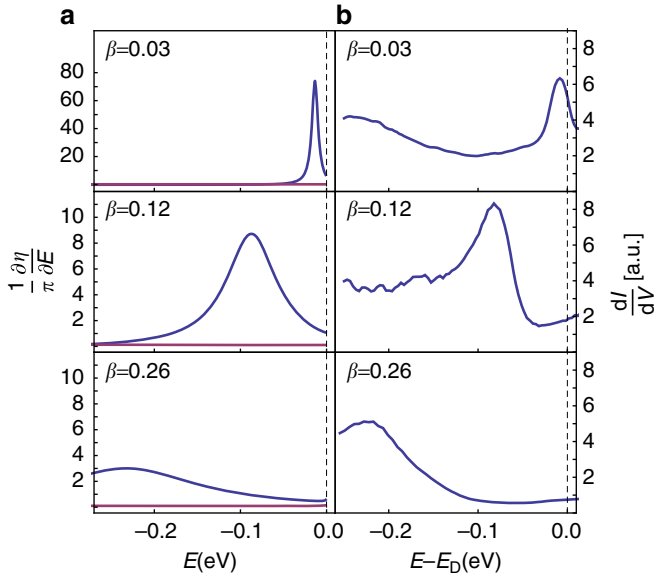

Fig. 2 Experimental and theoretical picture in the undercritical regime. **a** Theoretical behavior of $(1)/(\pi)\mathrm{d}\eta/\mathrm{d}E$ for $d=2$ showing quasi-bound states of a massless Dirac fermion in the undercritical regime $\beta<1/2$. In the scale-free low-energy, $EL\ll 1$ regime, the $m=-1$ (*blue*) branch contains a single peak and the $m=0$ (purple) branch shows no peak independently of the choice of boundary condition (see Supplementary Note 2). While increasing β, the resonance shifts to lower energy and becomes broader. **b** Excitation spectrum measured in graphene using STM as a function of the applied voltage V. The determination of the parameter β is explained in the text

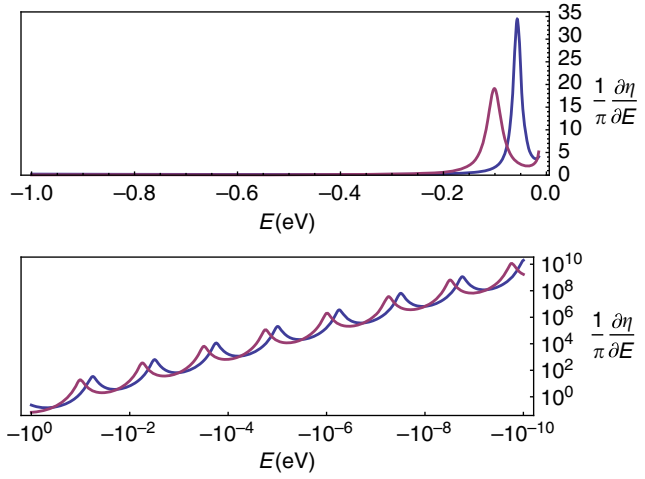

Fig. 3 Theoretical behavior of the low energy and scale-free part of the quasi-bound states spectrum in the overcritical regime for $d=2$ and $\beta=1.2>\beta_c(=1/2)$. The lower plot displays the detailed structure of the infinite geometric ladders. Note that the $m=-1$ (*blue*) and $m=0$ (*purple*) ladders are intertwined. These results are independent of the boundary condition

where $(\gamma^0,\ \gamma^j)$ are Dirac matrices. Here the dimensionless parameter monitoring the transition is $\beta=Z\alpha$, where Z is the Coulomb charge and α the fine structure constant. The QPT occurs at the critical value $\beta_c=(d-1)/2$ (Supplementary Note 1) (A related anomalous behavior in the Dirac Coulomb problem has been identified long ago[26] but its physical relevance was marginal since it required non existent heavy-nuclei Coulomb charges $Z\simeq 1/\alpha\simeq 137$ to be observed. Moreover, the problem of a massive Dirac particle is different due to the existence of a finite gap which breaks CS.). For resonant quasi-bound states, we look for scattering solutions of the form $\psi_{\mathrm{in}}+e^{2i\eta}\psi_{\mathrm{sc}}$, where $\eta(E)$ is the energy-dependent scattering phase shift and $\psi_{\mathrm{in,sc}}(r,\ E)$ are two component objects representing the radial part of the Dirac spinor which behave asymptotically as,

$$\psi_{\mathrm{in,sc}}(r,E)=r^{\frac{1-d}{2}}\left(V_{\mathrm{in,sc}}\,(2i|E|r)^{\mp i\beta}\,e^{\mp iEr}\right) \tag{4}$$

for $|E|r\gg 1$ and, using $\gamma\equiv\sqrt{\beta^2-\beta_c^2}$,

$$\psi_{\mathrm{in,sc}}(r,E)=r^{\frac{1-d}{2}}\left(U^{-}_{\mathrm{in,sc}}\,(2iEr)^{-i\gamma}+U^{+}_{\mathrm{in,sc}}(2iEr)^{i\gamma}\right), \tag{5}$$

for $|E|r\ll 1$ and for the lowest angular momentum channels. The two component objects $V_{\mathrm{in,sc}}$ and $U^{\pm}_{\mathrm{in,sc}}$ in Eqs. (4) and (5) are constants. It is easy to infer from (5) that $\beta=\beta_c$ plays a special role. Indeed for $\beta>\beta_c$, there exists a family of normalisable solutions that admit complex eigenvalues $E=-i\epsilon$, hence the Hamiltonian (3) is not self-adjoint ($H\neq H^{\dagger}$). To properly define this quantum problem, a regularisation is thus needed for the too strong potential at overcritical values of $\beta=Z\alpha$. This is achieved by introducing a cutoff length L and a boundary condition at $r=L$, which is equivalent to replacing the Coulomb potential at short distances by a well-behaved potential whose exact form is irrelevant in the low-energy regime $EL\ll 1$.

The resulting mixed boundary condition can be written as $h=\Psi_2(r,E)/\Psi_1(r,E)|_{r\to L^+}$, where $\Psi_{1,2}$ represent the two components of the aforementioned radial part of the Dirac spinor. The resulting scattering phase shift $\eta(E,\ L,\ h)$, which contains all the information about the regularisation, thus becomes a function of L and of the parameter h. The quasi-bound states energy spectrum is obtained from the scattering phase shift by means of the Krein–Schwinger relation[27, 28] which relates the change of density of states $\delta\rho$ to the energy derivative of η, (This is also related to the Wigner time delay[29] and to the Friedel sum rule)

$$\delta\rho(E)=\frac{1}{\pi}\frac{\mathrm{d}\eta(E)}{\mathrm{d}E}\,. \tag{6}$$

Theoretical structure of quasi-bound spectrum. From now on, and to compare to experimental results further discussed, we consider the case $d=2$, for which there is a single orbital angular momentum quantum number $m\in\mathbb{Z}$. The corresponding critical coupling becomes $\beta_c=|m+1/2|\geq 1/2$, giving rise to the s-wave channels, $m=0,\ -1$, for which $\beta_c=1/2$. Depending on the choice of boundary condition h, $\delta\rho(E)$ can be degenerate or non-degenerate over these two s-wave channels. This degeneracy originates from the symmetry of the $(2+1)$ Dirac Hamiltonian (3) under parity, $(x,\ y)\to(-x,\ y)$, and its existence is equivalent to whether or not the boundary condition breaks parity (Supplementary Note 2). In what follows, we will consider the generic case in which there is no degeneracy. In the undercritical, $\beta<\beta_c$, and low-energy regime $EL\ll 1$, we observe (Figs. 1b, 2a) a single quasi-bound state originating from only one of the s-wave channels and which broadens as β increases. In the overcritical regime $\beta>\beta_c$, this picture changes dramatically. (We emphasize that this picture remains valid for all values of $\beta>\beta_c$ and not only in the vicinity of β_c). The low-energy ($EL\ll 1$) scattering phase shift displays two intertwined, infinite geometric ladders of quasi-bound states (Figs. 1c, 3) at energies E_n still given by (2) but with $\zeta-\zeta_c$ now replaced by $\beta^2-\beta_c^2$. (Moreover, note that the energy scale ϵ_0 for the Dirac case is different from the inverse square Schrödinger case defined in equation (1)). This sharp transition at β_c belongs to the same universality class as presented for the inverse square Schrödinger problem, namely CS

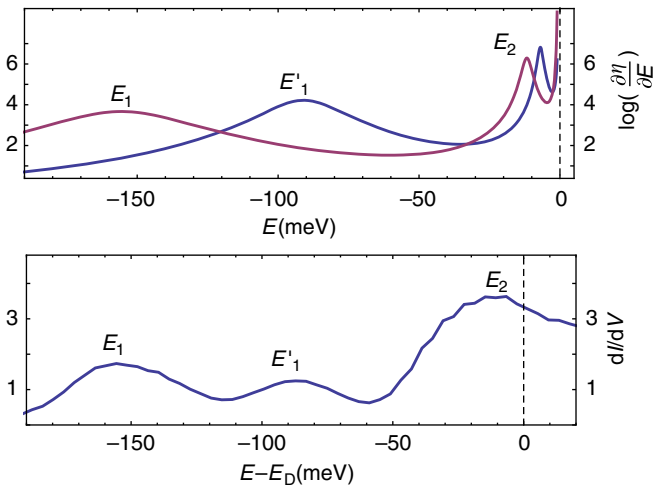

Fig. 4 Experimental and theoretical picture in the overcritical regime. *Upper plot*: Theoretical behavior of the low energy and scale-free part of the overcritical ($\beta = 1.33$) quasi-bound states spectrum obtained from (6). The *blue* (*purple*) *line* corresponds to $m = -1$ ($m = 0$). *Lower plot*: Experimental values of the (STM) tunnelling conductance measured at the position of charged vacancies in graphene. The labelling E_1, E_2, $E_1^{'}$ of the peaks is explained in the text

of the quasi-bound states spectrum is broken for $\beta > \beta_c$ into a DS phase characterized by a fractal distribution of quasi-bound states. The QPT thus reflects the lack of self-adjointness of the Hamiltonian equation (3) and the necessary regularisation procedure leads to a scale anomaly in which CS is broken into DS.

Experimental realization in graphene. A particularly interesting condensed matter system, where the previous considerations seem to be relevant is graphene in the presence of implanted Coulomb charges in conveniently created vacancies[30]. It is indeed known that low-energy excitations in graphene behave as a massless Dirac fermion field with a linear dispersion $\epsilon = \pm v_F|p|$ and a Fermi velocity $v_F \simeq 10^6$ m/s[31]. These characteristics have been extensively exploited to make graphene a very useful platform to emulate specific features of quantum field theory, topology and especially QED[23], since an effective fine structure constant $\alpha_G \equiv e^2/\hbar v_F$ of order unity is obtained by replacing the velocity of light c by v_F.

It has been recently shown that single-atom vacancies in graphene can stably host local charge[30]. Density functional theory calculations have shown that, when a carbon atom is removed from the honeycomb lattice, the atoms around the vacancy site rearrange into a lower energy configuration[32]. The resulting lattice reconstruction causes a charge redistribution, which in the ground state has an effective local charge of ≈+1. Recent Kelvin probe force microscopy measurements of the local charge at the vacancy sites are in good agreement with the Density functional theory predictions. Vacancies are generated by sputtering graphene with He^+ ions[33, 34]. Charge is modified and measured at the vacancy site by means of scanning tunnelling spectroscopy and Landau level spectroscopy as detailed in ref. [30]. Applying multiple pulses allows for a gradual increase in the vacancy charge, which in turn acts as an effective tunable Coulomb source. Moreover, the size of the source inside the vacancy is small (≈1 nm) as compared to the method of deposited metal clusters[35]. Using this method, we are able to observe the transition expected to occur at $\beta = 1/2$ and to measure and analyze three resonances for a broad range of β values.

To establish a relation between the measured differential conductance and the spectrum of quasi-bound states, we recall that the tunnel current $I(V)$ is proportional to both the density of states $\rho_t(\epsilon)$ of the STM tip and $\rho(\epsilon)$ of massless electronic excitations in graphene at the vacancy location. We also assume that the tunnel matrix element $|t|^2$ depends only weakly on energy and that both voltage and temperature are small compared to the Fermi energy and height of the tunnelling potential, so that the current $I(V) = G_t V$ is linear with V thus defining the tunnel conductance $G_t = 2\pi(e^2/\hbar)|t|^2\rho_t\rho(\epsilon)$. Assuming that ρ_t of the reference electrode (the tip) is energy independent, a variation $\delta\rho(\epsilon)$ of the local density of states at the vacancy leads to a variation $\delta I(V)$ of the current and thus to a variation $\delta G_t(V)$ of the tunnel conductance so that, at zero temperature, we obtain[36]

$$\frac{\delta G_t(V)}{G_t} = \frac{\delta\rho(\epsilon)}{\rho_0}, \tag{7}$$

where ρ_0 is the density of states in the absence of vacancy. By considering the vacancy as a local perturbation, each quasiparticle state is characterized by its scattering phase shift taken to be the phase shift $\eta(E)$ of the quasi-bound Dirac states previously calculated. Then, the change of density of states $\delta\rho(E)$ is obtained from equation (6) and combining together with equation (7) leads to the relation,

$$\frac{d\delta I}{dV} = \frac{G_t}{\pi\rho_0}\frac{d\eta(E)}{dE} \tag{8}$$

between the differential tunnel conductance and the scattering phase shift.

The measurements and the data analysis presented here were carried out as follows: positive charges are gradually injected into an initially prepared single atom vacancy and the differential conductance $\delta G_t(V)$ is measured at each step as a function of voltage. Since we are looking at the positions of resonant quasi-bound states, both quantities displayed in Figs. 2, 4 give the same set of resonant energies, independently of the energy-independent factor $G_t/\pi\rho_0$. For low enough values of the charge, the differential conductance displayed in Fig. 2b, shows the existence of a single quasi-bound state resonance. The behavior close to the Dirac point, namely in the low-energy regime independent on the short distance regularization, is very similar to the theoretical prediction of Fig. 2a. When the build up charge exceeds a certain value, we note the appearance of three resonances, emerging out of the Dirac point. We interpret these resonances as the lowest overcritical ($\beta > 1/2$) resonances, which we denote E_1, $E_1^{'}$, E_2, respectively. The corresponding theoretical and experimental behaviors displayed in Figs. 3, 4, show a very good qualitative agreement. To achieve a quantitative comparison solely based on the previous Dirac Hamiltonian equation (3), we fix L and the boundary condition h and deduce the theoretical β values corresponding to the respective positions of the lowest overcritical resonance E_1 (as demonstrated in Fig. 4). This allows to determine the lowest branch $E_1(\beta)$ for $n = 1$ represented in Fig. 5. Then, the experimental points $E_1^{'}$, E_2 are directly compared to their corresponding theoretical branch as seen in Fig. 5. We determine L and h, according to the ansatz $h = a(m + 1)$, and obtain the best correspondence for $L \simeq 0.2$ nm, $a \simeq -0.85$. We compare the experimental E_2/E_1 ratio with the universal prediction $E_{n+1}/E_n = e^{-\pi/\sqrt{\beta^2-1/4}}$ as seen in Fig. 6. A trend-line of the form $e^{-b/\sqrt{\beta^2-1/4}}$ is fitted to the ratios E_2/E_1, yielding a statistical value of $b = 3.145$ with standard error of $\Delta b = 0.06$ consistent with the predicted value π. An error of ± 1 mV is assumed for the position of the energy resonances.

A few comments are appropriate: (i) The points on the $E_2(\beta)$ curve follow very closely the theoretical prediction $E_{n+1}/E_n = e^{-\pi/\sqrt{\beta^2-1/4}}$. This result is insensitive to the choice

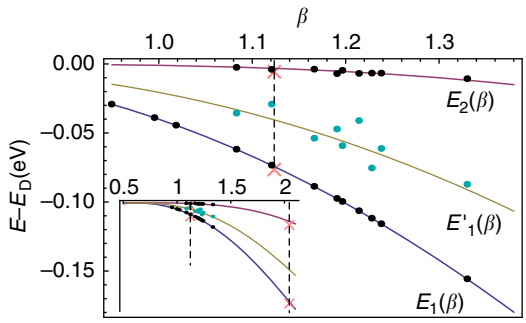

Fig. 5 Behavior of the energies $E_n(\beta)$ of the quasi-bound state spectrum. The curves are obtained from (2) for $E_1(\beta)$, $E_1^{'}(\beta)$, $E_2(\beta)$ as adapted to the massless Dirac case. The *black* and *cyan dots* correspond to the values measured in graphene. The two *pink x*'s are the values of Efimov energies measured in Caesium atoms[39, 47], which corresponds to the (overcritical) fixed Efimov value $\beta_E = 1.1236$. Additional experimental points obtained in refs [40, 41] are displayed in the *inset*

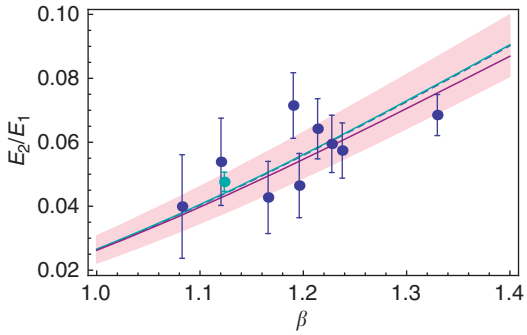

Fig. 6 Comparison between the experimentally obtained E_2/E_1 ratio and the universal factor $e^{-\pi/\sqrt{\beta^2-1/4}}$. *Blue points*: the ratio E_2/E_1 obtained from the position of the points in Fig. 5. Cyan point: Universal Efimov energy ratio as measured in Caesium atoms[39, 47]. *Blue line* (*dashed*): the corresponding optimized curve, fitted according to the model $e^{-b/\sqrt{\beta^2-1/4}}$ and corresponding to $b = 3.145$ with standard error of $\Delta b = 0.06$ consistent with the predicted value π. The *shaded pink* region is the $\pm 2\Delta b$ confidence interval of the curve. *Cyan* line: universal low-energy factor $e^{-\pi/\sqrt{\beta^2-1/4}}$. *Purple line*: theoretical ratio E_2/E_1 obtained from the exact solution of the Dirac equation. As $\beta \to 0.5$, $|E_n|$ becomes smaller therefore the green and purple curves coincide for low β. The *error bar* on the resonance energies is ±1 mV

of h, thus manifesting the universality of the ratio E_{n+1}/E_n. (ii) In contrast, the correspondence between the $E_1^{'}$ points and the theoretical branch is sensitive to the choice of h. This reflects the fact that while each geometric ladder is of the form equation (2) (with the appropriate $\zeta \to \beta$ change), the energy scale ϵ_0 is different between the two thus leading to a shifted relative position of the two geometric ladders in Fig. 3. The ansatz taken for h is phenomenological (Supplementary Note 2), however, we find that in order to get reasonable correspondence to theory, the explicit dependence on m is needed. More importantly, it is necessary to use a degeneracy breaking boundary condition to describe the $E_1^{'}(\beta)$ points. For instance, if the Coulomb potential is regularized by a constant potential for $r \le L$[37], then both angular momentum channels (i.e., the $E_1^{'}$ and E_1 points) become degenerate. The existence of the experimental $E_1^{'}$ branch is therefore a distinct signal that parity symmetry in the corresponding Dirac description equation (3) is broken. In graphene, exchanging the triangular sublattices is equivalent to a parity transformation. Creating a vacancy breaks the symmetry between the two sub-lattices and is therefore at the origin of broken parity in the Dirac model. (iii) The value $L \simeq 0.2$ nm is fully consistent with the low-energy requirement $E_1 L/\hbar v_F \simeq 0.03 \ll 1$ necessary to be in the regime relevant to observe the β-driven QPT.

Discussion

A further argument in support of the universality of this QPT is achieved by comparing the experimental results obtained in graphene with those deduced from a completely different physical problem. To that purpose, we dwell for a short while recalling the basics underlying Efimov physics[38]. Back to 1970, Efimov[10] studied the quantum problem of three identical nucleons of mass m interacting through a short range (r_0) potential. He pointed out that when the scattering length a of the two-body interaction becomes very large, $a \gg r_0$, there exists a scale-free regime for the low-energy spectrum, $\hbar^2/ma^2 \ll E \ll \hbar^2/mr_0^2$, where the corresponding bound-states energies follow the geometric series $\left(\sqrt{-E_n} = -\tilde{\epsilon}_0 e^{-\pi n/s_0}\right)$, where $s_0 \simeq 1.00624$ is a dimensionless number and $\tilde{\epsilon}_0$ a problem-dependent energy scale. Efimov deduced these results from an effective Schrödinger equation in $d = 3$ with the radial ($l = 0$) attractive potential $V(r) = -\left(s_0^2 + 1/4\right)/r^2$. Using Eqs. (1) and (2) and the critical value $\zeta_c = (d-2)^2/4 = 1/4$ for this Schrödinger problem, we deduce the ζ value for the Efimov effect to be $s_0^2 + 1/4 > \zeta_c$ corresponding to the overcritical regime of the QPT. The value of β matching to the Efimov geometric series factor e^{π/s_0} is $\beta_E = \sqrt{s_0^2 + 1/4} = 1.1236$, referred to as the fixed Efimov value. Despite being initially controversial, Efimov physics has turned into an active field especially in atomic and molecular physics where the universal spectrum has been studied experimentally[39–46] and theoretically[38]. The first two Efimov states E_n ($n = 1$, 2) have been recently determined using an ultracold gas of caesium atoms[47]. Although the Efimov spectrum always lies at a fixed and overcritical value of the coupling, unlike the case of graphene where β can be tuned, the universal character of the overcritical regime allows nevertheless for a direct comparison of these two extremely remote physical systems. To that purpose, we include the Efimov value β_E in the expression obtained for the massless Dirac fermion in a Coulomb potential and insert the corresponding data points obtained for cold atomic caesium in the graphene plot (Fig. 5) up to an appropriate scaling of $\tilde{\epsilon}_0$. The results are fully consistent thus showing in another way the universality presented.

There are other remote examples of systems displaying this universal QPT, e.g., flavoured QED3[48], and the XY model (Kosterlitz-Thouless[8] and roughening transitions[22]). Our results provide a useful and original probe of characteristic features of this universal QPT and motivate a more thorough study of this transition.

Methods

Our sample is stacked two layers of graphene on top of a thin BN flake (see Fig. 1f). The standard dry transfer procedure is followed to get this heterostructure. A large twisted angle between the two layers graphene is selected in order to weaken the coupling. The free-standing like feature for the top layer graphene is checked by the Landau levels spectroscopy. To achieve the diluted single vacancies, the sample is exposed to the helium ion beam for short time (100 eV for 5 s) followed by the high temperature annealing. The experiment is performed at 4.2 K with a home-built STM. The dI/dV (I is the current, V is the bias) is recorded by the standard lock-in technique, with a small AC modulation 2 mV at 473.1 Hz added on the DC bias. To tune the effective charge on the vacancy, we apply the voltage pulse (−2 V, 100 ms) with the STM tip directly locating on top of the vacancy.

Data availability. The data that support the findings of this study are available from the corresponding author upon request.

Received: 23 January 2017 Accepted: 12 July 2017
Published online: 11 September 2017

References

1. Akkermans, E. in *Fractal Geometry and Dynamical Systems in Pure and Applied Mathematics II: Fractals in Applied Mathematics* vol. 601, 1–21 (eds Carf, D., Lapidus, M. L., Pearse, E. P. J. & van Frankenhuijsen, M.) (American Mathematical Society (AMS), 2013).
2. Adler, S. L. Axial-vector vertex in spinor electrodynamics. *Phys. Rev.* **177**, 2426–2438 (1969).
3. Bell, J. S. & Jackiw, R. A PCAC puzzle: $\pi^0 \to \gamma\gamma$ in the σ-model. *Il Nuovo Cimento A* **60**, 47–61 (1969).
4. Case, K. M. Singular potentials. *Phys. Rev.* **80**, 797–806 (1950).
5. Landau, L. D. *Quantum Mechanics: Non-Relativistic Theory* (Butterworth-Heinemann, 1991).
6. Lévy-Leblond, J.-M. Electron capture by polar molecules. *Phys. Rev.* **153**, 1–4 (1967).
7. Camblong, H. E., Epele, L. N., Fanchiotti, H. & Garca Canal, C. A. Quantum anomaly in molecular physics. *Phys. Rev. Lett.* **87**, 220402 (2001).
8. Kaplan, D. B., Lee, J.-W., Son, D. T. & Stephanov, M. A. Conformality lost. *Phys. Rev. D* **80**, 125005 (2009).
9. Nisoli, C. & Bishop, A. R. Attractive inverse square potential, $U(1)$ gauge, and winding transitions. *Phys. Rev. Lett.* **112**, 070401 (2014).
10. Efimov, V. Energy levels arising from resonant two-body forces in a three-body system. *Phys. Lett. B* **33**, 563–564 (1970).
11. Efimov, V. Weakly-bound states of three resonantly-interacting particles. *Sov. J. Nucl. Phys* **12**, 589–595 (1971).
12. Jackiw, R. W. *Diverse Topics in Theoretical and Mathematical Physics* (World Scientific, 1995).
13. Meetz, K. Singular potentials in nonrelativistic quantum mechanics. *Il Nuovo Cimento* **34**, 690–708 (1964).
14. Gitman, D. M., Tyutin, I. & Voronov, B. L. *Self-adjoint Extensions in Quantum Mechanics: General Theory and Applications to Schrödinger and Dirac Equations with Singular Potentials* vol. 62 (Springer, 2012).
15. Albeverio, S., Høegh-Krohn, R. & Wu, T. T. A class of exactly solvable three-body quantum mechanical problems and the universal low energy behavior. *Phys. Lett. A* **83**, 105–109 (1981).
16. Beane, S. R. et al. Singular potentials and limit cycles. *Phys. Rev. A* **64**, 042103 (2001).
17. Mueller, E. J. & Ho, T.-L. Renormalization group limit cycles in quantum mechanical problems. Preprint at arXiv:cond-mat/0403283 (2004).
18. Braaten, E. & Phillips, D. Renormalization-group limit cycle for the $1/r^2$ potential. *Phys. Rev. A* **70**, 052111 (2004).
19. Hammer, H.-W. & Swingle, B. G. On the limit cycle for the $1/r^2$ potential in momentum space. *Ann. Phys.* **321**, 306–317 (2006).
20. Moroz, S. & Schmidt, R. Nonrelativistic inverse square potential, scale anomaly, and complex extension. *Ann. Phys.* **325**, 491–513 (2010).
21. De Martino, A., Klöpfer, D., Matrasulov, D. & Egger, R. Electric-dipole-induced universality for Dirac fermions in graphene. *Phys. Rev. Lett.* **112**, 186603 (2014).
22. Kolomeisky, E. B. & Straley, J. P. Universality classes for line-depinning transitions. *Phys. Rev. B* **46**, 12664–12674 (1992).
23. Shytov, A. V., Katsnelson, M. I. & Levitov, L. S. Atomic collapse and quasi-rydberg states in graphene. *Phys. Rev. Lett.* **99**, 246802 (2007).
24. Pereira, V. M., Nilsson, J. & Castro Neto, A. H. Coulomb impurity problem in graphene. *Phys. Rev. Lett.* **99**, 166802 (2007).
25. Nishida, Y. Vacuum polarization of graphene with a supercritical Coulomb impurity: low-energy universality and discrete scale invariance. *Phys. Rev. B* **90**, 165414 (2014).
26. Pomeranchuk, I. & Smorodinsky, J. On the energy levels of systems with $Z > 137$. *J. Phys.* **9**, 100 (1945).
27. Akkermans, E. Twisted boundary conditions and transport in disordered systems. *J. Math. Phys.* **38**, 1781–1793 (1997).
28. Akkermans, E., Dunne, G. & Levy, E. in *Optics of Aperiodic Structures: Fundamentals and Device Applications* (ed. Negro, L. D.) (Pan Stanford Publishing, 2013).
29. Smith, F. T. Lifetime matrix in collision theory. *Phys. Rev.* **118**, 349–356 (1960).
30. Mao, J. et al. Realization of a tunable artificial atom at a supercritically charged vacancy in graphene. *Nat. Phys.* **12**, 545–549 (2016).
31. Andrei, E. Y., Li, G. & Du, X. Electronic properties of graphene: a perspective from scanning tunneling microscopy and magnetotransport. *Rep. Prog. Phys.* **75**, 056501 (2012).
32. Liu, Y., Weinert, M. & Li, L. Determining charge state of graphene vacancy by noncontact atomic force microscopy and first-principles calculations. *Nanotechnology* **26**, 035702 (2015).
33. Lehtinen, O. et al. Effects of ion bombardment on a two-dimensional target: atomistic simulations of graphene irradiation. *Phys. Rev. B* **81**, 153401 (2010).
34. Chen, J.-H., Li, L., Cullen, W. G., Williams, E. D. & Fuhrer, M. S. Tunable Kondo effect in graphene with defects. *Nat. Phys.* **7**, 535–538 (2011).
35. Wang, Y. et al. Observing atomic collapse resonances in artificial nuclei on graphene. *Science* **340**, 734–737 (2013).
36. Akkermans, E. & Montambaux, G. In *Mesoscopic Physics of Electrons and Photons*, ch. 7 (Cambridge University Press, 2007).
37. Pereira, V. M., Kotov, V. N. & Castro Neto, A. H. Supercritical Coulomb impurities in gapped graphene. *Phys. Rev. B* **78**, 085101 (2008).
38. Braaten, E. & Hammer, H.-W. Universality in few-body systems with large scattering length. *Phys. Rep.* **428**, 259–390 (2006).
39. Kraemer, T. et al. Evidence for Efimov quantum states in an ultracold gas of caesium atoms. *Nature* **440**, 315–318 (2006).
40. Tung, S.-K., Jiménez-Garca, K., Johansen, J., Parker, C. V. & Chin, C. Geometric scaling of Efimov states in a ^{6}Li–^{133}Cs mixture. *Phys. Rev. Lett.* **113**, 240402 (2014).
41. Pires, R. et al. Observation of Efimov resonances in a mixture with extreme mass imbalance. *Phys. Rev. Lett.* **112**, 250404 (2014).
42. Pollack, S. E., Dries, D. & Hulet, R. G. Universality in three- and four-body bound states of ultracold atoms. *Science* **326**, 1683–1685 (2009).
43. Gross, N., Shotan, Z., Kokkelmans, S. & Khaykovich, L. Observation of universality in ultracold ^{7}Li three-body recombination. *Phys. Rev. Lett.* **103**, 163202 (2009).
44. Lompe, T. et al. Radio-frequency association of Efimov trimers. *Science* **330**, 940–944 (2010).
45. Nakajima, S., Horikoshi, M., Mukaiyama, T., Naidon, P. & Ueda, M. Measurement of an Efimov trimer binding energy in a three-component mixture of ^{6}Li. *Phys. Rev. Lett.* **106**, 143201 (2011).
46. Kunitski, M. et al. Observation of the Efimov state of the helium trimer. *Science* **348**, 551–555 (2015).
47. Huang, B., Sidorenkov, L. A., Grimm, R. & Hutson, J. M. Observation of the second triatomic resonance in Efimov's scenario. *Phys. Rev. Lett.* **112**, 190401 (2014).
48. Appelquist, T., Nash, D. & Wijewardhana, L. C. R. Critical behavior in (2 + 1)-dimensional QED. *Phys. Rev. Lett.* **60**, 2575–2578 (1988).

Acknowledgements

This work was supported by the Israel Science Foundation Grant No. 924/09. Funding for the experimental work provided by DOE-FG02-99ER45742 (STM/STS), NSF DMR 1207108 (fabrication and characterization).

Author contributions

O.O. and E.A.: Proposed observing the aforementioned quantum phase transition in graphene with a charged vacancy. They have contributed to interpreting and solving the theoretical model as well as analysing the experimental data and making contact with the theory. J.M., Y.J. and E.Y.A.: Conceived of and designed the experiment, as well as performed the measurements and analyzed the data. All authors contributed to discussions and preparation of the manuscript.

Additional information

Supplementary Information accompanies this paper at doi:10.1038/s41467-017-00591-8.

Competing interests: The authors declare no competing financial interests.

Reprints and permission information is available online at http://npg.nature.com/reprintsandpermissions/

Publisher's note: Springer Nature remains neutral with regard to jurisdictional claims in published maps and institutional affiliations.

Description of Supplementary Files

File Name: Supplementary Information
Description: Supplementary Figures, Supplementary Notes, Supplementary Methods and Supplementary References

File Name: Peer Review File

We present in supplementary figures 1 and 2 all overcritical and undercritical measurements, and their corresponding theoretical plots. In supplementary figure 3 we present the STM topography image of an isolated vacancy in graphene.

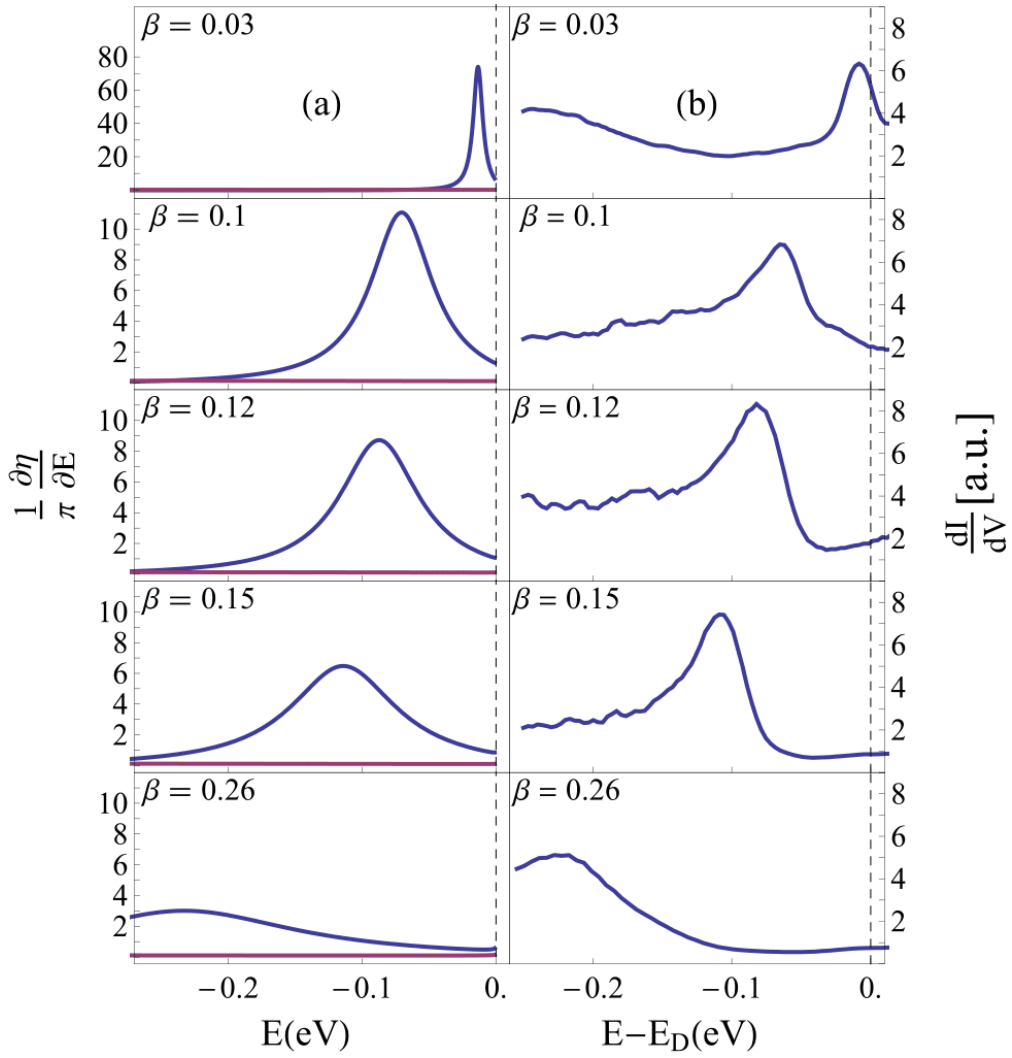

Supplementary Figure 1: **Experimental and theoretical picture in the undercritical regime.** a. Theoretical behaviour of the undercritical ($\beta < 1/2$) quasi-bound states spectrum of massless Dirac fermions. b. STM measurement of the quasi-particle spectrum at the position of the charged vacancy in the undercritical regime. See main text for more details.

Supplementary Note 1: Dirac Coulomb problem in $d+1$ dimensions – critical coupling, phase shift and quasi bound states

In what follows, we study a system described by a massless Dirac particle in the presence of an electric potential that has an inverse radial tail in $d+1$ dimensions. We show that beyond a critical coupling value, an anomalous breaking of conformal symmetry occurs and the system is described by a discrete scale invariant spectrum. We obtain for a general over critical coupling and short range behaviour of the potential, an expression for an infinite series of geometrically spaced quasi bound states.

The massless Dirac equation with an attractive potential $V(r) = -\frac{\beta}{r}$, $\beta \equiv Z\alpha$ in $d+1$ dimensions is

$$i\gamma^{\mu}\left(\partial_{\mu} + ieA_{\mu}\right)\psi\left(x^{\nu}\right) = 0 \tag{1}$$

where $\mu = 0 \ldots d$, A_{μ} is the electromagnetic potential (EM)

$$\begin{aligned} eA_0 &= -\beta/r \\ A_i &= 0 \quad i = 1, \ldots, d. \end{aligned} \tag{2}$$

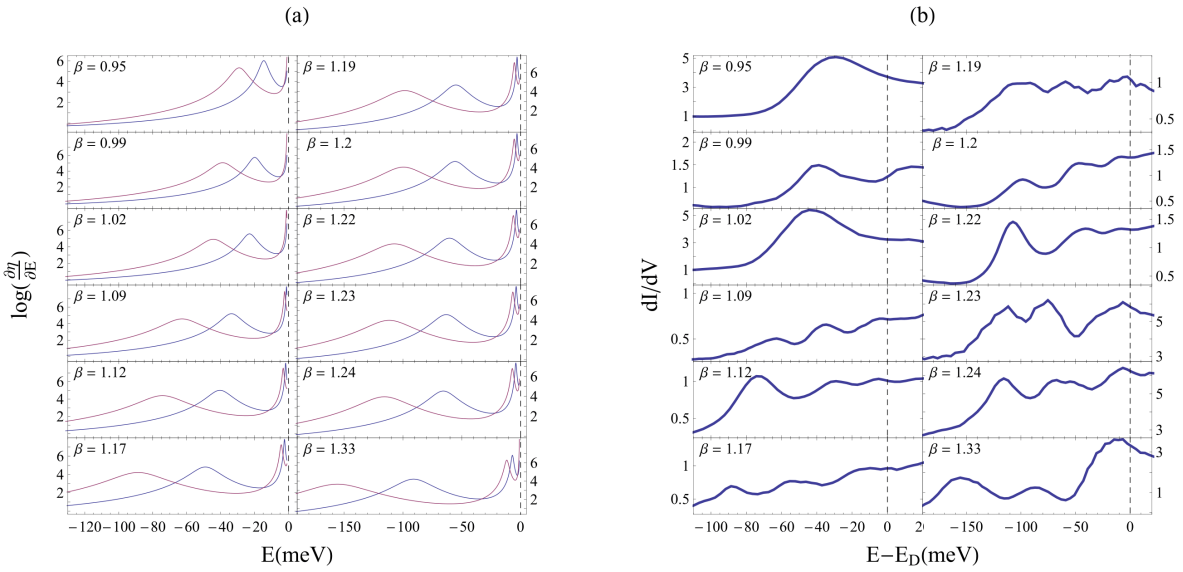

Supplementary Figure 2: **Experimental and theoretical picture in the overcritical regime.** a. Theoretical behaviour of the overcritical ($\beta > 1/2$) quasi-bound states spectrum of massless Dirac fermions. b. STM measurement of the quasiparticle spectrum at the position of the charged vacancy in the overcritical regime. See main text for more details.

and γ^μ are $d+1$ matrices satisfying the anti-commutation relation

$$\{\gamma^\mu, \gamma^\nu\} = 2\eta^{\mu\nu} \tag{3}$$

with $\eta_{\mu\nu}$ being the $d+1$ Minkowski metric with a 'mostly minus' sign convention. The Hamiltonian of the system is expressed as

$$H = \gamma^0 \gamma^j p_j - \beta/r \tag{4}$$

where $j = 1 \dots d$ and corresponds to the scale invariant eigenvalue equation $H\psi = E\psi$ equivalent to (1).

Utilizing rotational symmetry, the angular part of supplementary equation (1) can be solved and the radial dependence of $\psi(x^\nu)$ is given in terms of two functions $\Psi_2(r), \Psi_1(r)$ [1] determined by the following set of equations

$$\begin{aligned} \Psi_2'(r) + \frac{(d-1+2K)}{2r}\Psi_2(r) &= \left(E + \frac{\beta}{r}\right)\Psi_1 \\ -\Psi_1'(r) - \frac{(d-1-2K)}{2r}\Psi_1(r) &= \left(E + \frac{\beta}{r}\right)\Psi_2 \end{aligned} \tag{5}$$

where

$$K \equiv \begin{cases} \pm\left(l + \frac{d-1}{2}\right) & d > 2 \\ m + 1/2 & d = 2 \end{cases}, \tag{6}$$

$l = 0, 1, \dots$ and $m \in \mathbb{Z}$ are orbital angular momentum quantum numbers. In terms of these radial functions, the scalar product of two eigenfunctions $\psi, \tilde{\psi}$ is given by

$$\int dV\, \psi^\dagger \tilde{\psi} = \int dr\, r^{d-1} \left(\Psi_1^*(r)\tilde{\Psi}_1(r) + \Psi_2^*(r)\tilde{\Psi}_2(r)\right).$$

We introduce a short distance radial cut-off L and assume that there exist an electric Coulomb potential $V(r) = -\frac{\beta}{r}$ for $r > L$ and some interaction at $r < L$ that can be modelled by a BC at $r = L$. The equivalent mixed boundary condition of (5) can be written as follows [2]

$$h = \left.\frac{\Psi_2(r)}{\Psi_1(r)}\right|_{r \to L^+} \tag{7}$$

where h is determined by the short range physics and in general can depend on E, L and K. Specification of the cut-off L, coupling β, boundary condition h (and the already determined angular dependence) determine a specific set of solutions to equation (1).

Two independent solutions to equations (5) are given by $S_{\pm\gamma}$ with

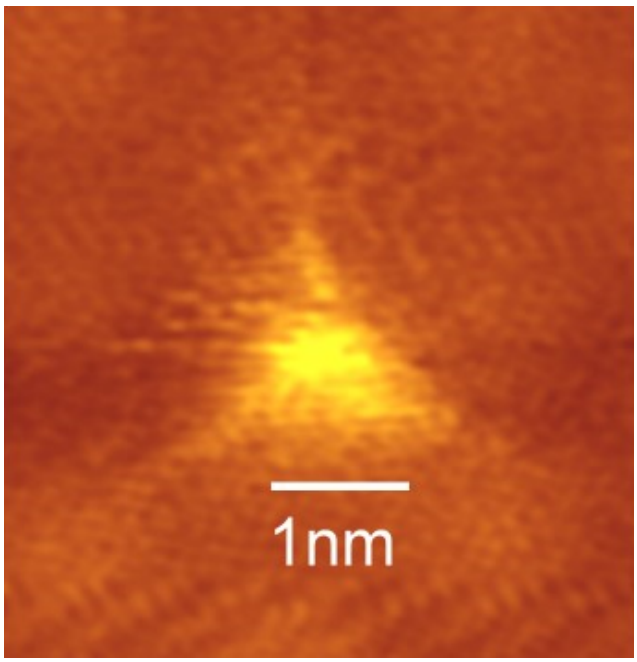

Supplementary Figure 3: **Characteristic topography signature of an isolated vacancy in graphene.** The triangular interference pattern arises due to the local crystal distortion and corresponding electronic state reconstruction. This is the feature that was used to identify single atom vacancies in this work.

$$\begin{aligned} S_\gamma(\rho) \equiv r^{\frac{1-d}{2}} e^{-\rho/2} \rho^{i\gamma} \Big[{}_1F_1\left(i(\gamma+\beta); 1+2i\gamma; \rho\right) \begin{pmatrix} 1 \\ i \end{pmatrix} \\ + \frac{\gamma+\beta}{K} {}_1F_1\left(1+i(\gamma+\beta); 1+2i\gamma; \rho\right) \begin{pmatrix} i \\ 1 \end{pmatrix} \Big] \end{aligned} \tag{8}$$

where ${}_1F_1\ (a,b,z)$ is Kummer's function [3], $\gamma \equiv \sqrt{\beta^2 - K^2}$ and $\rho \equiv 2iEr$. The $|E|\, r \ll 1$ behaviour of $S_{\pm\gamma}$ is given by

$$S_\gamma = r^{\frac{1-d}{2}} \rho^{i\gamma} \left(\begin{pmatrix} 1 + i\frac{\gamma+\beta}{K} \\ i + \frac{\gamma+\beta}{K} \end{pmatrix} + \mathcal{O}(|E|\, r) \right). \tag{9}$$

Solutions corresponding to outgoing and ingoing radial waves for $r \to \infty$ are given by the combinations

$$\begin{aligned} \psi_{\text{in}} &= \left(C_{\text{in}}^{\gamma} S_\gamma + C_{\text{in}}^{-\gamma} S_{-\gamma}\right) \\ &= r^{\frac{1-d}{2}} \left(\begin{pmatrix} 1 \\ -i \end{pmatrix} e^{-iEr - i\beta \log(2|E|r)} + \mathcal{O}\left(\frac{1}{|E|r}\right) \right) \\ \psi_{\text{sc}} &= \left(C_{\text{sc}}^{\gamma} S_\gamma + C_{\text{sc}}^{-\gamma} S_{-\gamma}\right) \\ &= r^{\frac{1-d}{2}} \left(\begin{pmatrix} 1 \\ i \end{pmatrix} e^{+iEr + i\beta \log(2|E|r)} + \mathcal{O}\left(\frac{1}{|E|r}\right) \right) \end{aligned} \tag{10}$$

where

$$\begin{aligned} C_{\text{sc}}^{\gamma} &\equiv K e^{-\frac{\pi\beta}{2}} \frac{\left(e^{2\pi\beta} - e^{-2\pi\gamma}\right) \Gamma(i(\gamma+\beta))}{\left(e^{2\pi\gamma} - e^{-2\pi\gamma}\right) \Gamma(1+2i\gamma)} \\ C_{\text{in}}^{\gamma} &\equiv e^{\pi\gamma} e^{\frac{3\pi\beta}{2}} \frac{\left(e^{-2\pi\beta} - e^{-2\pi\gamma}\right) \Gamma(1+i(\gamma-\beta))}{\left(e^{2\pi\gamma} - e^{-2\pi\gamma}\right) \Gamma(1+2i\gamma)} \end{aligned} \tag{11}$$

For the case $E < 0$. The log dependence in (10) is characteristic of the long range Coulomb tail and is irrelevant to the physics of the scattering problem [4]. Thus, a general solution to (5) can be written as

$$\begin{pmatrix} \Psi_1 \\ \Psi_2 \end{pmatrix} \propto \psi_{\text{in}}(\rho) + e^{2i\eta} \psi_{\text{sc}}(\rho) \tag{12}$$

where the scattering phase shift η is determined by the boundary condition (7) at $r = L$

$$e^{2i\eta(EL,h)} = -\left. \frac{\psi_{in,2}(\rho) - h\psi_{in,1}(\rho)}{\psi_{sc,2}(\rho) - h\psi_{sc,1}(\rho)} \right|_{\rho=2iEL} \tag{13}$$

The energy derivative of η is given by the logarithmic derivative of the RHS of (13)

$$\frac{d\eta}{dE} = \frac{1}{2i}\frac{d}{dE}\ln\left(-\frac{\psi_{in,2}(\rho) - h\psi_{in,1}(\rho)}{\psi_{sc,2}(\rho) - h\psi_{sc,1}(\rho)}\bigg|_{\rho=2iEL}\right) \tag{14}$$

The explicit expression is complicated and is therefore omitted. Resonant quasi-bound states appear for specific values of the energy E at which $d\eta/dE$ exhibits a sharp maxima. We would like to obtain an analytic expression for the position of the resonances in the regime $|E|\,L \ll 1$ appearing in Fig. 3 of the main text. Such an expression can in principle be extracted from (14). However, an easier route is available by allowing the energy parameter to be complex valued such that $E \to \varepsilon \equiv E_R - i\frac{W}{2}$ [5] and look for solutions of (5) and (7) with no e^{-iEr} plane wave solution for $r \to \infty$. The lifetime of the resonance is given by W^{-1} and is required to be positive. A solution with no ingoing wave is obtained by the requirement that $e^{-2i\eta(EL,h)} = 0$ or alternatively the vanishing of the denominator in (13) such that

$$h = \frac{\psi_{sc,2}(\rho)}{\psi_{sc,1}(\rho)}\bigg|_{\rho=2i\varepsilon L}. \tag{15}$$

Focusing our attention at the regime $|\varepsilon|\,L \ll 1$, one finds very different results depending on the value of β. For $\beta < \beta_c \equiv |K|$, γ is pure imaginary. Thus, from (9) and (10) we get that both $\psi_{sc,1,2} \propto \rho^{-\sqrt{K^2-\beta^2}}$ and therefore equation (15) is independent of ε to leading order in $|\varepsilon|\,L$. This inconsistency means that for fixed L and β there are no quasi bound states arbitrarily close to zero energy. In contrary, for $\beta > \beta_c$ and to leading order in $|\varepsilon|\,L$, equation (15) is given by

$$h_0 = \frac{C_s^{\gamma}\rho^{i\gamma}\left(i + \frac{\beta+\gamma}{K}\right) + (\gamma \to -\gamma)}{C_s^{\gamma}\rho^{i\gamma}\left(1 + i\frac{\beta+\gamma}{K}\right) + (\gamma \to -\gamma)} \tag{16}$$

where $h_0 \equiv h|_{E\to 0}$. Solving supplementary equation (16) for $\rho^{2i\gamma}$ gives $\rho^{2i\gamma} = z_0$ where $z_0 \equiv \frac{C_s^{-\gamma}((1-ih_0)(\beta-\gamma)-(h_0-i)K)}{C_s^{\gamma}((h_0-i)K-(1-ih_0)(\beta+\gamma))}$. Inserting $\rho \equiv 2i\varepsilon L$ and solving for ε yields

$$\varepsilon_n = -\epsilon_0 e^{i\Theta}e^{-\frac{\pi n}{\gamma}} \quad n \in \mathbb{Z} \tag{17}$$

where $\varepsilon_0 \equiv \frac{1}{2L}|z_0^{\frac{1}{2i\gamma}}| > 0$ and $\Theta \equiv \arg\left(iz_0^{\frac{1}{2i\gamma}}\right)$. The regime of validity of this result is for $n > n_{min}$, where n_{min} is such that $|\varepsilon_{n_{min}}|\,L \sim 1$. Using $\Gamma-$function identities, the phase Θ of $-\varepsilon_n$ can be simplified to

$$\begin{aligned}\Theta &= \arg\left(iz_0^{\frac{1}{2i\gamma}}\right)\\ &= \frac{\pi}{2} - \frac{1}{2\gamma}\log(|z_0|)\\ &= -\frac{\pi}{2} + \frac{1}{4\gamma}\log\left(\frac{\sinh(\pi(\beta+\gamma))}{\sinh(\pi(\beta-\gamma))}\right).\end{aligned} \tag{18}$$

Note that Θ is independent on the boundary condition h_0. Recall that $\gamma \equiv \sqrt{\beta^2-K^2}$, where K is given in (6) for $d \geq 2$. For $\beta > |K| \geq \frac{1}{2}$, $\arg(-\varepsilon_n)$ is a very slowly varying function bounded in the region $0 < \arg(-\varepsilon_n) < 0.046\pi$, as can be seen in supplementary figure 4. This is consistent with negative resonances $E_n = \mathrm{Re}(\varepsilon_n) < 0$ with width and $W_n \equiv -2\,\mathrm{Im}(\varepsilon_n) > 0$. Therefore, in the regime $|\varepsilon|\,L \ll 1$, ε_n describes a geometrically spaced set of infinitely many negative quasi bound states for all $\beta > |K|$, h, $d \geq 2$. The width of the resonance is given by $W_n \equiv -2\,\mathrm{Im}(\varepsilon_n) < 0.9\pi\,|\varepsilon_n|$ which describes resonances getting sharper indefinitely as $n \to \infty$. In the vicinity of the transition point $\beta - |K| \gtrsim 0$, $\arg(-\varepsilon_n) \cong -\frac{\pi}{1-e^{2|K|\pi}} + \mathcal{O}(\xi - |K|)^{1/2}$ which for $d = 2$, $m = 0 (\Leftrightarrow |K| = \frac{1}{2})$ agrees with the result of reference [6] in the main text.

Supplamentary Note 2: Dirac Coulomb system as a model for a charged vacancy in graphene

As explained in the main text, we model excitations around the vacancy as massless Dirac particles and neglect any interactions between them. Therefore, for $r > L$, L being the characteristic size of the vacancy, they are described by the Dirac equation (5) with $d = 2$. The full spinor in this case is given in polar coordinates by

$$\psi(r,\phi) = e^{im\phi}\begin{pmatrix}\Psi_1(r)\\ i\Psi_2(r)e^{i\phi}\end{pmatrix} \tag{19}$$

in a representation where $H = \vec{\sigma}\cdot\vec{p} - \beta/r$. The components of the spinor correspond to amplitudes of the wave function on each of the two graphene sublattices. In the near vacancy region, $r < L$ we assume some unknown interaction that can be taken into account by the boundary condition (7) at $r = L$. Conventionally used choices are:

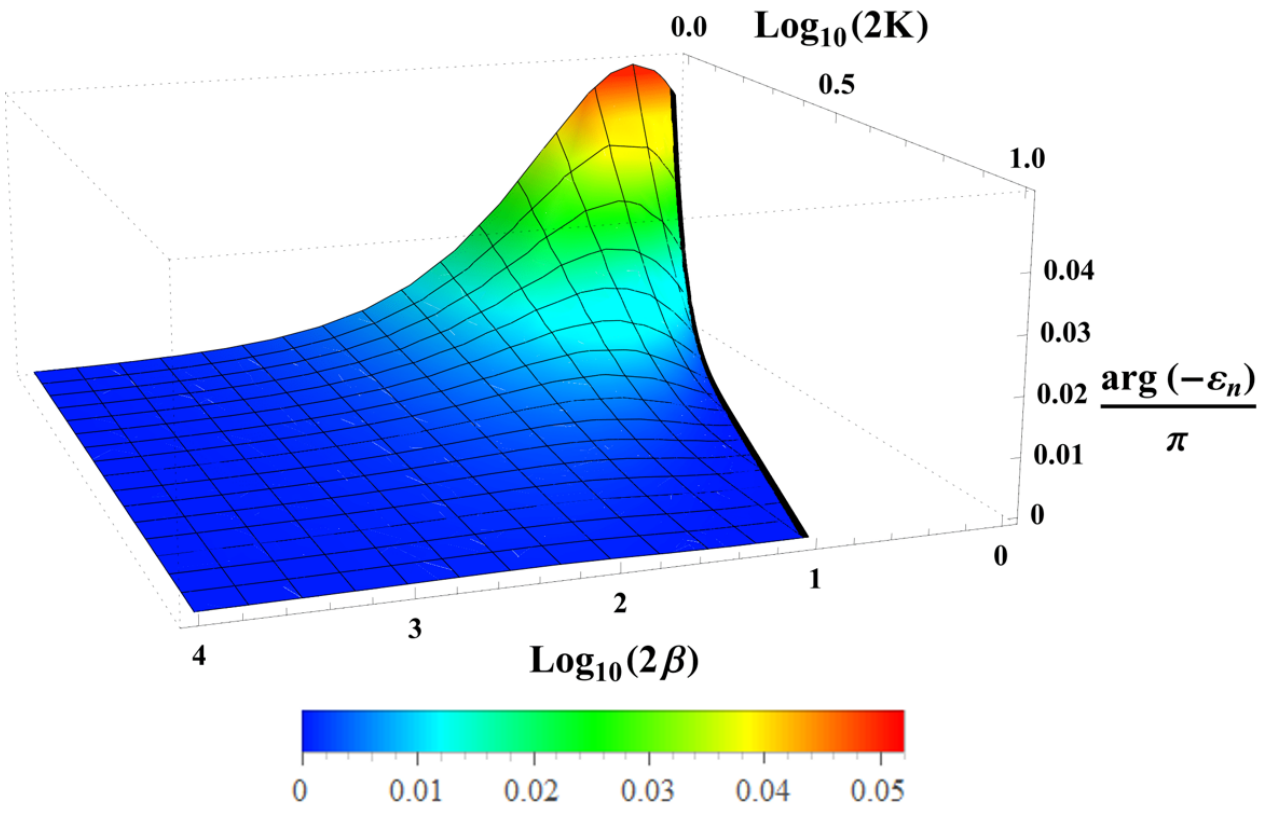

Supplementary Figure 4: **The phase of $-\varepsilon_n$ as a function of the coupling β and $|K|$ for $\beta > |K|$.** The bold black line represents $\xi = |K|$. It can be seen that the phase of $-\varepsilon_n$ takes values in the range $[0, 0.046\pi]$ for $d \geq 2$

.

(i) continuously connected constant potential $V_< = -\beta/L$ [7] corresponding to $h = J_{m+1}(\beta + EL)/J_m(\beta + EL)$, where $J_n(x)$ is Bessel's function; (ii) zero wavefunction on one of the graphene lattice sites [8] corresponding to $h = 0$; (iii) infinite mass term on boundary term [9] corresponding to $h = 1$. Generically, h can depend on E, L and m. From (6), the critical coupling is $\beta_c \equiv |m + 1/2| \leq 1/2$, giving rise to two angular momentum s-wave channels, $m = 0, -1$ for which $\beta_c = 1/2$.

An additional important property of our model is related to parity symmetry. Since mass or scalar potential terms are absent (and the Coulomb potential is radial), the Dirac equation in $2 + 1$ dimension is symmetric under 2 dimensional parity, P_y, in which $(x, y) \to (-x, y)$ [10]. The action of the parity operators on $\Psi(r, \phi)$ is defined as

$$\begin{aligned} \psi'(r,\phi) &\equiv P_y \psi(r, \pi - \phi) \\ &= \sigma_y \psi(r, \pi - \phi) \\ &= -ie^{i(-m-1)\phi} \begin{pmatrix} \Psi_2(r) \\ -i\Psi_1(r)e^{i\phi} \end{pmatrix}. \end{aligned} \tag{20}$$

This transformation can also be accounted for (up to an unimportant overall phase) by

$$\Psi_1(r) \to \Psi_2(r), \Psi_2(r) \to -\Psi_1(r), m \to -m - 1 \tag{21}$$

where $K \equiv m + 1/2$, thus $m \to -m - 1 \Leftrightarrow K \to -K$. Indeed, the Dirac equation (5), is invariant under (21).

From (21) it is apparent that solutions corresponding to angular momentum m and $-m-1$ are linked via parity symmetry. Since energy remains unchanged under parity, a natural question is whether the quasi bound energies are the same for angular momentum channels m and $-m-1$. The answer depends on the short distance region. For example, if we describe the $r < L$ regime by condition (i) then the quasi bound states will necessarily be degenerate over the m and $-m-1$ channels. The reason is that in this case, the potential of both regimes $r > L$, $r < L$ respects parity symmetry. As a result, h in (i) transforms like $\Psi_2(r)/\Psi_1(r)$ under (21), i.e., $h \to -h^{-1}$. Thus, by applying (21) on both side of (14) it is straightforward to obtain that $d\eta_m/dE = d\eta_{-m-1}/dE$. However, if the potential in the $r < L$ regime break parity, that is, the corresponding boundary condition does not transform as $h \to -h^{-1}$ under (21) (for example $h = 0, 1$), then $d\eta_m/dE \neq d\eta_{-m-1}/dE$ and the degeneracy will be broken. Specifically, for $m = 0, -1$ we find two interleaved geometric ladders of over critical states in the corresponding regime $\beta > \beta_c = 1/2$ as shown in the main text. The relative position of the two ladders typically depends on h and therefore is sensitive to the detail of the short range physics.

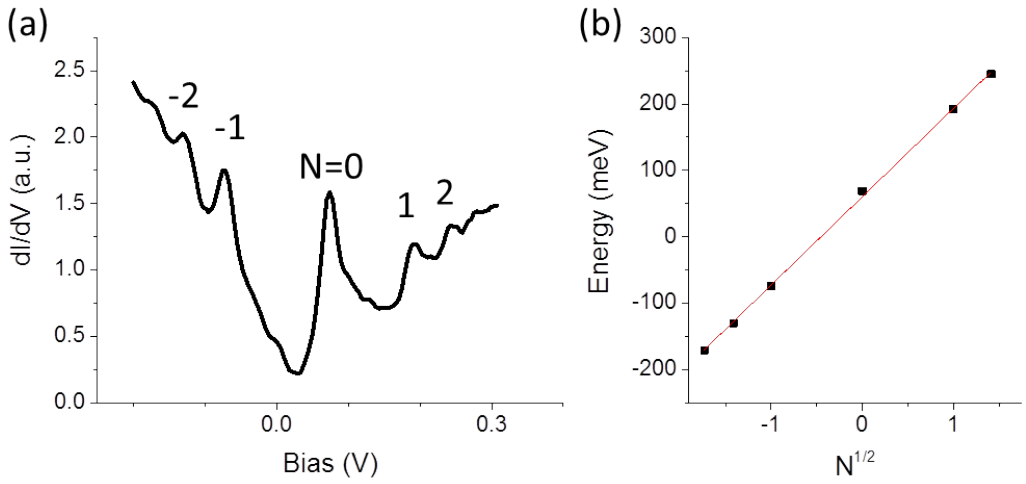

Supplementary Figure 5: **The Landau levels spectrum for twisted bilayer graphene under** 10T**.** (a) dI/dV curve on graphene at $B = 10$T with $V_b = -300$mV and $I = 20$pA. (b) Fit of the Landau level sequence in (a) used to extract the Fermi velocity.

All the figures in the main text describing the behaviour of $d\eta/dE$ as a function of E and the values of the quasi bound states $E_n(\beta)$ are extracted from the exact relation appearing in equation (14).

Supplementary Methods

Sample fabrication. In this work, we use G/G/BN on SiO_2 to perform the experiment. The hBN thin flakes were exfoliated onto the SiO_2 surface followed by a dry transfer process using a sacrificial PMMA thin film to stack the first graphene layer on the hBN flake. Before stacking the top layer graphene, the PMMA was removed with acetone and IPA, followed by furnace annealing in forming gas (10% H_2 and 90% Ar) at 230°C for 3 hours. The second layer graphene was stacked by using the same procedure as the first layer. Au/Ti electrodes were deposited by the standard SEM lithography for the STM contact. After the liftoff process, the sample was annealed again in furnace with forming gas to remove the PMMA residues. Subsequently, the sample is loaded in the UHV chamber for further annealing at $230°C$ overnight. To generate the single vacancies, the sample is exposed to a $100 - 140$eV He^+ ion beam followed by high temperature *in situ* annealing. The other stacked samples, G/BN/SiO_2 and G/G/SiO_2, were prepared by the same procedure.

Characterization by STM topography and Landau level (LL) spectroscopy. The STM experiment is performed at 4.2K using a cut PtIr tip. The dI/dV spectroscopy is performed using the standard lockin method with bias modulation typically 2mV at 473.1Hz. To charge the single vacancies, voltage pulses are applied directly at the desired vacancy site with the STM tip at ground potential. The intrinsic electronic properties of graphene can be effectively isolated from the random potential induced by the SiO_2 substrate by using an intermediate graphene layer and an hBN buffer underneath the layers. When the twist angle between the two stacked graphene layers exceeds 10° the two layers are electronically decoupled at the experimentally relevant energies. Therefore a large twist angle was chosen to ensure a linear dispersion near the Dirac point. LL spectroscopy provides a direct way to prove the layer decoupling. For single layer graphene, the energy level sequence is given by: $E_N = \mathrm{sign}(N) v_F \sqrt{2e\hbar |N| B}$, where N is the LL index, v_F is the Fermi velocity, $\hbar$ is the reduced Plank constant. For fixed magnetic field, the root N dependence for the sequence is the fingerprint of single layer graphene. supplementary figure 5(a) shows the LL spectrum of the G/G/BN sample at 10T. By fitting the LLs sequence (supplementary figure 5(b)), we obtain the value of the Fermi velocity $v_F = (1.2 \pm 0.02) \times 10^6 m/s$.

Supplementary References

[1] Dong, S.-H. *Wave Equations in Higher Dimensions* (Springer, 2011).

[2] Yang, C. N. Generalization of Sturm-Liouville theory to a system of ordinary differential equations with Dirac type spectrum. *Comm. Math. Phys.* **112**, 205–216 (1987).

[3] Abramowitz, M. & Stegun, I. A. *Handbook of mathematical functions: with formulas, graphs, and mathematical tables*. 55 (Courier Corporation, 1964).

[4] Walter Greiner, J. R., B. Mller. *Quantum Electrodynamics of Strong Fields* (Springer-Verlag Berlin Heidelberg, 1985).

[5] Friedrich, H. *Scattering Theory* (Springer-Verlag Berlin Heidelberg, 2013).

[6] Shytov, A. V., Katsnelson, M. I. & Levitov, L. S. Atomic Collapse and Quasi-Rydberg States in Graphene. *Phys. Rev. Lett.* **99**, 246802 (2007).

[7] Pereira, V. M., Kotov, V. N. & Castro Neto, A. H. Supercritical Coulomb impurities in gapped graphene. *Phys. Rev. B* **78**, 085101 (2008).

[8] Shytov, A. V., Katsnelson, M. I. & Levitov, L. S. Vacuum Polarization and Screening of Supercritical Impurities in Graphene. *Phys. Rev. Lett.* **99**, 236801 (2007).

[9] Pereira, V. M., Nilsson, J. & Castro Neto, A. H. Coulomb Impurity Problem in Graphene. *Phys. Rev. Lett.* **99**, 166802 (2007).

[10] WINKLER, R. & ZLICKE, U. Discrete symmetries of low-dimensional dirac models: A selective review with a focus on condensed-matter realizations. *The ANZIAM Journal* **57**, 3–17 (2015).

Rapid Communications

Scale anomaly of a Lifshitz scalar: A universal quantum phase transition to discrete scale invariance

Daniel K. Brattan*

Interdisciplinary Center for Theoretical Study, University of Science and Technology of China, 96 Jinzhai Road, Anhui, Hefei 230026, People's Republic of China

Omrie Ovdat† and Eric Akkermans‡

Department of Physics, Technion Israel Institute of Technology, Haifa 3200003, Israel

(Received 20 June 2017; published 12 March 2018)

We demonstrate the existence of a universal transition from a continuous scale invariant phase to a discrete scale invariant phase for a class of one-dimensional quantum systems with anisotropic scaling symmetry between space and time. These systems describe a Lifshitz scalar interacting with a background potential. The transition occurs at a critical coupling λ_c corresponding to a strongly attractive potential.

DOI: 10.1103/PhysRevD.97.061701

I. INTRODUCTION

Some of the most intriguing phenomena resulting from quantum physics are the violation of classical symmetries, collectively referred to as anomalies [1–4]. One class of anomalies describes the breaking of continuous scale symmetry at the quantum level. A remarkable example of these "scale anomalies" occurs in the case of a nonrelativistic particle in the presence of an attractive, inverse square potential [5–12], which describes the Efimov effect [13–15] and plays a role in various other systems [16–23]. Classically scale invariant [24], any system described by the Hamiltonian, $\hat{H}_S = p^2/2m - \lambda/r^2$, exhibits an abrupt transition in the spectrum at $2m\lambda_c = (d-2)^2/4$ [25] where d is the space dimension. For $\lambda < \lambda_c$, the spectrum contains no bound states close to $E = 0$; however, as λ goes above λ_c, an infinite series of bound states appears. Moreover, in this "over-critical" regime, the states arrange themselves in an unanticipated geometric series $E_n \propto \exp(-2\pi n/\sqrt{\lambda-\lambda_c})$, $n \in \mathbb{Z}$, accumulating at $E = 0$. The existence and geometric structure of such levels do not rely on the details of the potential close to its source and is a signature of residual discrete scale invariance since $\{E_n\} \to \{\exp(-2\pi/\sqrt{\lambda-\lambda_c}))E_n\} = \{E_n\}$. Thus, H_S exhibits a quantum phase transition at λ_c between a continuous scale invariant (CSI) phase and a discrete scale invariant phase (DSI). This transition has been associated with Berezinskii-Kosterlitz-Thouless (BKT) transitions [12,17,26–30].

Another system—the charged and massless Dirac fermion in an attractive Coulomb potential $\hat{H}_D = \gamma^0\gamma^j p_j - \lambda/r$ [31]—also belongs to the same universal class of systems with these abrupt transitions. The similarity between the spectra and transition of these Dirac and Schrödinger Hamiltonians motivates the study of whether a transition of this sort is possible for a generic scale invariant system. Specifically, these different Hamiltonians share a similar property—the power law form of the corresponding potential matches the order of the kinetic term. In this paper, we examine whether this property is a sufficient ingredient by considering a generalized class of one-dimensional Hamiltonians,

$$\hat{H}_N = (p^2)^N - \frac{\lambda_N}{x^{2N}}, \tag{1}$$

where N is an integer and λ_N a real coupling, and study if they exhibit a transition of the same universality class as $\hat{H}_S = \hat{H}_1$, $\hat{H}_D$.

Hamiltonian (1) describes a system with non-quadratic anisotropic scaling between space and time for $N > 1$. This "Lifshitz scaling symmetry" [32], manifest in (1), can be seen for example at the finite temperature multicritical points of certain materials [33,34] or in strongly correlated electron systems [35–37]. It may also have applications in particle physics [32], cosmology [38] and quantum gravity [39–43]. The non-interacting mode ($\lambda_N = 0$) can also appear very generically, for example in non-relativistic systems with spontaneous symmetry breaking [44].

Generalizing (1) to higher-dimensional flat or curved spacetimes also introduces intermediate scale invariant terms which are products of radial derivatives and powers

*danny.brattan@gmail.com
†somrie@campus.technion.ac.il
‡eric@physics.technion.ac.il

of the inverse radius. For $d > 1$ the potential in (1) can be generated by considering a Lifshitz scale invariant system with charge and turning on a background gauge field [32,45–47] consisting of the appropriate multipole moment. The procedures we use throughout this paper are readily extended to these situations and the simple model (1) is sufficient to capture the desired features.

Our main results are summarized as follows. In accordance with the $N = 1$ case, there is a quantum phase transition at $\lambda_{N,c} \equiv (2N-1)!!^2/2^{2N}$ for all $N > 1$ from a CSI phase to a DSI phase in the low energy regime $|E|^{1/2N} x_0 \ll 1$, where $x_0 > 0$ is a short distance cutoff. The CSI phase contains no bound states and the DSI phase is characterized by an infinite set of bound states forming a geometric series as given by Eq. (11). The transition and $\lambda_{N,c}$ value are independent of the short distance physics characterized by the boundary condition at $x = x_0$. For $(\lambda_N - \lambda_{N,c}) \to 0^+$, the analytic behavior of the spectrum is characteristic of the BKT scaling in analogy with $N = 1$ [12,17] and as shown by Eq. (17). We analyze the $x_0 = 0$ case, obtain its self adjoint extensions and spectrum and obtain similar results.

II. THE MODEL

Corresponding to (1) is the action of a complex scalar field in $(1+1)$ dimensions:

$$\int dt \int_{x=x_0}^{\infty} dx \frac{i}{2}(\Psi^* \partial_t \Psi - \text{c.c.}) - |\partial_x^N \Psi|^2 + \frac{\lambda_N}{x^{2N}} |\Psi|^2,$$

where c.c. indicates the complex conjugate. This field theory has manifest Lifshitz scaling symmetry, $(t, x) \mapsto (\Lambda^{2N} t, \Lambda x)$ when $x_0 \to 0$. The scaling exponent of Λ^2 is called the "dynamical exponent" and has value N in this case. The action represents a Lifshitz scalar with a single time derivative and can be recovered as the low energy with respect to mass limit of a charged, massive Lifshitz scalar which is quadratic in time derivatives [48]. The eigenstates of Hamiltonian (1) are given by stationary solutions of the subsequent equations of motion [49].

Consider the case $x_0 < x < \infty$ with $x_0 = 0$. The classical scaling symmetry of (1) implies that if there is one negative energy bound state then there is an unbounded continuum. Thus, the Hamiltonian is non-self-adjoint [51,52]. The origin of this phenomenon, already known from the $N = 1$ case, is the strong singularity of the potential at $x = 0$. To remedy this problem, the operator can be made self-adjoint by applying boundary conditions on the elements of the Hilbert space through the procedure of self-adjoint extension [53]. Alternatively, a suitable cutoff regularization at $x_0 > 0$ can be chosen to ensure self-adjointness as well as bound the spectrum from below by an intrinsic scale [8] leaving some approximate DSI at low energies.

For $N = 1$ in (1), the continuous scaling invariance of $\hat{H}_1$ is broken anomalously as a result of restoring self-adjointness. In particular, for $\lambda_1 > 1/4$, one obtains an energy spectrum given by $E_1 = -E_0 \exp(-(2\pi n)/\sqrt{\lambda_1 - \lambda_c})$ for $n \in \mathbb{Z}$. The energies are related by a discrete family of scalings which manifest a leftover DSI in the system.

In what follows, we shall demonstrate that in the case of large positive λ_N (attractive potential) one finds, for all N, a regime with a geometric tower of states using the method of self-adjoint extension. Subsequently, we bound the resulting spectrum from below, while maintaining DSI at low energies, by keeping $x_0 > 0$ and applying generic (self-adjoint) boundary conditions at a cutoff point. We obtain that a transition from CSI to DSI is a generic feature in the landscape of these Hamiltonians (1), independent of the choice of boundary condition and in a complete analogy with the $N = 1$ case [5–12]. By analytically solving the eigenvalue problem for all N, we obtain an expression for the critical λ_N and for the resulting DSI spectrum in the over-critical regime.

III. SELF-ADJOINT EXTENSION

To determine whether the Hamiltonians (1) can be made self-adjoint one can apply von Neumann's procedure [51–55]. This consists of counting the normalizable solutions to the energy eigenvalue equation with unit imaginary energies of both signs. When there are M linearly independent solutions of positive and negative sign, respectively, there is a $U(M)$ parameter family of conditions at $x = 0$ that can make the operator self-adjoint. If $M = 0$, it is essentially self-adjoint and if the number of positive and negative solutions do not match then the operator cannot be made self-adjoint.

For every N, there are N exponentially decaying solutions at infinity for $E = \pm i$. Normalizability then depends on their $x \to 0$ behavior which requires a complete solution of the eigenfunctions. The energy eigenvalue equation from (1) has an analytic solution in terms of generalized hypergeometric functions [56] (see the Supplemental material [57]) for arbitrary complex energy and λ_N. Near $x = 0$, the analytic solutions are characterized by the roots of the indicial equation,

$$\lambda_N = (-1)^N \Delta(\Delta - 1)(\Delta - 2)\ldots(\Delta - 2N + 1), \quad (2)$$

which can be obtained by inserting $\Psi(x) = x^{\Delta}(1 + \mathcal{O}(x^{2N}))$ into the eigenvalue equation and solving for Δ. We label the $2N$ solutions of (2) as Δ_i, $i = 1, \ldots, 2N$ and order by ascending real part followed by ascending imaginary part. Since (2) is real and symmetric about $N - 1/2$, all roots can be collected into pairs which sum to $2N - 1$ (see Fig. 1). In addition, because $N - 1/2 \geq -1/2$, there can be at most N roots with $\text{Re}(\Delta_i) \leq -1/2$. Thus, near $x = 0$, a generic combination of the N decaying solutions has the form

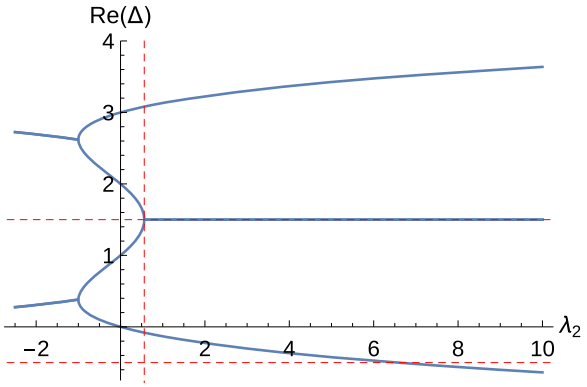

FIG. 1. A plot of the real part of the solution to the indicial equation (2) for $N = 2$ against λ_2. The dotted, red vertical line indicates where $\lambda_2 = 9/16$ above which the first pair of complex roots appears. The lowermost horizontal red line indicates where one of the roots becomes non-normalizable at positive λ_2 (i.e. $\lambda_2 = 105/16$) while the uppermost indicates the symmetry line responsible for pairing roots i.e. $\Delta = 3/2$.

$$\Psi(x) = \sum_{i=1}^{N} [(\epsilon x)^{\Delta_i}\phi_i + \cdots + (\epsilon x)^{\Delta_{i+N}} O_i + \ldots], \quad (3)$$

where E is the energy, $\epsilon \equiv |E|^{1/2N}$ and ϕ_i, O_i are complex numbers [58]. We have distinguished modes with the potential to be divergent as $x \to 0$ by the coefficients ϕ_i. Taking ratios of O_i and ϕ_i yields N-independent dimensionless scales.

To obtain the number of independent normalizable solutions M, we need to count the number m of roots Δ_i with real parts less than $-1/2$ as λ_N varies. When any root violates this bound we must take a linear combination of our N decaying functions to remove it from the near origin expansion and as a result $M = N - m$. This is easily accomplished by examining the analytic solutions in an expansion about $x = 0$.

Generically, for λ_N small in magnitude, $m = 0$, and there is an $U(N)$ self-adjoint extension [59]. As λ_N increases in absolute value and the real part of some roots go below $-1/2$ the dimension of the self-adjoint parameter decreases. Eventually $\hat{H}_N$ either becomes essentially self-adjoint (negative λ_N, repulsive potential) or has a $U(1)$ self-adjoint extension (positive λ_N, attractive potential). The different regimes are summarized for $N = 1, 2, 3$ in Table I.

Now that we have determined when our operator can be made self-adjoint we would like to obtain its energy spectrum. To that purpose, we define the boundary form, $[\Psi, \Phi](x)$, by computing the difference $\hat{H}_N - \hat{H}_N^\dagger$:

$$\langle\Phi|\hat{H}_N|\Psi\rangle - \langle\Phi|\hat{H}_N^\dagger|\Psi\rangle = [\Phi, \Psi](\infty) - [\Phi, \Psi](x_0), \quad (4)$$

$$\langle\Phi|\hat{H}_N|\Psi\rangle = \int_{x=x_0}^{\infty} dx\Phi^*(x)\hat{H}_N\Psi(x), \quad (5)$$

where

$$[\Phi, \Psi](x) = \sum_{j=1}^{2N}(-1)^{N+j-1} d_x^{j-1}\Phi^*(x) d_x^{2N-j}\Psi(x) \quad (6)$$

and the boundary form is calculated by moving the derivatives in $\langle\Phi|\hat{H}_N|\Psi\rangle$ to obtain $\langle\Phi|\hat{H}_N^\dagger|\Psi\rangle$ (see Supplemental material [57]). Setting $\Phi = \Psi$ and using the time-dependent Schrödinger equation, it is straightforward to show that

$$\partial_t\rho = \partial_x[\Psi, \Psi], \qquad \rho = |\Psi|^2, \quad (7)$$

so that the boundary form can be interpreted as the value of the probability current at $x = x_0$.

We are interested in evaluating (4) on the energy eigenfunctions and require it to vanish when taking $x_0 \to 0$ as this fixes any remaining free parameters of a general solution. For $E < 0$ there are N exponentially decaying solutions at infinity. A general energy eigenfunction is a sum of these and thus the boundary form (4) evaluated at infinity is zero. For $\hat{H}_N$ to be self-adjoint it is necessary to impose the same boundary conditions on the wave functions and their adjoints while ensuring that (6) vanishes.

By examining (2), it can be seen that for $\lambda_N > \lambda_{N,c} \equiv (2N-1)!!^2/2^{2N}$ there is a pair of complex roots whose real part is fixed to be $N - 1/2$, i.e.

$$\Delta_N = \Delta_{N+1}^* = (N - 1/2) - i\nu_N(\lambda_N), \quad (8)$$

$$\nu_N(\lambda_N) = \sqrt{\lambda_N - \lambda_{N,c}}(\alpha_N^{-1} + \mathcal{O}(\lambda_N - \lambda_{N,c})), \quad (9)$$

where α_N is a constant given explicitly in the Supplemental material [57]. At sufficiently positive λ_N, $\Delta_1, \ldots, \Delta_{N-1}$ are

TABLE I. The regimes of self-adjoint extension parameter with $N = 1, 2, 3$ for some values of λ_N. The bounds for $N = 1, 2$ are exact while those for $N = 3$ are approximate and determined by numerically solving the indicial Eq. (2). A table showing λ_N, for $N = 1, 2, 3$, to larger negative values can be found in the Supplemental material [57].

N	1		2		3	
λ	$-\frac{3}{4} < \lambda_1$	$\lambda_1 < -\frac{3}{4}$	$\frac{105}{16} < \lambda_2$	$-45 < \lambda_2 < \frac{105}{16}$	$693 \lesssim \lambda_3$	$-162 \lesssim \lambda_3 \lesssim 693$
Extension	$U(1)$	Self-adjoint	$U(1)$	$U(2)$	$U(1)$	$U(3)$

not normalizable and the pair (8) are the leading normalizable roots. This is illustrated in Fig. 1 for $N = 2$. Removing the $N - 1$ non-normalizable roots yields a single decaying wave function with arbitrary energy. As such, (3) becomes

$$\Psi(x) = \phi_N(\epsilon x)^{N-1/2-i\nu_N} + O_1(\epsilon x)^{N-1/2+i\nu_N} + \sum_{j\geq 2} O_j(\epsilon x)^{\Delta_{j+N}} + \ldots, \tag{10}$$

where the N dimensionless and energy-independent scales, O_j/ϕ_N, are now fixed. Substituting (10) for two energies E and $\tilde{E}$ into (6) yields a term $\propto (|E/\tilde{E}|^{2i\nu_N/N} - |O_1/\phi_N|^2)$ as $x_0 \to 0$. Thus, the self-adjoint boundary condition is equivalently an energy quantization condition relating an arbitrary reference energy $E_0 > 0$ to a geometric tower of energies:

$$E_n = -E_0 e^{-\frac{N\pi n}{\nu_N}}, \qquad n \in Z. \tag{11}$$

The reference energy E_0 is a free parameter and can be chosen arbitrarily.

IV. CUTOFF REGULARIZATION

We shall now consider $x_0 > 0$ and choose boundary conditions to give a lower bound to the energy spectrum while preserving approximate DSI near zero energy. We will impose the most general boundary condition on the cutoff point consistent with unitary time evolution [60]. As the $M = N$ decaying solutions are finite at all points $x_0 > 0$, independent of λ_N, this general boundary condition corresponds to an $U(N)$ self-adjoint extension.

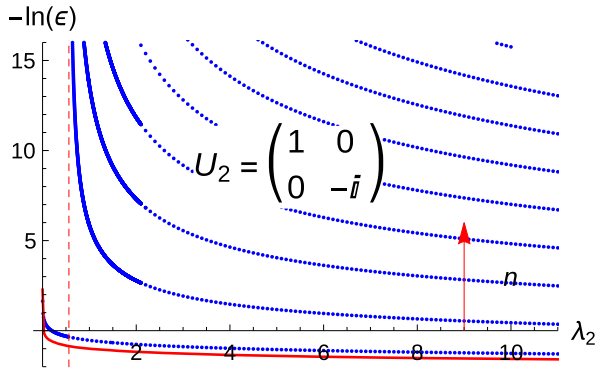

FIG. 2. A plot of the logarithm of ϵ against λ_2 for a cutoff position $x_0 = e^{-1}$ and boundary condition displayed. For $\lambda_2 < \lambda_{2,c} = 9/16$ there are no bound states satisfying $\epsilon x_0 \ll 1$ (although there is an isolated bound state outside this energy bound). The solid red line indicates the lower bound on the negative energies as discussed in the Supplemental material [57]. The dotted red line at $\lambda_{2,c}$ indicates where the first pair of complex roots appears, above which we can see the geometric tower abruptly appearing from $\epsilon = 0$.

To obtain the boundary condition, we diagonalize (6) by defining $\Psi_k^{\pm}(x_0)$,

$$x_0^{k-1} d_x^{k-1} \Psi(x_0) = \Psi_k^{+}(x_0) + \Psi_k^{-}(x_0), \tag{12}$$

$$x_0^{2N-k} d_x^{2N-k} \Psi(x_0) = e^{i\pi(k-\frac{1}{2})}[\Psi_k^{+}(x_0) - \Psi_k^{-}(x_0)] \tag{13}$$

for $1 \leq k \leq N$. After this redefinition, (6) evaluated at $x = x_0$ becomes proportional to

$$\mathbf{\Phi}^{+}(x_0)^{\dagger} \cdot \mathbf{\Psi}^{+}(x_0) - \mathbf{\Phi}^{-}(x_0)^{\dagger} \cdot \mathbf{\Psi}^{-}(x_0). \tag{14}$$

The vanishing of (14) can be achieved by setting

$$\mathbf{\Psi}^{+}(x_0) = U_N \mathbf{\Psi}^{-}(x_0), \tag{15}$$

for some arbitrary unitary matrix: U_N [53,61]. This additionally ensures that elements of the space of wave functions and its adjoint have the same boundary conditions, making $\hat{H}_N$ self-adjoint on said space. The matrix U_N can only be specified by supplying additional physical information beyond the form of the Hamiltonian.

As an illustration of the appearance of the geometric tower at $N > 1$, consider Figs. 2 and 3. The former plots ϵ for $N = 2$ against λ_2. It is plain that as soon as $\lambda_2 > 9/16$ (the dotted red line) there is a sudden transition from no bound states satisfying $\epsilon \ll x_0^{-1}$ (and one isolated bound state), to a tower of states. Similarly, Fig. 3 plots the logarithm of E_n/E_{n+1} for $N = 3$ as a function of λ_3 at low ϵx_0. The result, shown by the blue points in Fig. 3, is a good match with π/ν_3 with ν_3 defined by (8).

For general N, $\lambda_N > \lambda_{N,c}$ and small enough energies, we shall now argue that one always finds DSI with the scaling defined in (11) using a small ϵ expansion. Determining the

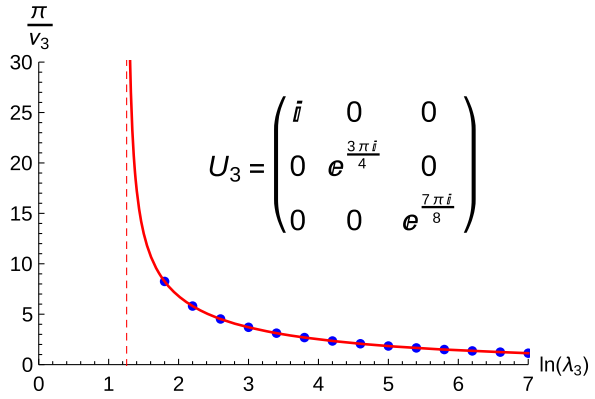

FIG. 3. A plot of π/ν_3 against $\ln \lambda_3$ for a cutoff position $x_0 = e^{-1}$ and boundary condition displayed. The solid red line indicates the numerical result from solving (2) for the roots defined in (8). The blue dots are calculated by numerically determining the gradient of $\ln E_n/E_{n+1}$ against n for several n corresponding to $\epsilon x_0 \ll 1$. The red dotted line indicates the critical λ_3.

energy eigenstates analytically for arbitrary boundary conditions is made difficult for $N > 1$ due to the presence of multiple distinct complex roots in the small energy expansion. However, we shall show that one pair makes a contribution that decays more slowly as $\epsilon \to 0$ than any other and derive an approximation in this limit.

Consider (3) evaluated at $x \sim x_0$ which is a good approximation to the wave function when $\epsilon x_0 \ll 1$. Imposing decay fixes N of the $2N$ free parameters. Without loss of generality we can take them to be O_i so that $O_i = G_i{}^j \phi_j$ for some complex $(N \times N)$-matrix G. The N remaining free parameters ϕ_i will be fixed by wave function normalization and boundary conditions at the cutoff point (15). The generic dependence of ϕ_i on ϵ, x_0 for $\epsilon x_0 \ll 1$ is extractable. Applying the redefinition $\tilde{\phi}_i \equiv \phi_i (\epsilon x_0)^{\Delta_i}$ implies

$$O_i (\epsilon x_0)^{\Delta_{i+N}} \to G_i{}^j (\epsilon x_0)^{\Delta_{i+N} - \Delta_j} \tilde{\phi}_j. \tag{16}$$

Given our canonical ordering of the roots and that $\lambda > \lambda_c$ we have $\mathrm{Re}(\Delta_{i+N} - \Delta_j) \geq 0$ with equality only when $i = 1$ and $j = N$. For $\epsilon x_0 \ll 1$ the leading contributions to the wave function (3) have the form

$$\Psi(x) = \sum_{i=1}^{N} \tilde{\phi}_i \left(\frac{x}{x_0}\right)^{\Delta_i} + G_1{}^N \tilde{\phi}_N (\epsilon x_0)^{2i\nu_N} \left(\frac{x}{x_0}\right)^{\Delta_{N+1}}$$

where ϵx_0 only enters the leading term through a phase and all other contributions to O_i from the $\tilde{\phi}_i$ drop out as they come with ϵx_0 to a real positive power. The displayed terms above are the relevant ones at low energies for solving (15). Moreover these leading terms are invariant under the discrete scaling transformation and thus we have DSI. As a result, applying (15) will necessarily give the energy spectrum (11) for $\epsilon x_0 \ll 1$ with E_0 a number depending on $U(N)$ and the cutoff x_0.

We can use our expression (9) for ν_N in terms of λ_N to find:

$$\frac{E_n}{E_0} = -\exp\left(-\frac{N\pi n \alpha_N}{\sqrt{\lambda_N - \lambda_{N,c}}(1 + \mathcal{O}(\lambda_N - \lambda_{N,c}))}\right), \tag{17}$$

characteristic of the BKT scaling for $\lambda_N \to \lambda_{N,c}$.

With the above considerations we can say that a CSI to DSI transition, at $\epsilon x_0 \ll 1$, is a generic feature of our models is for the consequences of DSI to be relevantindependent of the completion of the potential near the origin. This is in complete analogy with the $N = 1$ case. Thus, the Hamiltonian (1) need only be effective for the consequences of DSI to be relevant.

ACKNOWLEDGMENTS

The work of D. K. B. was supported in part by the Israel Science Foundation under Grant No. 504/13 and is currently supported by a key grant from the National Science Foundation of China with Grant No. 11235010. This work was also supported by the Israel Science Foundation Grant No. 924/09. D. K. B. would like to thank the Technion and University of Haifa at Oranim for their support. D. K. B. would also like to thank Matteo Baggioli and Yicen Mou for reading early drafts.

[1] S. L. Adler, Phys. Rev. **177**, 2426 (1969).
[2] J. S. Bell and R. Jackiw, Nuovo Cimento A **60**, 47 (1969).
[3] J. G. Esteve, Phys. Rev. D **34**, 674 (1986).
[4] B. R. Holstein, Am. J. Phys. **61**, 142 (1993).
[5] K. M. Case, Phys. Rev. **80**, 797 (1950).
[6] V. de Alfaro, S. Fubini, and G. Furlan, Nuovo Cimento Soc. Ital. Fis. **34**, 569 (1976).
[7] L. D. Landau, *Quantum Mechanics: Non-relativistic Theory* (Butterworth-Heinemann, Oxford, 1991).
[8] H. E. Camblong, L. N. Epele, H. Fanchiotti, and C. A. G. Canal, Phys. Rev. Lett. **85**, 1590 (2000).
[9] G. N. J. Añaños, H. E. Camblong, and C. R. Ordóñez, Phys. Rev. D **68**, 025006 (2003).
[10] H. W. Hammer and B. G. Swingle, Ann. Phys. (N.Y.) **321**, 306 (2006).
[11] E. Braaten and D. Phillips, Phys. Rev. A **70**, 052111 (2004).
[12] D. B. Kaplan, J.-W. Lee, D. T. Son, and M. A. Stephanov, Phys. Rev. D **80**, 125005 (2009).
[13] V. Efimov, Phys. Lett. B **33**, 563 (1970).
[14] V. Efimov, Sov. J. Nucl. Phys. **12**, 589 (1971).
[15] E. Braaten and H.-W. Hammer, Phys. Rep. **428**, 259 (2006).
[16] J.-M. Lévy-Leblond, Phys. Rev. **153**, 1 (1967).
[17] E. B. Kolomeisky and J. P. Straley, Phys. Rev. B **46**, 12664 (1992).
[18] K. S. Gupta and S. G. Rajeev, Phys. Rev. D **48**, 5940 (1993).
[19] H. E. Camblong, L. N. Epele, H. Fanchiotti, and C. A. G. Canal, Phys. Rev. Lett. **87**, 220402 (2001).
[20] C. Nisoli and A. R. Bishop, Phys. Rev. Lett. **112**, 070401 (2014).
[21] T. R. Govindarajan, V. Suneeta, and S. Vaidya, Nucl. Phys. **B583**, 291 (2000).
[22] H. E. Camblong and C. R. Ordonez, Phys. Rev. D **68**, 125013 (2003).
[23] S. Bellucci, A. Galajinsky, E. Ivanov, and S. Krivonos, Phys. Lett. B **555**, 99 (2003).
[24] R. W. Jackiw, *Diverse Topics in Theoretical and Mathematical Physics* (World Scientific, Singapore, 1995).

[25] Thus, for $d = 2$, an attractive potential is always overcritical.
[26] K. Jensen, A. Karch, D. T. Son, and E. G. Thompson, Phys. Rev. Lett. **105**, 041601 (2010).
[27] K. Jensen, Phys. Rev. D **82**, 046005 (2010).
[28] K. Jensen, Phys. Rev. Lett. **107**, 231601 (2011).
[29] B. Derrida and M. Retaux, J. Stat. Phys. **156**, 268 (2014).
[30] H. Gies and G. Torgrimsson, Phys. Rev. Lett. **116**, 090406 (2016).
[31] O. Ovdat, J. Mao, Y. Jiang, E. Y. Andrei, and E. Akkermans, Nat. Commun. **8**, 507 (2017).
[32] J. Alexandre, Int. J. Mod. Phys. A **26**, 4523 (2011).
[33] R. M. Hornreich, M. Luban, and S. Shtrikman, Phys. Rev. Lett. **35**, 1678 (1975).
[34] G. Grinstein, Phys. Rev. B **23**, 4615 (1981).
[35] E. Fradkin, D. A. Huse, R. Moessner, V. Oganesyan, and S. L. Sondhi, Phys. Rev. B **69**, 224415 (2004).
[36] A. Vishwanath, L. Balents, and T. Senthil, Phys. Rev. B **69**, 224416 (2004).
[37] E. Ardonne, P. Fendley, and E. Fradkin, Ann. Phys. (Amsterdam) **310**, 493 (2004).
[38] S. Mukohyama, Classical Quantum Gravity **27**, 223101 (2010).
[39] M. Reuter, Phys. Rev. D **57**, 971 (1998).
[40] S. Kachru, X. Liu, and M. Mulligan, Phys. Rev. D **78**, 106005 (2008).
[41] P. Horava, Phys. Rev. Lett. **102**, 161301 (2009).
[42] P. Horava, Phys. Rev. D **79**, 084008 (2009).
[43] H. Gies, B. Knorr, S. Lippoldt, and F. Saueressig, Phys. Rev. Lett. **116**, 211302 (2016).
[44] T. Brauner, Symmetry **2**, 609 (2010).
[45] P. Horava, Phys. Lett. B **694**, 172 (2010).
[46] S. R. Das and G. Murthy, Phys. Rev. Lett. **104**, 181601 (2010).
[47] C. F. Farias, M. Gomes, J. R. Nascimento, A. Yu. Petrov, and A. J. da Silva, Phys. Rev. D **85**, 127701 (2012).
[48] S. Pal and B. Grinstein, J. High Energy Phys. 12 (2016) 012.
[49] Additional boundary terms will be required to make the variation of the action vanish on boundary conditions that make the corresponding Hamiltonian operator self-adjoint [50].
[50] M. Asorey, D. Garcia-Alvarez, and J. M. Munoz-Castaneda, in Proceedings of 7th Workshop on Quantum Field Theory Under the Influence of External Conditions (QFEXT 05) Barcelona, Catalonia, Spain, *J. Phys. A* 39, 6127 (2006).
[51] G. Bonneau, J. Faraut, and G. Valent, Am. J. Phys. **69**, 322 (2001).
[52] A. Ibort, F. Lledó, and J. M. Pérez-Pardo, Ann. Inst. Henri Poincaré **16**, 2367 (2015).
[53] D. M. Gitman, I. V. Tyutin, and B. L. Voronov, arXiv: 0903.5277.
[54] K. Meetz, Nuovo Cimento **34**, 690 (1964).
[55] D. M. Gitman, I. Tyutin, and B. L. Voronov, *Self-adjoint Extensions in Quantum Mechanics: General Theory and Applications to Schrödinger and Dirac Equations with Singular Potentials*, Vol. 62 (Springer, New York, 2012).
[56] Y. Luke, *The Special Functions and Their Approximations, Mathematics in Science and Engineering* (Elsevier Science, New York, 1969).
[57] See Supplemental Material at http://link.aps.org/supplemental/10.1103/PhysRevD.97.061701 for details relative to the eigenvalue spectrum of the Hamiltonian $\hat{H}_N$ in Eq. (1), the cutoff regularisation procedure and an explicit expression of the constant α_N in Eq. (9).
[58] We have also assumed that the Δ_i do not differ by integer powers to avoid the complication of logarithmic terms in the Frobenius series represented by (3).
[59] In fact, for λ_N small enough the Δ_i are real and one can find isolated bound states for some choices of the parameter $U(N)$.
[60] The Hamiltonian is to be made self-adjoint in the portion of the half-line considered.
[61] D. Gitman, I. Tyutin, and B. Voronov, *Self-adjoint Extensions in Quantum Mechanics: General Theory and Applications to Schrödinger and Dirac Equations with Singular Potentials: 62 (Progress in Mathematical Physics)* (Birkhauser, 2012).

Scale anomaly of a Lifshitz scalar: a universal quantum phase transition to discrete scale invariance
Supplementary materials

Daniel K. Brattan*
Interdisciplinary Center for Theoretical Study, University of Science and Technology of China, 96 Jinzhai Road, Hefei, Anhui, 230026 PRC.

Omrie Ovdat† and Eric Akkermans‡
Department of Physics, Technion Israel Institute of Technology, Haifa 3200003, Israel.
(Dated: June 11, 2017)

SELF-ADJOINT EXTENSION

The eigenfunctions

The energy eigenvalue equation with Hamiltonian

$$\hat{H}_N = (-1)^N \frac{d^{2N}}{dx^{2N}} - \frac{\lambda_N}{x^{2N}} \, . \tag{S1}$$

has an analytic solution in terms of generalised hypergeometric functions [S1] for arbitrary energy and λ_N. These analytic solutions are specified by the roots of the indicial equation,

$$\lambda_N = (-1)^N \prod_{k=0}^{2N-1} (\Delta - k) \, , \tag{S2}$$

which can be obtained by inserting $\Psi(x) = x^{\Delta}(1 + \mathcal{O}(x^{2N}))$ into the eigenvalue equation and solving for Δ. We label the $2N$ solutions of (S2) as $\Delta_i, i = 1, \ldots, 2N$ and order by ascending real part followed by ascending imaginary part. These roots can be collected into pairs which sum to $2N - 1$. The Δ_i also allow us to rewrite the differential operator as

$$x^{2N}\hat{H}_N = (-1)^N \prod_{j=1}^{2N} \left(x\frac{d}{dx} - \Delta_{\sigma(j)} \right) \, , \tag{S3}$$

where σ is an arbitrary permutation of the integers $1, \ldots, 2N$.

Let $\mathbf{\Delta}_i$ be the vector of solutions to (S2) with Δ_i omitted, then generic solutions of the differential equation associated with $\hat{H}_N$ and energy eigenvalue E are given by the sum:

$$\Psi(x;\phi_j) = \sum_{i=1}^{2N} e^{i\Delta_i\phi_j} \left(\frac{\epsilon x}{2N}\right)^{\Delta_i} \Gamma\left(\frac{\mathbf{\Delta}_i - \Delta_i}{2N}\right) {}_0F_{2N-1}\left[\begin{matrix} - \\ 1 - \frac{\Delta_i - \mathbf{\Delta}_i}{2N} \end{matrix} ; E\left(\frac{x}{2N}\right)^{2N} \right] \, , \tag{S4}$$

$$\phi_j = \frac{1}{2N}\left(\theta - 2\pi(N + (w + j))\right) \, , \quad j = 1, 2, \ldots, 2N \, , \tag{S5}$$

where w is an integer chosen such that $|\phi_j| < \pi(1 + \frac{1}{2N})$, $E = |E|e^{i\theta}$ and $\epsilon = |E|^{\frac{1}{2N}}$. For negative energies the choices of ϕ_j are symmetric about zero, which may or may not be included in the set. The functions ${}_0F_{2N-1}$ are generalised hypergeometric functions [S1].

We now wish to determine the wavefunction corresponding to a $U(1)$ self-adjoint extension at sufficiently positive λ_N, i.e. where there are only $N+1$ normalisable roots. To do this, consider a general decaying wavefunction which is given by a sum over the N exponentially decaying basis wavefunctions defined in (S4):

$$\Psi(x) = \sum_{j=1}^{N} A_j \Psi(x;\phi_j) \, , \tag{S6}$$

where A_j are some arbitrary complex constants defining the wavefunction. Without loss of generality let Δ_1 have a real part less than $-1/2$. To remove this root from our general expression we require that

$$\sum_{j=1}^{N} A_j e^{i\Delta_1\phi_j} \left(\frac{\epsilon x}{2N}\right)^{\Delta_1} \Gamma\left(\frac{\mathbf{\Delta}_1 - \Delta_1}{2N}\right) {}_0F_{2N-1}\left[\begin{matrix} - \\ 1 - \frac{\Delta_1 - \mathbf{\Delta}_1}{2N} \end{matrix} ; E\left(\frac{x}{2N}\right)^{2N} \right] \equiv 0 \, , \tag{S7}$$

near $x = 0$. We can drop all the j independent terms leaving

$$\sum_{j=1}^{N} A_j e^{i\Delta_1\phi_j} = 0 \, . \tag{S8}$$

The A_j are constrained. Similarly, for the other $N - 2$ non-normalisable roots in the $U(1)$ regime which we can summarise by the matrix equation:

$$\left(e^{i\Delta_i\phi_j}\right) A_j = 0 \, . \tag{S9}$$

We note that the matrix is of dimension $(N - 1) \times N$ and, as the rows are generically linearly independent, the vector A_j parameterizes the one-dimensional null space.

Let a_j denote the components of this unit normalised vector that solves (S9). The desired $U(1)$ wavefunction

is then given by

$$\Psi(x) = A\sum_{i=1}^{N}\left(\frac{\epsilon x}{2N}\right)^{\Delta_i}\left(\sum_{j=1}^{N} a_j e^{i\Delta_i\phi_j}\right)\Gamma\left(\frac{\boldsymbol{\Delta}_i-\Delta_i}{2N}\right) {}_0F_{2N-1}\left[\begin{matrix} - \\ 1-\frac{\Delta_i-\boldsymbol{\Delta}_i}{N}\end{matrix}; E\left(\frac{x}{2N}\right)^{2N}\right] \tag{S10}$$

where A is an overall normalisation constant and the energy is completely arbitrary. To fix the energy we require a boundary condition from $x = 0$ as discussed in the main text. The details follow as discussed there.

CUT-OFF REGULARISATION

Constraints on the cut-off boundary conditions

We can diagonalize the boundary form on the cut-off by defining $\Psi_k^{\pm}(x_0)$,

$$x_0^{k-1}d_x^{k-1}\Psi(x_0) = \Psi_k^{+}(x_0) + \Psi_k^{-}(x_0)\,, \tag{S11}$$

$$x_0^{2N-k}d_x^{2N-k}\Psi(x_0) = e^{i\pi(k-\frac{1}{2})}\left[\Psi_k^{+}(x_0) - \Psi_k^{-}(x_0)\right] \tag{S12}$$

for $1 \leq k \leq N$. After this redefinition we find the boundary form is given by:

$$\begin{aligned}&\frac{1}{2}(ix_0)^{2N-1}\left[\Phi,\Psi\right](x_0)\\ &= \boldsymbol{\Phi}^{+}(x_0)^{\dagger}\cdot\boldsymbol{\Psi}^{+}(x_0) - \boldsymbol{\Phi}^{-}(x_0)^{\dagger}\cdot\boldsymbol{\Psi}^{-}(x_0)\,.\end{aligned} \tag{S13}$$

The vanishing of the boundary form [S2, S3] can be achieved by setting

$$\boldsymbol{\Psi}^{+}(x_0) = U_N\boldsymbol{\Psi}^{-}(x_0)\,,\quad \boldsymbol{\Phi}^{+}(x_0) = U_N\boldsymbol{\Phi}^{-}(x_0)\,. \tag{S14}$$

It is well-known that a generic self-adjoint extension does not preserve time-reversal invariance [S4], nor does it guarantee that the spectrum is bounded from below. The former property is equivalent to having real-valued ground state wavefunctions [S4] and can be imposed on the system by limiting the self-adjoint extensions to those which satisfy

$$\det\left(\mathbb{1}_N - U_N^{*}U_N\right) = 0\,. \tag{S15}$$

To bound the spectrum from below consider the expectation value of the energy on some unit normalised state $|\Psi\rangle$:

$$\begin{aligned}\langle\Psi|\hat{H}_N|\Psi\rangle = &\sum_{j=1}^{N}(-1)^{N+j-1}d_{x_0}^{j-1}\Psi^{*}(x_0)d_{x_0}^{2N-j}\Psi(x_0)\\ &+\int_{x_0}^{\infty}dx\,\left[|\partial_x^N\Psi|^2 - \frac{\lambda_N}{x^{2N}}|\Psi|^2\right]\,.\end{aligned}$$

Using the redefinitions of (S11) one can show that $\langle\Psi|\hat{H}_N|\Psi\rangle$ is greater than or equal to

$$\begin{aligned}&\frac{1}{x_0^{2N}}\left[(-1)^N x_0\left(\boldsymbol{\Psi}^{-}(x_0)\right)^{\dagger}\left[i\left(U_N - U_N^{\dagger}\right)\right]\boldsymbol{\Psi}^{-}(x_0)\right.\\ &\left.\qquad - \lambda_N\right]\,.\end{aligned} \tag{S16}$$

Thus, if the Hermitian part of the unitary matrix has eigenvalues of the correct sign we can ensure that the spectrum is bounded from below by the minimum of the potential [S5].

Example: cut-off regularisation energies for $N = 1$

In the case of $N = 1$ it is known that for $\lambda_1 > \frac{1}{4}$, if the logarithmic derivative of the wavefunction is chosen to be any real number one finds at low energies discrete scale invariance [S6]. This classic result follows by noting that (S13) implies

$$\frac{x_0\Psi'(x_0)}{\Psi(x_0)} = \tan\left(\frac{\theta}{2}\right) \qquad \theta \neq \pm\pi\,, \tag{S17}$$

as a rewriting of the boundary condition. The cases of $\pm\pi$ correspond to Dirichlet and Neumann conditions for the wavefunction at the cut-off and can be thought of as limits. Taking small energies is equivalent to taking the cut-off to zero where for $N = 1$ the wavefunction has the form:

$$\begin{aligned}\Psi(x_0) = &\tilde{A}\left(\frac{\epsilon x_0}{2}\right)^{\frac{1}{2}}\left|\Gamma\left(-i\nu_1\right)\right|^{\frac{1}{2}}\\ &\cos\left(\nu_1\ln\left(\frac{\epsilon x_0}{2}\right) + \frac{\phi_1}{2}\right) + \mathcal{O}^{\frac{3}{2}}(x_0)\,,\end{aligned} \tag{S18}$$

$$e^{i\phi_1} = \frac{\Gamma\left(-i\nu_1\right)}{\Gamma\left(i\nu_1\right)}\,,\qquad \nu_1 = \sqrt{\lambda_1 - \frac{1}{4}}\,, \tag{S19}$$

with $\tilde{A}$ some normalisation constant. Substituting (S18) into (S17) we find

$$\tan\left(\frac{\theta}{2}\right) = \sqrt{\lambda_1 - \frac{1}{2}}\frac{\cos\left(\nu_1\ln\left(\frac{\epsilon x_0}{2}\right) + \frac{\phi_1+\alpha}{2}\right)}{\cos\left(\nu_1\ln\left(\frac{\epsilon x_0}{2}\right) + \frac{\phi_1}{2}\right)}\,, \tag{S20}$$

$$e^{i\alpha} = \frac{\frac{1}{2}+i\nu_1}{\frac{1}{2}-i\nu_1}\,. \tag{S21}$$

Fixing θ we can numerically solve this equation for an ϵ. Taking this as a reference energy, the symmetry of the right hand side ensures that $\epsilon\exp\left(-\pi n/\nu_1\right)$ is also a solution where $n \in \mathbb{N}$ is required for the approximation (S18) to apply. Hence, for $N = 1$ the cut-off regularisation gives approximate discrete scale invariance at low energies.

$N=1$	$3/4<\lambda_1$	$\lambda_1<3/4$		
extension parameter	$U(1)$	essentially self-adjoint		
$N=2$	$105/16<\lambda_2$	$-1<\lambda_2<105/16$	$\lambda_2<-1$	
extension parameter	$U(1)$	$U(2)$	essentially self-adjoint	
$N=3$	$693\lesssim\lambda_3$	$-162\lesssim\lambda_3\lesssim 693$	$-36201\lesssim\lambda_3\lesssim -162$	$\lambda_3\lesssim -36201$
extension parameter	$U(1)$	$U(3)$	$U(2)$	essentially self-adjoint

TABLE I. A table showing the distinct regimes of self-adjoint extension parameter for $N=1,2,3$. The bounds for $N=1,2$ are exact while those for $N=3$ are approximate and determined by numerically solving the indicial equation (S2).

Relating the energies to the critical coupling

By examining (S2) it can be seen that for $\lambda_N > \lambda_{N,c} \equiv (2N-1)!!^2/2^{2N}$ there is a pair of complex roots whose real part is fixed to be $N-1/2$ i.e.

$$\Delta_N = \Delta^*_{N+1} = (N-1/2) - i\nu_N(\lambda_N)\ , \tag{S22}$$

$$\nu_N(\lambda_N) = \sqrt{\lambda_N - \lambda_{N,c}}\left(\alpha_N^{-1} + \mathcal{O}(\lambda_N - \lambda_{N,c})\right)\ , \tag{S23}$$

where α_N is related to the value of the second derivative of the indicial equation (S2) with respect to Δ at $\Delta = N-1/2$. The precise form of $\alpha(N)$ is given by:

$$\alpha_N^2 = \frac{\lambda_{N,c}}{2}\left(\gamma_1\left(N+\frac{1}{2}\right) - \gamma_1\left(\frac{1}{2}-N\right)\right)\ . \tag{S24}$$

* danny.brattan@gmail.com
† somrie@campus.technion.ac.il
‡ eric@physics.technion.ac.il

[S1] Y. Luke, *The Special Functions and Their Approximations*, Mathematics in Science and Engineering (Elsevier Science, 1969).

[S2] D. M. Gitman, I. V. Tyutin, and B. L. Voronov, (2009), 10.1088/1751-8113/43/14/145205, arXiv:0903.5277 [quant-ph].

[S3] D. Gitman, I. Tyutin, and B. Voronov, *Self-adjoint Extensions in Quantum Mechanics: General Theory and Applications to Schrödinger and Dirac Equations with Singular Potentials: 62 (Progress in Mathematical Physics)* (Birkhuser, 2012).

[S4] G. Bonneau, J. Faraut, and G. Valent, Am. J. Phys. **69**, 322 (2001), arXiv:quant-ph/0103153 [quant-ph].

[S5] We should emphasise that the implication is one-way i.e. the energies can still be bounded below if the Hermitian part of the unitary matrix does not eigenvalues of the correct sign but this must be determined by examining the energy spectrum.

[S6] A. M. Essin and D. J. Griffiths, American Journal of Physics **74**, 109 (2006).

IOP Publishing Journal of Physics A: Mathematical and Theoretical

J. Phys. A: Math. Theor. **51** (2018) 435401 (15pp) https://doi.org/10.1088/1751-8121/aadfae

On the landscape of scale invariance in quantum mechanics

Daniel K Brattan[1], Omrie Ovdat[2] and Eric Akkermans[2]

[1] Interdisciplinary Center for Theoretical Study, University of Science and Technology of China, 96 Jinzhai Road, Hefei, Anhui, 230026, People's Republic of China
[2] Department of Physics, Technion Israel Institute of Technology, Haifa 3200003, Israel

E-mail: danny.brattan@gmail.com, somrie@campus.technion.ac.il and eric@physics.technion.ac.il

Received 5 July 2018, revised 4 September 2018
Accepted for publication 7 September 2018
Published 26 September 2018

Abstract

We consider the most general scale invariant radial Hamiltonian allowing for anisotropic scaling between space and time. We formulate a renormalisation group analysis of this system and demonstrate numerically the existence of a universal quantum phase transition from a continuous scale invariant phase to a discrete scale invariant phase. Close to the critical point, the discrete scale invariant phase is characterised by an isolated, closed, attracting trajectory in renomalisation group space (a limit cycle). Moving in appropriate directions in the parameter space of couplings this picture is altered to one controlled by a quasi periodic attracting trajectory (a limit torus) or fixed points. We identify a direct relation between the critical point, the renormalisation group picture and the power laws characterising the zero energy wave functions.

Keywords: quantum, phase, transition, discrete, scale, invariance, limit cycle

(Some figures may appear in colour only in the online journal)

1. Introduction

Classical symmetries broken at the quantum level are termed anomalous. Since their discovery [1–4], anomalies have become a very active field of research in physics. One class of anomalies describes the breaking of continuous scale invariance (CSI). In the generic case, quantisation of a classically scale invariant Hamiltonian is ill-defined and necessitates the introduction of a regularisation scale [5] which breaks CSI altogether. Recently, a sub-class of scale anomalies has been discovered in which a residual discrete scale invariance (DSI) remains after regularisation. Models exhibiting this phenomenon include a non-relativistic particle in the presence

of an attractive, inverse square radial potential $\hat{H}_S = p^2 - \lambda/r^2$ [6–13] ($M = 1/2$), the charged and massless Dirac fermion in an attractive Coulomb potential $\hat{H}_D = \gamma^0\gamma^j p_j - \lambda/r$ [14] and a class of one dimensional Lifshitz scalars [15] with $\hat{H}_L = \left(p^2\right)^N - \lambda/x^{2N}$ [16]. Any system described by these classically scale invariant Hamiltonians exhibits an abrupt transition in the spectrum at some $\lambda = \lambda_c$. For $\lambda < \lambda_c$, the spectrum contains no bound states close to $E = 0$, however, as λ goes above λ_c, an infinite sequence of bound (quasi-bound for $\hat{H}_D$) states appears. In addition, in this 'over-critical' regime, the states surprisingly form a geometric sequence

$$E_n = E_0 \exp\left(-n\alpha/\sqrt{\lambda - \lambda_c}\right), \tag{1}$$

accumulating at $E = 0$ where $n \in \mathbb{Z}$, $\alpha > 0$ and E_0 is a number that depends on the regularisation. The existence and structure of the levels is 'universal', that is, it does not rely on the details of the potential close to its source. This feature is a signature of residual DSI since $\{E_n\} \to \{\exp\left(-2\pi/\sqrt{\lambda - \lambda_c}\right))E_n\} = \{E_n\}$. Thus, a quantum phase transition occurs at λ_c between a CSI phase and a DSI phase. This transition has been associated with Berezinskii–Kosterlitz–Thouless (BKT) transitions [13, 17–22] and has found applications in the Efimov effect [23–25], graphene [14], QED3 [26] and other phenomena [17, 27–34].

A useful tool in the characterisation of this phenomenon is the renormalisation group (RG) [35]. For the case of $\hat{H}_{S,D,L}$, it consists of introducing an initial short distance scale L and defining model dependent parameters such as λ, and the boundary conditions, according to physical information. At low energies with respect to the cut-off L, a RG formalism allows one to determine the dependence of these parameters on L and thus how physical, regularisation independent, information can be extracted from a scheme dependent result. For example, an attractive fixed point represents a class of parameters describing the same low energy predictions, characterised by the effective Hamiltonian corresponding to the fixed point. In that sense, the fixed point Hamiltonian describes universal physics. However, termination at a fixed point is not the only possible outcome of a RG flow. In principle, there are three other distinct behaviours that one can find: limit cycles, limit tori and strange attractors [36]; all of which are rare in applications of RG.

The study of $\hat{H}_S$ and $\hat{H}_D$ using RG [12, 13, 17, 37–39] shows that the quantum critical phase transition is characterised by two fixed points (UV and IR) for $\lambda < \lambda_c$ which combine and annihilate at $\lambda = \lambda_c$. For $\lambda > \lambda_c$ all the flows are log-periodic in the cut-off and therefore exhibit DSI, independent of the choice of initial boundary condition and scale. The meaning is that for every choice of initial L and boundary condition, there is an infinite equivalent set of scales described by a geometric ladder. This is manifested in (1) as it implies $E_{n+k+1}/E_{n+k} = E_{n+1}/E_n$ for all $n, k \in \mathbb{Z}$. Remarkably, even in the absence of fixed points, there is universal information in this regime represented by the geometric series factor E_{n+1}/E_n.

Hamiltonians $\hat{H}_{S,D,L}$ share the property of scaling uniformly under $r \mapsto \Lambda r$. This suggests widening our perspective to consider all possible radial Hamiltonians with CSI and spherical symmetry. Such Hamiltonians are given by[3]

$$\hat{H}_N = \hat{p}^{2N} + \sum_{i=1}^{2N} \frac{\lambda_i}{r^i} d_r^{2N-i}, \qquad \hat{p}^2 = -d_r^2 - \frac{d-1}{r} d_r + \frac{\ell(\ell + d - 2)}{r^2}, \tag{2}$$

[3] In writing (2) we have ignored the possibility of δ-function interactions which scale correctly only in certain dimensions. When such terms can be included in (2) they can generally be represented as a choice of boundary conditions [40] rather than being introduced explicitly.

where $N > 0$ is an integer, $\lambda_i \in \mathbb{R}$, $d_r \equiv \frac{\mathrm{d}}{\mathrm{d}r}$, ℓ is the total angular momentum quantum number and d is the number of spatial dimensions.

Under $r \mapsto \Lambda r$ the Hamiltonians (2) scale as $\hat{H}_N \mapsto \Lambda^{-2N}\hat{H}_N$ making the Schrödinger equation scale invariant with $t \mapsto \Lambda^{2N}t$. Anisotropic scaling between space and time is collectively referred to as 'Lifshitz symmetry' [15]. This scaling symmetry can be seen for example at the finite temperature multicritical points of certain materials [41, 42] and in strongly correlated electron systems [43–45]. Quartic dispersion relations ($E \sim \boldsymbol{p}^4$) can also be found in graphene bilayers [46] and heavy fermion metals [47] or bose gases [48–51]. Lifshitz symmetry may also have applications in particle physics [15], cosmology [52] and quantum gravity [53–57]. Moreover, instances of the Hamiltonians in (2) can be recovered from Lifshitz field theories coupled to background gauge fields [15, 58] of the appropriate multipole moment. Coupling the charged particles to a magnetic monopole in two dimensions, or an infinite solenoid in three, is one way to generate the derivative interactions of (2).

In this paper we formulate a RG description for systems described by (2) and study its solutions numerically. We show that departure from scale invariance characterised by fixed point annihilation, and subsequently universal DSI, is a generic feature in the landscape of Hamiltonians (2). Depending on the values of λ_i, we find additional possibilities including: isolated periodic flow (non-linear limit cycle) and quasi-periodic flow (limit tori) as shown by figures 2 and 4 respectively. In addition, we show that these types of RG flows can be simply determined from the characteristic power laws of the $E = 0$ wave function (zero modes).

2. CSI in quantum mechanics

The scaling symmetry of (2) implies that if there is one negative energy bound state then there is an unbounded continuum. Thus, the existence of any bound state necessitates that the Hamiltonian is not self-adjoint [59, 60]. The origin of this phenomenon is the strong singularity of the potential terms at $r = 0$. To render the quantum problem well defined we introduce a cut-off $L > 0$ and choose boundary conditions that make the Hamiltonian self-adjoint. The cut-off explicitly breaks scale invariance and we will track the behaviour of the system for $\epsilon L \ll 1$, with $\epsilon = |E|^{1/(2N)}$ and E the energy, using a RG approach. Observables, such as bound state energies, that respect this limit will be approximately independent of the value of the cut-off L and thus robust.

An analytic general solution of

$$\hat{H}_N\psi(r) = E\psi(r), \qquad r \in [L, \infty), \tag{3}$$

is given in terms of generalized hypergeometric functions [61] (see appendix A). Importantly, there is an equal number of normalisable eigenfunctions with positive and negative imaginary energies (N to be exact, see appendix A). Therefore, according to von Neumann's second theorem [62], there is a $U(N)$ parameter family of self-adjoint boundary conditions at $r = L$ (self-adjoint extensions of $\hat{H}_N$). The complete family of boundary conditions is obtained from an impenetrable wall condition corresponding to the vanishing of the radial component of probability current $J(r)$ at $r = L$. In particular,

$$J(L) \propto \int_{r=L}^{\infty} \mathrm{d}r \, \left[\psi^*(r)\hat{H}_N\psi(r) - \psi(r)\hat{H}_N\psi^*(r)\right], \tag{4}$$

where $\hat{H}_N$ is a differential operator as given by (2) and we absorbed a Jacobian factor into the definition of $\psi(r)$. Using integration by parts on (4) we can reduce this expression to a boundary term. Assuming decay at infinity, this becomes a quadratic form evaluated at $r = L$

in terms of $L^{k-1}d_r^{k-1}\psi(L)$ and their conjugates. By diagonalising the quadratic form $J(L)$, it can be reduced to [62]:

$$J(L) \propto \mathrm{i}\left[|\boldsymbol{\psi}^+(L)|^2 - |\boldsymbol{\psi}^-(L)|^2\right], \tag{5}$$

where $\boldsymbol{\psi}^{\pm}(L)$ are N-vectors whose components are linear combinations of the $L^{k-1}d_r^{k-1}\psi(L)$. The self-adjoint boundary conditions, being those that set (5) to zero, are thus

$$\boldsymbol{\psi}^+(L) = U_N\boldsymbol{\psi}^-(L) \tag{6}$$

where U_N is an arbitrary $(N\times N)$-unitary matrix[4]. The matrix U_N describes implicit model dependent parameters that are specified by additional physical information.

As will be exhibited in more detail later, the characteristic low energy behaviour of system (3) is determined by $2N$ powers Δ_i describing the $E=0$ eigenfunctions of $\hat{H}_N$. These are obtained by inserting $\psi\propto r^{\Delta}$ into $\hat{H}_N\psi=0$ and solving for the roots of the resultant polynomial in Δ. Since $\lambda_i\in\mathbb{R}$ in (2), Δ_i^* belongs to the set of roots whenever Δ_i does. In addition, $\hat{H}_N=\hat{H}_N^\dagger$ implies that $2N-1-\Delta_i$ is also a root (see appendix B). As a result, in the complex z plane, the roots Δ_i are symmetric with respect to the lines $\mathrm{Im}[z]=0$, $\mathrm{Re}[z]=N-1/2$.

It will be useful for deriving a RG equation to rewrite (3) in terms of $\boldsymbol{\psi}^{\pm}(r)$ at $r=L$. This consists of splitting (3) into a set of first order coupled ODEs in $r^{k-1}d_r^{k-1}\psi(r)$, $k=1,\ldots,2N$ and applying the transformation that diagonalised J. The result is an equation of the form

$$rd_r\begin{pmatrix}\boldsymbol{\psi}^+(r)\\ \boldsymbol{\psi}^-(r)\end{pmatrix} = \begin{pmatrix}C_{++} & C_{+-}\\ C_{-+} & C_{--}\end{pmatrix}\begin{pmatrix}\boldsymbol{\psi}^+(r)\\ \boldsymbol{\psi}^-(r)\end{pmatrix}. \tag{8}$$

Scale invariance ensures that the matrix of Cs is dimensionless and therefore depends only on ϵr. The precise form of the Cs will only be necessary when working with a particular Hamiltonian; to determine qualitative features of the RG space we will not require these details.

3. Renormalisation group flow

Consider an eigenfunction of Hamiltonian (2) of energy E and satisfying the boundary condition defined by U_N at $r=L$. Defining $U_N\equiv U_N(L)$ and imposing that (6) holds for the given state after performing an infinitesimal transformation $L\mapsto\Lambda L$ implies that $U_N(L)$ must satisfy the following equation:

$$Ld_L\boldsymbol{\psi}^+(L) = Ld_LU_N(L)\boldsymbol{\psi}^-(L) + U_N(L)Ld_L\boldsymbol{\psi}^-(L). \tag{9}$$

We replace the derivatives of the field using (8), and $\boldsymbol{\psi}^+(L)$ for $\boldsymbol{\psi}^-(L)$ using (6), to find:

$$\left(Ld_LU_N - C_{+-} + U_NC_{--} - C_{++}U_N + U_NC_{-+}U_N\right)\boldsymbol{\psi}^- = 0, \tag{10}$$

[4] It is important to note a global symmetry of the boundary conditions. Namely, given some $U_N(L)$ defining the boundary conditions then

$$\left(V_1\boldsymbol{\psi}^+(L)\right) = \tilde{U}_N(L)\left(V_2\boldsymbol{\psi}^-(L)\right), \tag{7}$$

yields the same boundary conditions where $\tilde{U}_N(L)=V_1U_N(L)V_2^\dagger$ for any unitary matrices V_1, V_2. The reader therefore, by choosing a different diagonalisation of the probability current $J(L)$, can arrive at a different value for $U_N(L)$ to that presented. However, there are still N^2 distinct β-functions as this global symmetry only allows us to set the value of $U_N(L)$ arbitrarily at a single point along the RG flow.

where E and explicit L dependence enters into (10) through the Cs. Assuming $\epsilon L \ll 1$ removes this dependence rendering (10) translationally invariant in E, L. In this regime, (10) holds for every eigenfunction and its corresponding $\boldsymbol{\psi}^-(L)$, meaning the term in brackets is zero. Multiplying through (10) by $-iU_N^{-1}$ gives the flow equation for $U_N(L)$:

$$-\mathrm{i}LU_N^{-1}d_L U_N = \mathrm{i}C_{--} - \mathrm{i}U_N^{-1}C_{+-} + \mathrm{i}C_{-+}U_N - \mathrm{i}U_N^{-1}C_{++}U_N. \tag{11}$$

This is essentially a generalisation of the approach taken by [13, 37]. For $N = 1$, defining $g = \tan(-\mathrm{i}\ln U_1)$, equation (11) reduces into their result.

4. Fixed point annihilation—a generic feature in the landscape of scale invariant Hamiltonians

We numerically obtained the trajectories corresponding to (11) and solved for the zeros of the RHS (the β function) in a variety of cases. We find a range of distinct flows terminating in fixed points, limit cycles and limit tori. We find that a few simple properties of the $E = 0$ power laws Δ_i determine what is the characteristic RG picture as summarised in table 1. In particular, the RG space will contain unitary fixed points[5] if and only if there are no roots Δ_i on the symmetry line $\mathrm{Re}[z] = N - 1/2$. This implies the following general result: consider a Hamiltonian $\hat{H}_N$ corresponding to some choice of $\lambda_i \in \mathbb{R}$ in (2) such that there are no roots Δ_i on the symmetry line $\mathrm{Re}[z] = N - 1/2$. Then, continuously tuning the λ_i's such that at least one pair of roots settle on $\mathrm{Re}[z] = N - 1/2$ will generate a transition characterized by fixed point annihilation. In this context, fixed point annihilation of $\hat{H}_S = p^2 - \lambda_2/r^2$ is only one case, corresponding to $N = 1$, $\lambda_1 = 0$. In general we observe that there are 2^N unitary fixed points which annihilate in pairs.

As an example, consider figure 1 which represents the flow of the fixed points of (11) for the system:

$$\left[\left(d_r^2 + \frac{1}{r}d_r - \frac{m^2}{r^2}\right)^2 - \frac{\lambda}{r^4} - E\right]\left(r^{-\frac{1}{2}}\psi(r)\right) = 0 \tag{12}$$

which describes a particle with kinetic energy $E = \boldsymbol{p}^4$ on a two-dimensional plane interacting with a potential whose strength is controlled by the parameter λ. The integer m represents the angular momentum while the additional factor of $r^{-1/2}$ is a Jacobian factor such that the probability current is defined as in (4). Choosing $m = 2$ henceforth, the boundary conditions are specified by U_2 matrices with respect to the basis

$$\begin{aligned}\psi_1^{\pm}(L) \approx{}& 0.033\,\psi(L) \pm 0.033\mathrm{i}\,L\psi'(L)\\ &+ 0.254\,L^2\psi''(L) \pm 0.254\mathrm{i}\,L^3\psi'''(L),\end{aligned} \tag{13a}$$

$$\begin{aligned}\psi_2^{\pm}(L) \approx{}& 1.937\,\psi(L) \mp 1.937\mathrm{i}\,L\psi'(L)\\ &- 0.254\,L^2\psi''(L) \pm 0.254\mathrm{i}\,L^3\psi'''(L).\end{aligned} \tag{13b}$$

Different values of m will yield different numerical coefficients in (13*a*) and (13*b*), as each choice of m in (12) corresponds to a distinct Hamiltonian.

[5] A unitary fixed point corresponds to a unitary matrix. A non-unitary fixed point will similarly be given by a non-unitary matrix.

Table 1. Summary of the relation between the distinct RG flows describing Hamiltonians (2) and the power laws characterising the zero energy wave functions.

Conditions on $\{\Delta_i\}$		Characteristic RG picture
All roots on symmetry line ($\mathrm{Re}\,[z] = N - 1/2$)	$\mathrm{Im}\,[\Delta_i]/\mathrm{Im}\,[\Delta_j] \in \mathbb{Q}$	RG space filled by many limit cycles (figure 3) with no fixed points
	$\mathrm{Im}\,[\Delta_i]/\mathrm{Im}\,[\Delta_j] \notin \mathbb{Q}$	RG space filled by many limit tori with no fixed points
Some roots off the symmetry line ($\mathrm{Re}\,[z] = N - 1/2$)	For roots with $\mathrm{Re}\,[\Delta_i] = N - 1/2$ if $\mathrm{Im}\,[\Delta_i]/\mathrm{Im}\,[\Delta_j] \in \mathbb{Q}$	Isolated limit cycles (figure 2) with no fixed points
	For roots with $\mathrm{Re}\,[\Delta_i] = N - 1/2$ if $\mathrm{Im}\,[\Delta_i]/\mathrm{Im}\,[\Delta_j] \notin \mathbb{Q}$	Isolated limit torus (figure 4) with no fixed points
No roots on symmetry line ($\mathrm{Re}\,[z] = N - 1/2$)		2^N fixed points

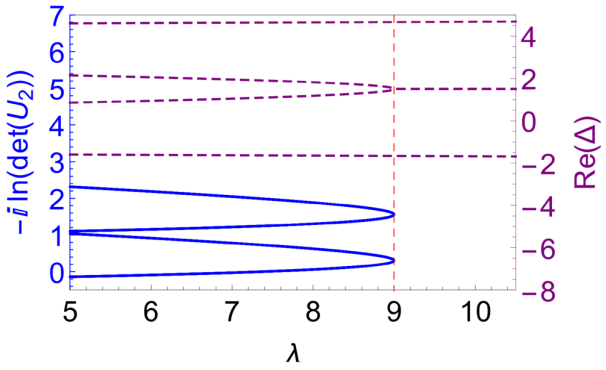

Figure 1. A plot demonstrating fixed point annihilation described by Hamiltonian (12). The solid blue lines represent the fixed points of the RG flow equation (11) while the dashed purple lines display the real parts of the roots Δ_i; both against the coupling λ. The RG space is four dimensional and for brevity the fixed points are projected onto a one dimensional axis corresponding to the value of $-\mathrm{i}\ln(\det U_2)$. The dotted red line indicates the critical coupling $\lambda_c = 9$ below which there are no powers Δ_i on the line $\mathrm{Re}[z] = N - 1/2 = 3/2$.

For $\lambda < 9$, there are four unitary fixed points (and a further two non-unitary). When $\lambda > \lambda_c = 9$, the red dotted line of figure 1, there are no unitary fixed points. In terms of the roots Δ_i, the value $\lambda_c = 9$ is the exact point at which roots move onto the symmetry line $\mathrm{Re}[z] = 3/2$, as seen in figure 1. An additional illustration of this phenomenon for $N = 3$ is given in appendix C.

When considering the phenomena of fixed point annihilation, a pertinent question is what is the characteristic RG picture in the over critical regime, i.e. the regime with no fixed points. Recent studies [11, 12, 38, 39] show that for $N = 1$ the flow in the over critical regime is completely periodic. In other words, regardless of the initial condition, the boundary parameter is periodic in $\ln L$ generating a DSI RG picture. The appearance of this type of flow has been considered as evidence for the relevance of RG limit cycles in physical applications.

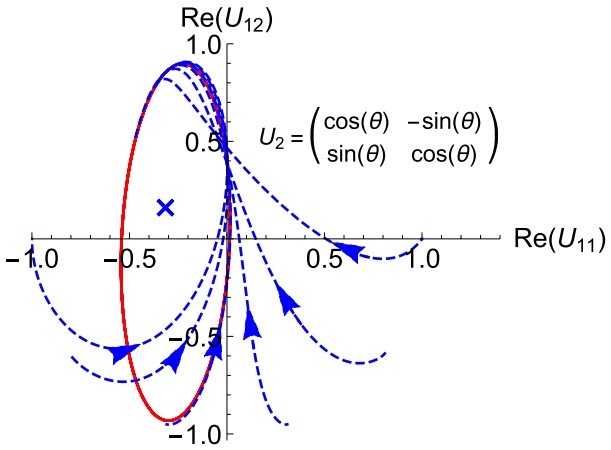

Figure 2. A two dimensional projection of the (four dimensional) RG picture of the system $\hat{H}_2 = d_r^4 - 2/r^4$. Boundary conditions are with respect to $\psi_1^{\pm}(L) = \frac{1}{\sqrt{2}}\left(L\psi'(L) \mp \mathrm{i}L^2\psi''(L)\right)$ and $\psi_2^{\pm}(L) = \frac{1}{\sqrt{2}}\left(\psi(L) \pm \mathrm{i}L^3\psi'''(L)\right)$. The initial conditions for the dashed blue flows are specified by choosing $\theta = -\pi, \ldots, -\pi/10, 0$ for the U_2 matrix as displayed. We see that all the trajectories flow towards a limit cycle. There exists a non-unitary fixed point, denoted by the blue cross, which is enclosed by the cycle when we project down onto any two dimensional subspace.

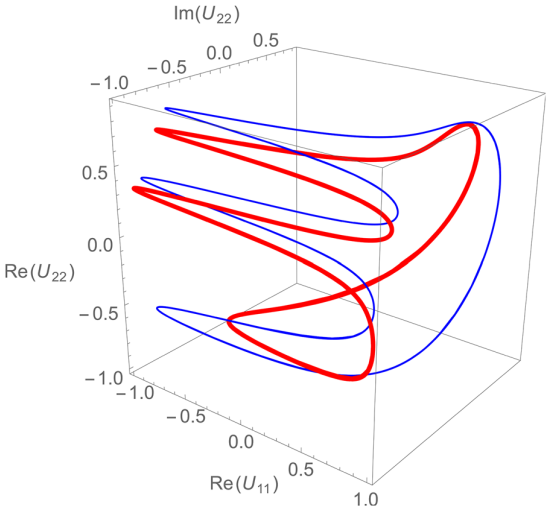

Figure 3. A three dimensional projection of the (four dimensional) RG picture for the system $\hat{H}_2 = d_r^4 + \frac{25}{2}\frac{1}{r^2}d_r^2 - 25\frac{1}{r^3}d_r + \frac{585}{16}\frac{1}{r^4}$. The boundary conditions are $U_2 = -\mathbb{1}_2$ (red and thick) and $U_2 = \exp(-3\pi\mathrm{i}/4)\mathbb{1}_2$ (blue and thin) at $L = e^1$ with respect to the basis $\psi_1^{\pm}(L) \approx \mp 0.016\mathrm{i}\psi(L) - 0.016L\psi'(L) \pm 0.199\mathrm{i}L^2\psi''(L) + 0.199L^3\psi'''(L)$ and $\psi_2^{\pm}(L) \approx \mp 2.500\mathrm{i}\psi(L) + 2.500L\psi'(L) \mp 0.199\mathrm{i}L^2\psi''(L) + 0.199L^3\psi'''(L)$. We see that a small modification of the boundary condition corresponds to two different nearby periodic trajectories. The space is filled by closed trajectories. Any choice of initial condition, that is the initial boundary condition, will flow on one of them.

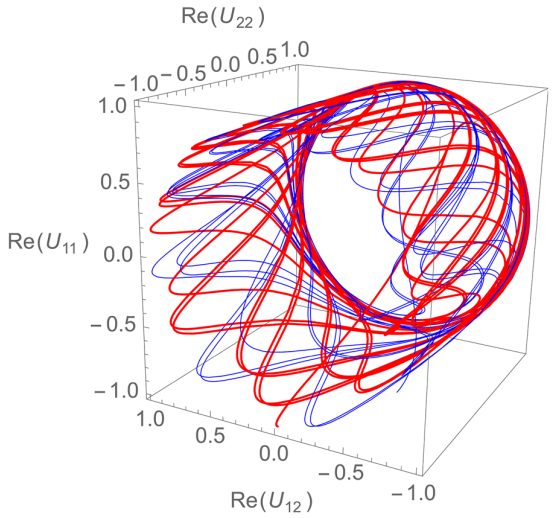

Figure 4. A three dimensional projection of the (nine dimensional) RG picture for the system $\hat{H}_3 \approx -d_r^6 - 16.2\frac{1}{r^2}d_r^4 + 64.9\frac{1}{r^3}d_r^3 - 195.3\frac{1}{r^4}d_r^2 + 392.0\frac{1}{r^5}d_r - 299.1\frac{1}{r^6}$. The basis with respect to which we determine U_3 is particularly long, and as such we display it in appendix D along with an exact expression for $\hat{H}_3$. The initial condition for the red, thick curve is $U_3(1) = -\mathbb{1}_3$ and $U_3(1) = \exp(\mathrm{i}\pi/4)\mathbb{1}_3$ for the blue and thin curve. The curves represent two different initial conditions that are attracted to a quasi periodic trajectory as $L \to 0$. This type of attractor is characterised by a trajectory that never closes on itself and fills a compact RG subspace.

For $N > 1$, we find that the $N = 1$ case is a single instance in a rich set of possibilities. In the overcritical regime, and close to the critical point, there is an isolated closed trajectory to which all other trajectories are attracted as $L \to 0$ (see figure 2). As opposed to completely periodic flow, this intrinsically non-linear flow picture, is in fact the rigorous definition of a limit cycle [63]. To our knowledge, this is the only manifestation of a limit cycle in a physical application to date. The difference with respect to the $N = 1$ case is simply displayed in terms of the behaviour of the $E = 0$ wave functions, i.e. the roots Δ_i. For $N > 1$, near the critical point and in the overcritical regime, the two complex conjugate roots on the symmetry line $\mathrm{Re}[z] = N - 1/2$ are accompanied by $2(N-1) \neq 0$ roots off the line. If we move in a direction in the λ_i parameter space such that all the roots are on the symmetry line, the limit cycle will disappear in favour of an RG space filled entirely by periodic flows (figure 3) or quasi-periodic flows. The former is obtained when the imaginary part of all the roots on the symmetry line has a common divisor and later when they do not. If we allow roots outside the symmetry line as well as multiple roots on the symmetry line (with imaginary parts not having a common divisor), then all the flows are attracted to an isolated quasi-periodic trajectory as seen in figure 4. This trajectory, known as a limit torus, is characterised by a curve that never closes on itself and fills a compact RG subspace.

In order to obtain further insight on the over critical regime, we calculated the spectrum in various cases corresponding to the distinct flows described by figures 2–4. For $\hat{H}_S = p^2 - \lambda/r^2$, corresponding to $N = 1$, $\lambda_1 = 0$ and $\lambda_2 = -\lambda$, DSI manifests in the geometric progression of the spectrum given by (1). For $N > 1$ and in the case where the flow is periodic (figures 2 and 3) we find that the spectrum can be described by a union of multiple geometric towers as seen

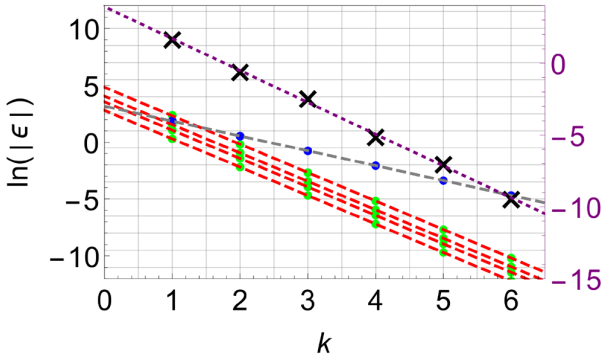

Figure 5. Negative bound state energies of various Hamiltonians corresponding to the distinct flows described by figures 2–4 where k is some arbitrary integer labeling of the energy levels. The blue and green dots represent bound state energies for the Hamiltonians $\hat{H}_2 = d_r^4 + \frac{(125+388\pi^2)}{50}\frac{1}{r^2}d_r^2 - \frac{(125+388\pi^2)}{25}\frac{1}{r^3}d_r + \frac{(9+4\pi^2)(225+676\pi^2)}{400}\frac{1}{r^4}$ and (12) (with $\lambda = 100$ in this latter case). The black crosses represent negative energy levels for the Hamiltonian of figure 4. All boundary condition parameters are given by the identity matrix and the cut-off is $L = e^{-1}$. The first pair of these systems are of the class corresponding to figures 2 and 3 respectively. In the former, the spectrum is a composition of four intertwined geometric towers of energy (the four red dashed lines), while in the latter there is one (the grey dashed line). The Hamiltonian corresponding to the black crosses is a limit torus case and the purple dotted line represents a best fit to the data, given by black crosses. These crosses do not sit precisely on the purple line indicating that there is no discrete scale invariance.

for example in figure 5. When the flow is quasi-periodic the spectrum is no longer DSI as is also exhibited in figure 5.

5. Summary

We considered a large class of quantum mechanical scale invariant systems (2) and formulated a RG description controlled by a short distance cut-off L. The resulting picture shows that the quantum phase transition characterised by fixed point annihilation and DSI is a generic phenomenon exhibited by the class of Hamiltonians (2). We found that the transition point is related to the value of the roots characterising the zero energy wave function solutions. Hermiticity of the Hamiltonian imposes that these powers be symmetric with respect to the line $\mathrm{Re}[z] = N - 1/2$ and the appearance of roots on this line is in direct correspondence with the transition point. We hope that our results will provide further insight and intuition on the quantum behaviour of scale invariant systems in quantum mechanics and quantum field theory.

Acknowledgments

The work of DB is supported by key grants from the NSF of China with grant numbers: 11235010 and 11775212. This work was also supported by the Israel Science Foundation Grant No. 924/09. DB would like to thank Matteo Baggioli for reading an early draft.

Appendix A. Analytic solution of $\hat{H}_N\Psi(r) = E\Psi(r)$

Consider the differential equation $\hat{H}_N\Psi(r) = E\Psi(r)$ where

$$\hat{H}_N = \hat{p}^{2N} + \sum_{i=1}^{2N} \frac{\lambda_i}{r^i} d_r^{2N-i}, \tag{A.1}$$

with $\lambda_i \in \mathbb{R}$. For $E = 0$, there are $2N$ independent solutions given by $\psi \propto r^{\Delta_i}$, $i = 1, \ldots, 2N$ obtained by inserting $\psi \propto r^{\Delta}$ into $\hat{H}_N\psi = 0$ and solving for the roots of the resultant polynomial in Δ

$$0 = (\Delta - \Delta_1)\ldots(\Delta - \Delta_{2N})\,. \tag{A.2}$$

We assume that all roots are distinct for simplicity as this avoids dealing with logarithms in the Frobenius solution [64]. For $E \neq 0$ and of arbitrary complex value, the general solution of (A.1) is expressed in terms of generalised hypergeometric functions ${}_pF_q\left[\begin{matrix}a_1,\ldots,a_p\\ b_1,\ldots,b_q\end{matrix};z\right]$ [61, pg 136]:

$$\psi(r;\phi_j) = \sum_{i=1}^{2N} \mathrm{e}^{\mathrm{i}\Delta_i\phi_j}\left(\frac{\epsilon r}{2N}\right)^{\Delta_i}\Gamma\left(\frac{\boldsymbol{\Delta}_i - \Delta_i}{2N}\right) \times\ {}_0F_{2N-1}\left[\begin{matrix}-\\ 1 - \frac{\Delta_i - \boldsymbol{\Delta}_i}{2N}\end{matrix};|E|\left(\frac{r}{2N}\right)^{2N}\right], \tag{A.3}$$

$$\phi_j = \frac{1}{2N}\left(\theta - 2\pi(N + (w + j))\right), \qquad j = 1, 2, \ldots, 2N, \tag{A.4}$$

where $\boldsymbol{\Delta}_i$ is the vector of solutions to (A.2) with Δ_i omitted, w is an integer chosen such that $|\phi_j| < \pi(1 + \frac{1}{2N})$, $E = |E|\mathrm{e}^{\mathrm{i}\theta}$ and $\epsilon = |E|^{\frac{1}{2N}}$.

At large r only the leading derivative term $(-1)^N d_r^{2N}$ of the kinetic term is important and the wavefunctions behave as $\psi(r) \sim \exp(\alpha r)$ with $\alpha^{2N} = (-1)^N E$. Setting $E = \pm\mathrm{i}$ we find

$$\alpha = \exp\left(\mathrm{i}\pi\left(\frac{1}{2} + \frac{n}{N} \pm \frac{1}{4N}\right)\right), \tag{A.5}$$

respectively with $n = 0, \ldots, 2N - 1$. For each $E = \pm\mathrm{i}$ there are exactly N values of n giving $\pi/2 < \arg(\alpha) < 3\pi/2$. Thus one has N decaying wavefunctions of negative and positive imaginary energies giving a $U(N)$ self-adjoint extension. The relationship between these asymptotic behaviours and (A.3) is:

$$\psi(r;\phi_j) \sim \exp\left(-\epsilon r\mathrm{e}^{\mathrm{i}\phi_j}\right) \tag{A.6}$$

for non-zero ϵ (see [61]).

Appendix B. Constraints on the power laws characterising the $E = 0$ wavefunctions

The space of wave functions upon which $\hat{H}_N$ acts is equipped with an inner product defined given by

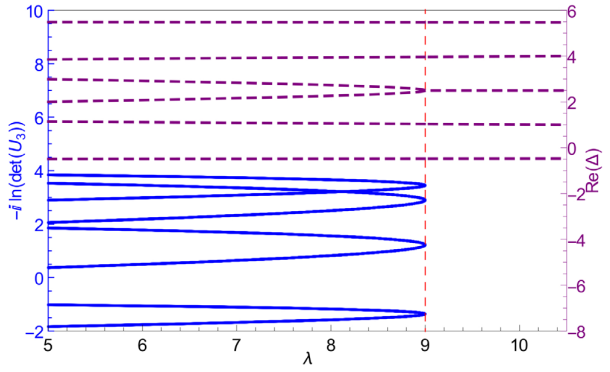

Figure B1. A plot demonstrating fixed point annihilation for a two dimensional system with orbital angular momentum ($m = 1$) interacting with a potential (C.1). The solid blue lines represent the fixed points of the RG flow equation (11) while the dashed purple lines display the real parts of the roots Δ_i; both against the coupling λ. The dotted red line indicates the critical coupling $\lambda_c = 9$ above which there is DSI.

$$\langle\phi|\psi\rangle = \int_{r=L}^{\infty} \mathrm{d}r\ \phi^*(r)\psi(r) \tag{B.1}$$

where we have absorbed a Jacobian factor into the definition of the wave functions and $L \geqslant 0$. Hamiltonian (2) can be factorised as

$$\hat{H}_N = (-1)^N \hat{D}_{2N} \ldots \hat{D}_1 \tag{B.2}$$

where:

$$\hat{D}_i = d_r - \left(\frac{\Delta_i - i + 1}{r}\right), \tag{B.3}$$

$i = 1, \ldots, 2N$, and Δ_i are the roots of (A.2). This can be seen by acting with the $\hat{D}_i$'s on r^{Δ}, Δ arbitrary. The formal adjoints of (B.3), are defined by $\langle\phi|\hat{D}_i^\dagger|\psi\rangle = \langle\hat{D}_i\phi|\psi\rangle$, ignoring any boundary terms. By integrating by parts the right hand side, $\hat{D}_i^\dagger$ is given by

$$\begin{aligned}\hat{D}_i^\dagger &= -\left[d_r + \left(\frac{\Delta_i^* - i + 1}{r}\right)\right] \\ &= -\left[d_r - \left(\frac{(2N - 1 - \Delta_i^*) - (2N - i + 1) + 1}{r}\right)\right].\end{aligned}$$

Similarly, the formal adjoint of $\hat{H}_N$ is given by

$$\hat{H}_N^\dagger = (-1)^N \hat{D}_1^\dagger \ldots \hat{D}_{2N}^\dagger. \tag{B.4}$$

For $\hat{H}_N = \hat{H}_N^\dagger$ we can identify $\hat{D}_i^\dagger = -\hat{D}_{2N-i+1}$. As a result, if Δ_i belongs to the set $\{\Delta_i\}$ then so does $2N - 1 - \Delta_i^*$. Furthermore, since λ_i in (2) are real, both Δ_i and Δ_i^* belong to the set of roots. Thus, if Δ_i^* is a root, then $2N - 1 - \Delta_i$ is a root which implies that if Δ_i is a root then $2N - 1 - \Delta_i$ is a root.

Appendix C. Fixed point flow for $N = 3$

Consider figure B1 which represents the flow of the fixed points of (11) for the system:

$$\left[\left(d_r^2 + \frac{1}{r}d_r - \frac{m^2}{r^2}\right)^3 + \frac{\lambda}{r^6} + E\right]\left(r^{-\frac{1}{2}}\psi(r)\right) = 0. \tag{C.1}$$

This represents a particle with kinetic energy $E = \boldsymbol{p}^6$ on a two-dimensional plane interacting with a potential whose strength is controlled by the parameter λ. The integer m represents the angular momentum while the additional factor of $r^{-1/2}$ is a Jacobian factor such that the probability current is defined as in equation (4) of the main text. Choosing $m = 1$ henceforth, the boundary conditions are specified by U_3 matrices with respect to the basis

$$\begin{aligned}\psi_1^{\pm}(L) \approx{}& \mp 0.0067i\,\psi(L) + (0.0066 \mp 0.0001\mathrm{i})\,L\psi'(L)\\ &- (0.0014 \pm 0.0159\mathrm{i})\,L^2\psi''(L) + (0.0156 \mp 0.0307\mathrm{i})\,L^3\psi'''(L)\\ &- (0.0031 \pm 0.1461\mathrm{i})\,L^4\psi^{(4)}(L) + 0.1493\,L^5\psi^{(5)}(L),\end{aligned} \tag{C.2}$$

$$\begin{aligned}\psi_2^{\pm}(L) \approx{}& (0.0049 \pm 0.1020\mathrm{i})\,\psi(L) - (0.1004 \pm 0.2103\mathrm{i})\,L\psi'(L)\\ &+ (0.0111 \mp 0.7618\mathrm{i})\,L^2\psi''(L) + 0.7731\,L^3\psi'''(L)\\ &- (0.1640 \mp 0.0783\mathrm{i})\,L^4\psi^{(4)}(L)\\ &- (0.0795 \mp 0.0039\mathrm{i})\,L^5\psi^{(5)}(L),\end{aligned} \tag{C.3}$$

$$\begin{aligned}\psi_3^{\pm}(L) \approx{}& 2.9105\,\psi(L) + (0.1013 \mp 2.8055\mathrm{i})\,L\psi'(L)\\ &+ (0.3449 \pm 0.7747\mathrm{i})\,L^2\psi''(L) - (0.0449 \pm 0.3595\mathrm{i})\,L^3\psi'''(L)\\ &- (0.1626 \pm 0.0059\mathrm{i})\,L^4\psi^{(4)}(L) \pm 0.1687\mathrm{i}\,L^5\psi^{(5)}(L).\end{aligned} \tag{C.4}$$

Different values of m will yield different numerical coefficients in (C.2)–(C.4), as each choice of m in (C.1) corresponds to a distinct Hamiltonian. For $\lambda < 9$, there are eight unitary fixed points. When $\lambda > \lambda_c = 9$, the red dotted line of figure B1, there are no unitary fixed points. In terms of the roots Δ_i, the value $\lambda_c = 9$ is the exact point at which roots move onto the symmetry line $\mathrm{Re}[z] = 5/2$, as seen in figure B1.

Appendix D. Hamiltonians and boundary conditions for $N = 3$ limit tori

The Hamiltonian that represents a limit torus flow in figure 4 of the main text is:

$$\begin{aligned}\hat{H}_3 = {}& -d_r^6 - \left(\frac{\pi^2}{4} + \frac{55}{4}\right)\frac{1}{r^2}d_r^4 + \left(\pi^2 + 55\right)\frac{1}{r^3}d_r^3\\ &- \left(\frac{39\pi^2}{8} + \frac{2355}{16}\right)\frac{1}{r^4}d_r^2 + \left(\frac{27\pi^2}{2} + \frac{1035}{4}\right)\frac{1}{r^5}d_r\\ &- \left(\frac{549\pi^2}{64} + \frac{13\,725}{64}\right)\frac{1}{r^6}.\end{aligned} \tag{D.1}$$

The basis for the U_3 matrices describing the boundary conditions are given by:

$$\begin{aligned}\psi_1^{\pm}(L) \approx & \mp 0.000\,318i\,\psi(L) + (0.000\,312 \mp 0.000\,006\mathrm{i})\,L\psi'(L) \\ & - (0.005\,096 \mp 0.010\,420\mathrm{i})\,L^3\psi'''(L) \\ & + (0.000\,061 \pm 0.005\,192\mathrm{i})\,L^2\psi''(L) \\ & - (0.000\,996 \pm 0.053\,012\mathrm{i})\,L^4\psi^{(4)}(L) \\ & + 0.054\,026\,L^5\psi^{(5)}(L),\end{aligned} \tag{D.2}$$

$$\begin{aligned}\psi_2^{\pm}(L) \approx & -(0.001\,6482 \pm 0.137\,145\mathrm{i})\,\psi(L) \\ & - (0.132\,819 \mp 0.276\,935\mathrm{i})\,L\psi'(L) \\ & + 0.864\,357\,L^3\psi'''(L) + (0.026\,730 \pm 0.836\,773I)\,L^2\psi''(L) \\ & + (0.172\,537 \pm 0.082\,749\mathrm{i})\,L^4\psi^{(4)}(L) \\ & + (0.085\,444 \mp 0.001\,0269\mathrm{i})\,\psi^{(5)}(L),\end{aligned} \tag{D.3}$$

$$\begin{aligned}\psi_3^{\pm}(L) \approx & 7.185\,486\,\psi(L) + (0.346\,217 \pm 6.821\,721\mathrm{i})\,L\psi'(L) \\ & + (1.056\,720 \mp 2.257\,285\mathrm{i})\,L^2\psi''(L) \\ & + (0.021\,347 \pm 1.111\,986\mathrm{i})\,L^3\psi'''(L) \\ & + (0.064\,511 \mp 0.003\,274\mathrm{i})\,L^4\psi^{(4)}(L) \pm 0.067\,951\mathrm{i}\,\psi^{(5)}(L).\end{aligned} \tag{D.4}$$

Appendix E. Fixed point annihilation—methods and additional results

We have used two methods to check that our numerical calculations give the correct values for the stable fixed point. The first of these requires setting the left hand side of the RG-flow equation,

$$-\mathrm{i}LU_N^{-1}d_LU_N = \mathrm{i}C_{--} - \mathrm{i}U_N^{-1}C_{+-} + \mathrm{i}C_{-+}U_N - \mathrm{i}U_N^{-1}C_{++}U_N, \tag{E.1}$$

to zero and solving the resultant matrix polynomial for U_N. For $N = 1$ this is simply solving a quadratic equation. For $N > 1$ we have a matrix quadratic equation which is more difficult to solve. Nonetheless the methods discussed in [65] allow one to do this and we refer the interested reader to the book.

A second, more practical, method is to use the general form of the wavefunction for $\epsilon L \ll 1$. The generic wavefunction for small $\epsilon L \ll 1$ has the form

$$\psi(r) = \sum_{i=1}^{N}\left[(\epsilon r)^{\Delta_i}\,\phi_i + \ldots + (\epsilon r)^{\Delta_{i+N}}\,O_i + \ldots\right], \tag{E.2}$$

where ϕ_i and O_i are complex constants and $\epsilon = |E|^{1/N}$. Half of these coefficients will be fixed by conditions at infinity while the other half will be fixed by boundary conditions on the cut-off. As the wavefunction $\psi(r)$ can be expanded in small ϵr so can $\boldsymbol{\psi}^{\pm}(r)$. Hence the boundary condition at $r = L$ takes the form

$$\begin{aligned}0 = & \sum_{i=1}^{N}(\epsilon L)^{\Delta_i}\,\phi_i\left(\boldsymbol{\psi}^{+}_{\Delta_i} - U_N\boldsymbol{\psi}^{-}_{\Delta_i}\right) \\ & + (\epsilon L)^{\Delta_{i+N}}\,O_i\left(\boldsymbol{\psi}^{+}_{\Delta_{i+N}} - U_N\boldsymbol{\psi}^{-}_{\Delta_{i+N}}\right) + \ldots\end{aligned} \tag{E.3}$$

where $\epsilon L \ll 1$ and $\psi^{\pm}_{\Delta_i}$ is the coefficient of $\phi_i(\epsilon L)^{\Delta_i}$ or $O_i(\epsilon L)^{\Delta_{i+N}}$ in the expansion of $\psi^{\pm}(L)$.

Solutions to the energy eigenvalue problem at some $r = L$ satisfy (E.3). Suppose we require (E.3) to be satisfied for every L such that $\epsilon L \ll 1$. Then the terms in (E.3) must vanish separately. Moreover, after fixing conditions at $r = L$ we will require N remaining degrees of freedom (a collection of N of the ϕ_i and O_i) to fix boundary conditions at infinity. Thus, it must be the case that N of the ϕ_i and O_i are identically zero while for the remaining N terms the equation $\left(\psi^{+}_{\Delta_i} - U_N \psi^{-}_{\Delta_i}\right) \equiv 0$ is satisfied (so that N of the ϕ_i and O_i are undetermined). These latter conditions allow for a total of $2N!/N!^2$ solutions of U_N, each of which is a fixed point (as it is invariant under rescaling).

We have numerically checked the number of fixed points using the method of [65]. It should be noted that while (E.3) seemingly yields $(2N)!/N!^2$ possible fixed points, not all of them are unitary. In particular, we have seen that if one chooses to include two Δ_i that sum to $2N - 1$ in the definition of U_N then the resultant fixed point will be non-unitary. Thus, we find that there always 2^N unitary fixed points. We tested one thousand uniformly distributed random values for Δ_i with $\mathrm{Re}[\Delta_i], \mathrm{Im}[\Delta_i] \in [-10, 10]$ (satisfying the constraints explained in appendix B) and determined the number of unitary fixed points for $N = 2, 3$ using the method of [65]. Indeed, applying this method in the case where there are roots on the line $\mathrm{Re}[z] = N - 1/2$ yields only non-unitary fixed points and 2^N unitary fixed points when there is no root with $\mathrm{Re}[z] = N - 1/2$.

ORCID iDs

Eric Akkermans https://orcid.org/0000-0002-2441-1344

References

[1] Adler S L 1969 *Phys. Rev.* **177** 2426–38
[2] Bell J S and Jackiw R 1969 *Nuovo Cimento* A **60** 47–61
[3] Esteve J G 1986 *Phys. Rev.* D **34** 674–7
[4] Holstein B R 1993 *Am. J. Phys.* **61** 142–7
[5] Coleman S and Jackiw R 1971 *Ann. Phys.* **67** 552–98
[6] Case K M 1950 *Phys. Rev.* **80** 797–806
[7] de Alfaro V, Fubini S and Furlan G 1976 *Il Nuovo Cimento* A **34** 569–612
[8] Landau L D 1991 *Quantum Mechanics: Non-Relativistic Theory* (Oxford: Heinemann)
[9] Camblong H E, Epele L N, Fanchiotti H and Garcia Canal C A 2000 *Phys. Rev. Lett.* **85** 1590–3
[10] Añanos G N J, Camblong H E and Ordóñez C R 2003 *Phys. Rev.* D **68** 025006
[11] Hammer H W and Swingle B G 2006 *Ann. Phys.* **321** 306–17
[12] Braaten E and Phillips D 2004 *Phys. Rev.* A **70** 052111
[13] Kaplan D B, Lee J W, Son D T and Stephanov M A 2009 *Phys. Rev.* D **80** 125005
[14] Ovdat O, Mao J, Jiang Y, Andrei E Y and Akkermans E 2017 *Nat. Commun.* **8** 507
[15] Alexandre J 2011 *Int. J. Mod. Phys.* A **26** 4523–41
[16] Brattan D K, Ovdat O and Akkermans E 2018 *Phys. Rev.* D **97** 061701
[17] Kolomeisky E B and Straley J P 1992 *Phys. Rev.* B **46** 12664–74
[18] Jensen K, Karch A, Son D T and Thompson E G 2010 *Phys. Rev. Lett.* **105** 041601
[19] Jensen K 2010 *Phys. Rev.* D **82** 046005
[20] Jensen K 2011 *Phys. Rev. Lett.* **107** 231601
[21] Derrida B and Retaux M 2014 *J. Stat. Phys.* **156** 268–90
[22] Gies H and Torgrimsson G 2016 *Phys. Rev. Lett.* **116** 090406
[23] Efimov V 1970 *Phys. Lett.* B **33** 563–4
[24] Efimov V 1971 *Sov. J. Nucl. Phys.* **12** 589–95
[25] Braaten E and Hammer H W 2006 *Phys. Rep.* **428** 259–390

[26] Herbut I F 2016 *Phys. Rev.* D **94** 025036
[27] Lévy-Leblond J M 1967 *Phys. Rev.* **153** 1–4
[28] Gupta K S and Rajeev S G 1993 *Phys. Rev.* D **48** 5940–5
[29] Camblong H E, Epele L N, Fanchiotti H and García Canal C A 2001 *Phys. Rev. Lett.* **87** 220402
[30] Nisoli C and Bishop A R 2014 *Phys. Rev. Lett.* **112** 070401
[31] Govindarajan T R, Suneeta V and Vaidya S 2000 *Nucl. Phys.* B **583** 291–303
[32] Camblong H E and Ordonez C R 2003 *Phys. Rev.* D **68** 125013
[33] Bellucci S, Galajinsky A, Ivanov E and Krivonos S 2003 *Phys. Lett.* B **555** 99–106
[34] Brattan D K 2018 *Phys. Rev.* D **98** 036005
[35] Wilson K G and Kogut J 1974 *Phys. Rep.* **12** 75–199
[36] Cambel A 1993 *Applied Chaos Theory: a Paradigm for Complexity* (Amsterdam: Elsevier)
[37] Mueller E J and Ho T L 2004 (arXiv:cond-mat/0403283)
[38] Gorsky A and Popov F 2014 *Phys. Rev.* D **89** 061702
[39] Nishida Y 2016 *Phys. Rev.* B **94** 085430
[40] Gitman D M, Tyutin I V and Voronov B L 2010 *J. Phys. A: Math. Theor.* **43** 145205
[41] Hornreich R M, Luban M and Shtrikman S 1975 *Phys. Rev. Lett.* **35** 1678–81
[42] Grinstein G 1981 *Phys. Rev.* B **23** 4615–30
[43] Fradkin E, Huse D A, Moessner R, Oganesyan V and Sondhi S L 2004 *Phys. Rev.* B **69** 224415
[44] Vishwanath A, Balents L and Senthil T 2004 *Phys. Rev.* B **69** 224416
[45] Ardonne E, Fendley P and Fradkin E 2004 *Ann. Phys.* **310** 493–551
[46] McCann E and Koshino M 2013 *Rep. Prog. Phys.* **76** 056503
[47] Ramires A, Coleman P, Nevidomskyy A H and Tsvelik A M 2012 *Phys. Rev. Lett.* **109** 176404
[48] Miao J, Liu B and Zheng W 2015 *Phys. Rev.* A **91** 033404
[49] Radić J, Natu S S and Galitski V 2015 *Phys. Rev.* A **91** 063634
[50] Po H C and Zhou Q 2015 *Nat. Commun.* **6** 8012
[51] Wu J, Zhou F and Wu C 2017 *Phys. Rev.* B **96** 085140
[52] Mukohyama S 2010 *Class. Quantum Grav.* **27** 223101
[53] Reuter M 1998 *Phys. Rev.* D **57** 971–85
[54] Kachru S, Liu X and Mulligan M 2008 *Phys. Rev.* D **78** 106005
[55] Horava P 2009 *Phys. Rev. Lett.* **102** 161301
[56] Horava P 2009 *Phys. Rev.* D **79** 084008
[57] Gies H, Knorr B, Lippoldt S and Saueressig F 2016 *Phys. Rev. Lett.* **116** 211302
[58] Das S R and Murthy G 2010 *Phys. Rev. Lett.* **104** 181601
[59] Bonneau G, Faraut J and Valent G 2001 *Am. J. Phys.* **69** 322
[60] Ibort A, Lledó F and Pérez-Pardo J M 2015 *Ann. Henri Poincaré* **16** 2367–97
[61] Luke Y 1969 *The Special Functions and Their Approximations* (*Mathematics in Science and Engineering*) (Amsterdam: Elsevier)
[62] Gitman D, Tyutin I and Voronov B 2012 *Self-adjoint Extensions in Quantum Mechanics: General Theory and Applications to Schrödinger and Dirac Equations with Singular Potentials* (*Progress in Mathematical Physics* vol 62) (Basel: Birkhäuser)
[63] Strogatz S H 1994 *Nonlinear Dynamics and Chaos* (Boca Raton, FL: CRC Press)
[64] Borden B and Luscombe J 2017 Power-series solutions of odes *Essential Mathematics for the Physical Sciences* (Bristol: IOP Publishing) pp 3-1–3-27 (https://doi.org/10.1088/978-1-6817-4485-8)
[65] Lancaster P and Rodman L 1995 *Algebraic Riccati Equations* (Oxford: Oxford Science Publications)

4 Submitted Publications

1. O. Ovdat, Y. Don, E. Akkermans, "Vacancies in Graphene: Dirac Physics and Fractional Vacuum Charges", arXiv 1807.10297 (2018) (Submitted).

Vacancies in Graphene : Dirac Physics and Fractional Vacuum Charges

Omrie Ovdat, Yaroslav Don, and Eric Akkermans*
Department of Physics, Technion – Israel Institute of Technology, Haifa 3200003, Israel

The study of neutral vacancies in graphene is a topic of growing interest. A single vacancy induces a localized stable charge of order unity interacting with other charges of the conductor through an unscreened Coulomb potential. It also breaks the symmetry between the two triangular graphene sublattices hence inducing zero energy states at the Dirac points. Here we show the fractional and pseudo-scalar nature of this vacancy charge. A continuous Dirac model is presented which relates zero modes to vacuum fractional charge and to a parity anomaly. This relation constitutes an Index theorem and is achieved by using particular chiral boundary conditions, which map the vacancy problem onto edge state physics. Vacancies in graphene thus allow to realize prominent features of $2+1$ quantum electrodynamics but without coupling to a gauge field. This essential difference makes vacancy physics relatively easy to implement and an interesting playground for topological switching and computation.

I. INTRODUCTION AND PRECISE STATEMENT OF RESULTS

Graphene has a remarkable low energy spectrum described by an effective Dirac model, whose interest resides in its ability to account for a wealth of fundamental aspects specific to massless Dirac fermions. Vacancies[1–18], obtained by removing neutral carbon atoms, have important consequences for the physics of graphene: (i) Zero energy modes. In the presence of $N_A + N_B$ vacancies, where N_A (N_B) is the number of vacancies corresponding to sublattice T_A (T_B), the tight binding Hamiltonian has $|N_A - N_B|$ zero energy eigenvalues with vanishing wave function on the minority sublattice[1–6]. (ii) Charge. Density functional theory calculations[7] show that when a carbon atom is removed, the induced electronic rearrangement leads to a lower energy configuration and to an overall local electric charge in the ground state. In addition, tunnelling and Landau level spectroscopy[6] provide experimental support for the existence of this local charge and show, with very good agreement, an energy spectrum corresponding to an unscreened $V \sim -1/r$ Coulomb potential[8]. (iii) Symmetry breaking. For $N_A \neq N_B$, sublattice symmetry is broken and so is parity in the continuum limit. For a single vacancy, the degeneracy lifting between the two lowest angular momentum channels $j = \pm 1/2$, a clear indication of parity symmetry breaking, has been indeed observed[8].

We present a continuous Dirac model of graphene, valid at low energy and applicable to an arbitrary configuration of isolated vacancies, which accounts for the above features and shows their direct relation. The localized, fractional and pseudo-scalar nature of the vacancy charge is a consequence of the asymmetry between positive and negative parts of the spectrum as expressed by the occurrence of zero energy modes (Fig. 1a). This fractional charge does not display Friedel-like density oscillations and essentially differs from the screening resulting from the insertion of external charge defects[19–25]. We show that the amount of charge associated with $N_A + N_B$ vacancies is proportional to $|N_A - N_B|$. The vacuum charge density and its corresponding charge are obtained by solving the scattering problem of massless Dirac fermions by one vacancy while imposing on their wave function a new type of 'chiral' boundary conditions. This choice unveils the topological nature of the charge and its relation to zero modes under the form of an Index theorem. We emphasize how the phenomena of a charged vacancy presented here, realizes the physics of fermion number fractionalisation[26–42] with the topological content of the magnetic flux Φ now replaced by vacancies with properly chosen boundary conditions such that

$$N_A - N_B \leftrightarrow \Phi. \tag{1}$$

We generalize these results to multi-vacancy configurations and we demonstrate the interest of topological features to achieve remote charge switching (Fig. 1b).

II. DIRAC MODEL

In graphene, carbon atoms condense into a planar honeycomb bipartite lattice built from two triangular sublattices T_A and T_B. The Bravais lattice with a two-atom unit cell and its reciprocal are triangular and the hexagonal Brillouin zone has two inequivalent crystallographic Dirac points K and K'. Around each of them, the low energy excitation spectrum is conveniently described by non-interacting and in-plane massless Dirac fermions with the effective continuous Hamiltonian,

$$H = -i\,\boldsymbol{\sigma}\cdot\boldsymbol{\nabla} = \begin{pmatrix} 0 & D \\ D^\dagger & 0 \end{pmatrix} \tag{2}$$

($\hbar = v_{\rm F} = 1$), $D = -i\partial_x - \partial_y = e^{-i\theta}\left(-i\partial_r - \frac{1}{r}\partial_\theta\right)$ and $\boldsymbol{\sigma} = (\sigma_x, \sigma_y)$. This description was shown to be valid at low energies even in the presence of electron-electron interactions up to logarithmic corrections to the Fermi velocity[43,44] (see Supplementary Note 1). The operators D and $D^\dagger$ are defined on the direct sum $\mathcal{H}_A \oplus \mathcal{H}_B$ of Hilbert spaces associated to T_A and T_B and the corresponding quantum states are two-component spinors

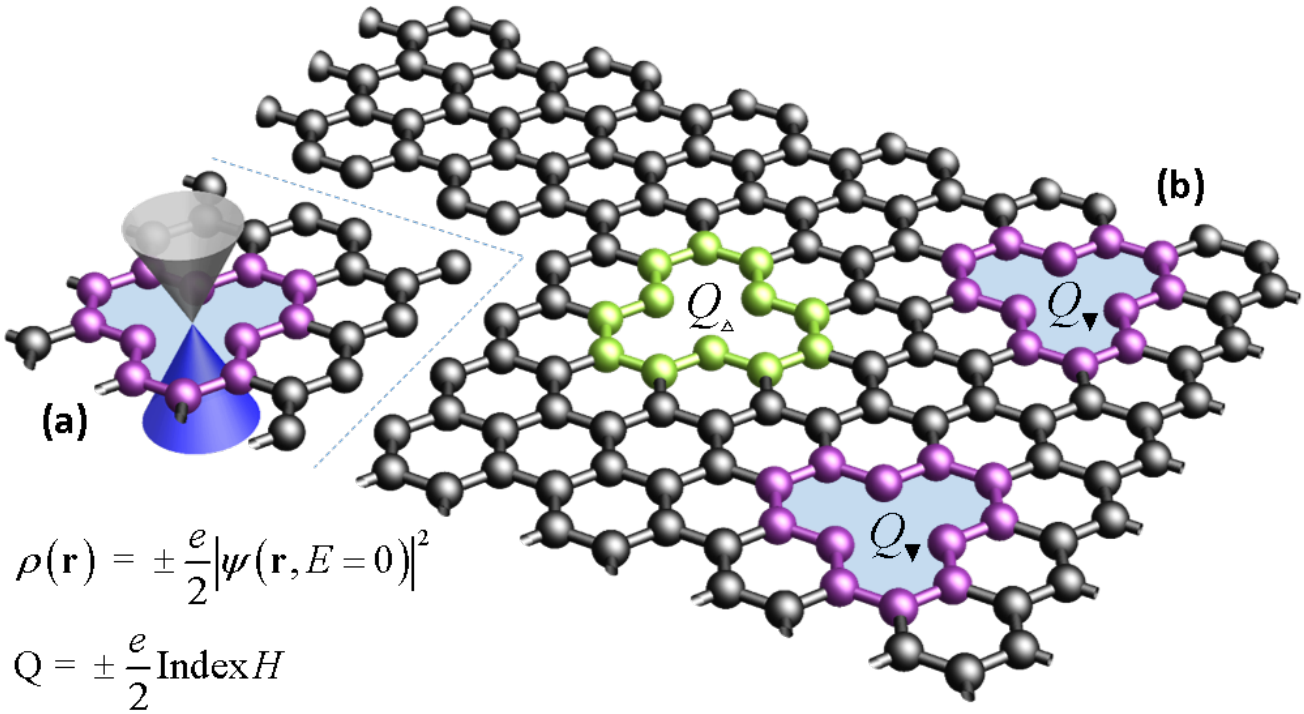

Figure 1. **Schematic visualization of the main results. (a)** By removing a single carbon atom, a vacancy is created which holds a finite fractional charge $Q = \pm\frac{e}{2}\,\mathrm{Index}\,H$. This vacuum charge is associated to the emergence of zero energy modes whose bookkeeping is given by Index H, a topological quantity in nature which preserves the symmetry between positive and negative parts of the Dirac spectral cone. The zero mode eigenfunction $\psi(\boldsymbol{r}, E=0)$ and its corresponding charge density $\rho(\boldsymbol{r})$ are localized at the vacancy boundary (purple). **(b)** Multiple vacancies. A configuration of $N_A = 2$ A-vacancies and $N_B = 1$ B-vacancies is represented. The charge distribution is still constrained by the number of zero modes and its related Index $H = |N_A - N_B|$, but $\rho(\boldsymbol{r})$ is now markedly modified compared to a single vacancy. For $|N_A - N_B| \neq 0$, charges vanish on the minority vacancies, a situation we denote $Q_{\triangle} = 0$, while being finite on the majority vacancies. These charges denoted by $Q_{\blacktriangledown}$, albeit of topological nature, are different from the single vacancy fractional charge, and depend on the spatial configuration of all vacancies. Their value is determined by integrating the charge density deduced from the ansatz Eq. (22) for the zero energy eigenfunctions, over two lattice spacings around the vacancy.

$\psi(\boldsymbol{r}) = \left(\psi^A \;\; \psi^B\right)^T$, with $\psi^{A,B}$ being quantum amplitudes on T_A and T_B respectively at a coarse grained position $\boldsymbol{r}$. The spectrum of H spans the continuum, but positive and negative parts can be mapped one onto the other, a symmetry expressed by

$$\{H, \sigma_z\} = 0\,, \tag{3}$$

and hereafter called chiral, which is a consequence of the bipartite structure of the lattice. Moreover, the honeycomb lattice is invariant under spatial inversion $\boldsymbol{r} \mapsto -\boldsymbol{r}$ which decomposes into two mirror symmetries where parity,

$$x \mapsto x,\; y \mapsto -y, H \mapsto \sigma_x H \sigma_x, \tag{4}$$

exchanges the two sublattices T_A and T_B.

The vacuum charge density,

$$\rho(\boldsymbol{r}) = -e \sum_{n, E_n<0} \psi_n^\dagger(\boldsymbol{r})\,\psi_n(\boldsymbol{r}) + e \sum_{n, E_n<0} \psi_n^\dagger(\boldsymbol{r})\,\psi_n(\boldsymbol{r})\Big|_{\text{free}}, \tag{5}$$

corresponds to the particle density associated with electrons filling all the negative energy states relative to the same quantity in absence of any potentials. Utilizing the completeness relation $\rho(\boldsymbol{r})$ takes the symmetric form[45,46],

$$\rho(\boldsymbol{r}) = \frac{e}{2}\sum_n \mathrm{sign}(E_n)\,\psi_n^\dagger(\boldsymbol{r})\,\psi_n(\boldsymbol{r})\,. \tag{6}$$

For an infinite system, the charge density $\rho(\boldsymbol{r})$ is a total divergence (see[46,47] and Supplementary Note 2),

$$\rho(\boldsymbol{r}) = \frac{e}{2}\,\mathrm{sign}(M)\,\boldsymbol{\nabla}\cdot\boldsymbol{\Delta}(\boldsymbol{r}) \tag{7}$$

where the regularising mass parameter $M \to 0$ removes the sign ambiguity in (6) in the presence of zero modes. The ambiguity associated with $E = 0$ results from the necessity to determine whether or not $E = E_F = 0$ states are occupied or not. The introduction of a small mass term is one way to regularize this ambiguity. The mass term shifts the zero modes to $\pm M$ which, depending on

the sign, discriminates between occupying the zero modes or not. The matrix element

$$\boldsymbol{\Delta}(\boldsymbol{r}) \equiv \frac{1}{2}\langle \boldsymbol{r}| \operatorname{tr}\big(\boldsymbol{\sigma}\sigma_z \frac{1}{H - i0}\big)|\boldsymbol{r}\rangle \tag{8}$$

is a two-dimensional vector and "tr" is over spinor indices.

Despite being defined over the entire energy spectrum, $\rho(\boldsymbol{r})$ turns out to be related to a quantity evaluated at the Fermi energy, a noteworthy result since (2) is merely valid close to $E = 0$. Furthermore, (7) is directly related to features of the zero-energy subspace. Its dimension, $\dim\ker D + \dim\ker D^\dagger$, obtained by counting all solutions of $D\psi_B = D^\dagger\psi_A = 0$, cannot generally be determined, but the relation,

$$\operatorname{Index} H = -\operatorname{sign}(M) \int d\boldsymbol{r}\, \boldsymbol{\nabla}\cdot\boldsymbol{\Delta}(\boldsymbol{r}) \tag{9}$$

holds for $\operatorname{Index} H \equiv \dim\ker D - \dim\ker D^\dagger$[45,46]. Combining (7) and (9) leads to

$$Q \equiv \int d\boldsymbol{r}\rho(\boldsymbol{r}) = -\frac{e}{2}\operatorname{Index} H\,. \tag{10}$$

In the absence of vacancies, there are no zero modes thus $\operatorname{Index} H$ vanishes and so does the charge Q and $\rho(\boldsymbol{r})$. However, this may not be the case in the presence of vacancies.

III. SCATTERING DESCRIPTION OF SINGLE VACANCY

The removal of one carbon atom creates a neutral vacancy, here arbitrarily assigned to be an A-vacancy[48]. The corresponding excitation spectrum in the continuum limit is obtained by considering scattering solutions of the Dirac Hamiltonian (2) on a plane with a puncture of radius R. Generically, the spectral imprint of a small defect is expected to be significant only near zero energy, which is consistent with the Dirac picture. Since $\rho(\boldsymbol{r})$ depends on the behaviour at zero energy, we look for zero modes, i.e., solutions of $D\psi_B = D^\dagger\psi_A = 0$. The general solution is

$$\psi(r,\theta) \equiv \sum_{m\in\mathbb{Z}} e^{im\theta}\begin{pmatrix}\psi_m^A(r)\\ i\psi_m^B(r)e^{i\theta}\end{pmatrix} \tag{11}$$

with $\psi_m^A(r) = A_m r^m$, $\psi_m^B(r) = B_m r^{-m-1}$ and (A_m, B_m) constants. Requiring $\psi(r\to\infty,\theta) = 0$, we keep harmonics $m < 0$ for $\psi_m^A(r)$ and $m \geq 0$ for $\psi_m^B(r)$.

A. Chiral boundary conditions

We choose appropriate boundary conditions on the scattering potential so as to preserve chiral symmetry (3), a necessary condition to use expressions (7)–(10).

Table I. **Boundary condition.** Boundary conditions for an A/B-vacancy imposed on the radial components $\psi_m^{A,B}$. The conditions differ only for $m = 0, -1$ ($j = \pm 1/2$).

	A-vacancy		B-vacancy	
m	$\psi_m^A(R)$	$\psi_m^B(R)$	$\psi_m^A(R)$	$\psi_m^B(R)$
≤ -2	0		0	
-1	0			0
0	0			0
≥ 1		0		0

Local boundary conditions e.g., Dirichlet, $\psi(\boldsymbol{r})|_{\text{vac}} = 0$ lead either to an over determination or to particle-hole pair creation (Neumann)[49]. We propose instead a new set of chiral boundary conditions,

$$\begin{aligned}\psi_m^A(r=R) &= 0, \quad m \leq 0,\\ \psi_m^B(r=R) &= 0, \quad m > 0,\end{aligned} \tag{12}$$

a close relative of non-local boundary conditions introduced in the study of Index theorems for Dirac operators[50–52]. This choice (12) preserves the chiral symmetry and thereby represent a perfectly reflecting barrier of probability density (Supplementary Note 3). Implemented on the power law wave function (11), conditions (12) uniquely lead to a single zero mode

$$\psi(\boldsymbol{r}) \equiv \begin{pmatrix}0\\ iB_0 e^{i\theta}/r\end{pmatrix} \tag{13}$$

by projecting onto the $m = 0$ subspace for $\psi_m^B(r)$ and having $\psi_m^A \equiv 0$. It is worth noting that this eigenfunction reproduces the tight binding result[3] justified by the absence of any characteristic scale. This zero mode is quasi-bound, that is, decaying but non-normalizable and thus appears as a pronounced peak in the density of states at the Fermi energy. An analogous choice of boundary conditions for a B-vacancy , presented in Tab. I, leads to the single zero mode $\psi(\boldsymbol{r}) \equiv \begin{pmatrix}A_{-1}/r & 0\end{pmatrix}^T$[53].

B. Parity symmetry breaking

Chiral boundary conditions (12) do not preserve parity which in the continuous limit, corresponds to $m \leftrightarrow -m-1$, $\psi_m^A \leftrightarrow -\psi_{-m-1}^B$ and $\psi_m^B \leftrightarrow \psi_{-m-1}^A$. Indeed, unlike the parity preserving choice,

$$\begin{aligned}\psi_m^A(r=R) &= 0, \quad m > 0,\\ \psi_m^B(r=R) &= 0, \quad m \leq 0,\end{aligned} \tag{14}$$

under conditions (12), the $m = 0$ solution $\psi_0^B(r) = ie^{i\theta}/r$ does not transform into the vanishing $m = -1$ solution $\psi_{-1}^A(r)$. We thus conclude that the presence of a vacancy necessarily breaks parity and removes the $j = \pm 1/2$ degeneracy, where $j \equiv m + 1/2$. This point is particularly relevant in light of recent observation of $j = \pm 1/2$ degeneracy breaking by STM spectroscopy at a vacancy site[8].

C. Results - single vacancy

To relate the existence of the zero mode to a finite vacuum charge density as given in (9)–(10), we must directly calculate the Index in (9). To that aim, we use the regularized expression[47],

$$\text{Index}\, H = \lim_{z\to 0} \text{Tr}\left(\frac{z}{H^B+z} - \frac{z}{H^A+z}\right) \tag{15}$$

where $H^B \equiv D^\dagger D$ and $H^A \equiv DD^\dagger$. The "Tr" operation here is over all states. Hereafter we take $\text{sign}\, M \equiv 1$ in (9), thus arbitrarily fixing the sign of the charge for an A-vacancy. Extending chiral boundary conditions (12) to non-zero energy scattering states involved in (15), shows how the angular momentum contributions cancel out except for $j = \pm 1/2 \leftrightarrow m = -1, 0$. A thorough calculation (Supplementary Note 4) yields

$$\text{Index}\, H = -\frac{1}{2\pi R}\lim_{z\to 0}\int d\boldsymbol{r}\, \boldsymbol{\nabla}\cdot\left(\frac{K_0(\sqrt{z}r)K_1(\sqrt{z}r)}{K_0(\sqrt{z}R)K_1(\sqrt{z}R)}\hat{r}\right) \tag{16}$$

where $K_n(x)$ are the modified Bessel functions of the second kind. Integrating (16) in the region $R < r < \infty$, $0 < \theta < 2\pi$ and inserting into (10) gives

$$Q = -\frac{e}{2}\,\text{Index}\, H = -\frac{e}{2}\cdot\left(\lim_{z\to 0} 1\right) = -\frac{e}{2}\cdot 1. \tag{17}$$

The charge density $\rho(\boldsymbol{r})$ can be read off the integrand[54] in (16)

$$\rho(\boldsymbol{r}) = -\frac{e}{4\pi R}\boldsymbol{\nabla}\cdot\left(\frac{K_0(\sqrt{z}r)K_1(\sqrt{z}r)}{K_0(\sqrt{z}R)K_1(\sqrt{z}R)}\hat{r}\right). \tag{18}$$

In the limit of a pointlike vacancy, $R \to 0$, $\rho(\boldsymbol{r})$ vanishes $\forall r \neq 0$. Since $\int d\boldsymbol{r}\,\rho(\boldsymbol{r}) = -e/2$, independent of R, $\rho(\boldsymbol{r})$ can be represented by the δ-function distribution

$$\lim_{R\to 0}\rho(\boldsymbol{r}) = -\frac{1}{2\pi}\boldsymbol{\nabla}\cdot\left(\frac{e/2}{r}\hat{r}\right). \tag{19}$$

For finite R, $\rho(\boldsymbol{r})$ can be approximated from (18) with an arbitrarily small finite value of z acting as an IR cutoff. For $r\sqrt{z} \gg 1$, $\rho(r)/\rho(R) \approx \exp(-2\sqrt{z}r)$ and for $r\sqrt{z} \ll 1$, $R\sqrt{z} \ll 1$, $\rho(r)/\rho(R) \approx R^2/r^2$. Thus, the charge density decays close to the vacancy as $\sim 1/r^2$ and decays exponentially, far from the vacancy (see Fig. 2).

The resulting charge density $\rho(\boldsymbol{r})$, is thus a total divergence with a fractional vacuum charge $Q = -e/2$, localized at the boundary of the vacancy (Fig. 2, 3). The corresponding induced potential is Coulomb-like, i.e. decays as $1/r$. The same conclusions apply to a B-vacancy but with an opposite sign of the charge (Supplementary Note 4). This sign flip $Q \to -Q$ in the exchange $T_A \leftrightarrow T_B$ points to the pseudo-scalar nature of the vacuum charge. Hence a non-zero Q provides a clear signal for the breaking of parity symmetry of the ground state and the lifting of the $j = \pm 1/2$ degeneracy. Including spin degeneracy, the overall "fractional charge" is $2 \times Q = \pm e$.

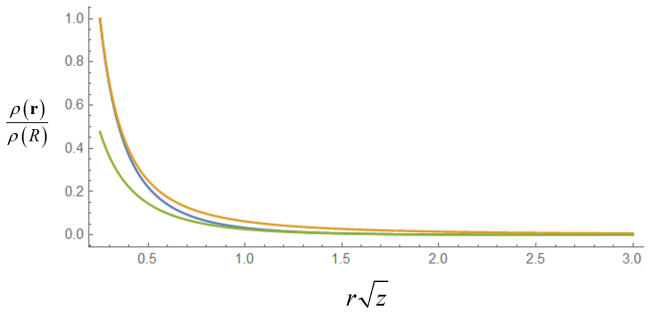

Figure 2. **Single vacancy charge density.** Blue: Characteristic behaviour of $\rho(\boldsymbol{r})/\rho(R)$ in (18) as a function of $x \equiv r\sqrt{z}$ with $y \equiv R\sqrt{z} = 0.25$. Orange: the function y^2/x^2. Green: The function $\pi y^2 e^{-2x}/x$

It is interesting to further understand the origin of this finite charge. The creation of a vacancy leads to an asymmetry between positive and negative energy states. An ill-defined albeit suggestive way to visualize it is offered by the spatial integral of (6) which together with (10) gives

$$Q = \frac{e}{2}\left(\sum_{E_n>0} 1 - \sum_{E_n<0} 1\right) = -\frac{e}{2}\,\text{Index}\, H\,. \tag{20}$$

This "spectral asymmetry", of topological origin[50], eventually amounts to a counting of zero modes only.

All together, the fractional pseudo-scalar charge, the resulting Coulomb-like potential[55] and the lifting of the $j = \pm 1/2$ degeneracy provide a comprehensive explanation to the observation of a vacancy charge and parity breaking obtained by STM measurements at a vacancy location in graphene[8]. Note that the charge density (19) does not display otherwise expected Friedel-like oscillations for the screening of a scalar charge. This is yet another indication of the topological nature of the charge expressed by a finite Index (10), resulting only from the choice of boundary conditions (12) and insensitive to both perturbations and specific features of large energy dispersion law. These findings constitute an original example of a non-zero Index in an open space, independent of the existence of an underlying gauge field (above one spatial dimension). A finite Q thus describes the physics of a topological defect.

IV. MULTIPLE VACANCIES AND TOPOLOGICAL SWITCH

We now generalize the previous results to arbitrary configurations of a finite number of isolated vacancies. The zero mode wave functions are now difficult to obtain primarily due to multiple scattering between vacancies and the lack of rotational symmetry. Since the size of

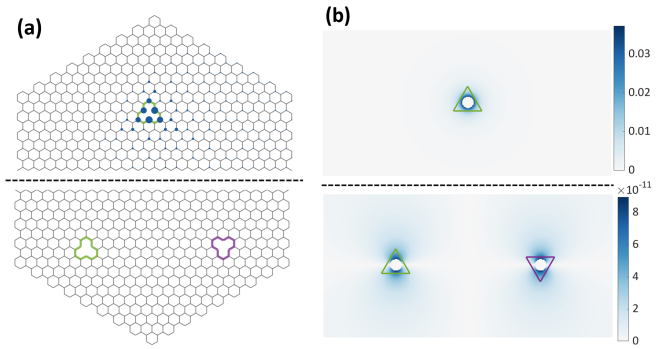

Figure 3. **Charge of vacancy configurations. Top:** Single A-vacancy ($N_A = 1$, $N_B = 0$). There is one zero mode, Index $H = |N_A - N_B| = 1$ and a finite fractional charge $Q = e/2$. **Bottom:** $N_A = N_B = 1$. Adding a B-vacancy, the zero mode disappears, Index $H = |N_A - N_B| = 0$, and so does the fractional charge on both vacancy locations represented for visual aid, by the green (A-vacancy) and purple (B-vacancy) outlines. **(a)** Tight binding calculation of the spatial charge density $|\rho(\boldsymbol{r})|$ obtained from definition Eq. (6) and depicted by the blue spots. The total charge in a two lattice spacing radius is $Q \approx 10^{-1}$ (in units of $e/2$) for the single vacancy (Top) and $Q_{\triangle}$, $Q_{\triangledown} \approx 10^{-8}$ for $N_A = N_B = 1$ (Bottom). A small positive mass term $M \approx +10^{-9}$ has been used together with armchair boundary conditions which suppress charge accumulation on the boundary (Supplementary Note 5). **(b)** Continuous Dirac model calculation of the spatial charge density $|\rho(\boldsymbol{r})|$ for the same situations as in **(a)**. These results are obtained using low energy scattering theory (Supplementary Note 6). Note the different scales displayed on the right color code.

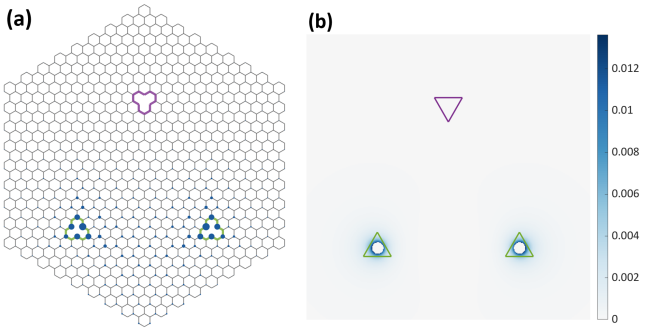

Figure 4. **Configuration of three vacancies $N_A = 2$, $N_B = 1$.** There is one zero mode, Index $H = |N_A - N_B| = 1$, so that the two A-vacancies (green upward outline) have a finite and equal charge $Q_{\blacktriangle}$ in this symmetric configuration and the B-vacancy (purple downward outline) is not charged $Q_{\triangledown} = 0$. **(a)** Tight binding calculation of the spatial charge density $|\rho(\boldsymbol{r})|$ obtained from definition Eq. (6) and depicted by the blue spots. The total charge is $Q_{\blacktriangle} \approx 10^{-1}$ (in units of $e/2$) and $Q_{\triangledown} \approx 10^{-4}$ on each A,B vacancy respectively. A small positive mass term $M \approx +10^{-9}$ has been used together with armchair boundary conditions which suppress charge accumulation on the boundary (Supplementary Note 5). **(b)** Continuous Dirac model calculation of the spatial charge density $|\rho(\boldsymbol{r})|$ for the same situation as in **(a)**. These results are obtained using low energy scattering theory (Supplementary Note 6). The homogeneous purple region around the A-vacancies is $\approx 10^{-5}$.

each vacancy is the lattice spacing, we assume constant wave function along the boundary of each vacancy making them point-like scatterers[56]. Starting from the zero mode eigenfunctions,

$$\psi_{\blacktriangle}(z) = \frac{1}{z^* - z_A^*}\begin{pmatrix}0\\1\end{pmatrix}, \quad \psi_{\blacktriangledown}(z) = \frac{1}{z - z_B}\begin{pmatrix}1\\0\end{pmatrix} \tag{21}$$

established for a single A or B-vacancy located in $z_{A,B}$, we propose the ansatz,

$$\psi_N(z) = \begin{pmatrix}0\\1\end{pmatrix}\sum_{k=1}^{N_A}\frac{q_{kA}}{z^* - z_{kA}^*} + \begin{pmatrix}1\\0\end{pmatrix}\sum_{k=1}^{N_B}\frac{q_{kB}}{z - z_{kB}} \tag{22}$$

for a configuration of $N = N_A + N_B$ vacancies located in $z_{kA,kB}$'s. This spinor wavefunction $\psi_N \equiv \begin{pmatrix}\psi_N^A & \psi_N^B\end{pmatrix}^T$ reproduces all the single vacancy features previously obtained by means of chiral boundary conditions (12), provided we require $\psi_N^A(z_{kA}) = \psi_N^B(z_{kB}) = 0$. The resulting constraints on the parameters $q_{kA,kB}$ take the matrix form,

$$M\boldsymbol{q}_B = 0, \quad M^\dagger \boldsymbol{q}_A = 0, \tag{23}$$

where $M_{ij} = (z_{iA} - z_{jB})^{-1}$ is a $N_A \times N_B$ Cauchy matrix of full rank $\forall z_{iA}, z_{jB}$[57]. Assuming, without loss of generality, that $N_A \geq N_B$, then $\operatorname{rank} M = \operatorname{rank} M^\dagger = N_B$ and the solution of $M\boldsymbol{q}_B = 0$ becomes the trivial one $\boldsymbol{q}_B = 0$, while $M^\dagger \boldsymbol{q}_A = 0$ has $N_A - N_B$ independent solutions, i.e., $|N_A - N_B|$ zero modes for arbitrary N_A, N_B. As expected, this result coincides with the number of zero modes proven to exist in any vacancy filled bipartite lattice[1–5]. Moreover, for $N_A \geq N_B$, all the zero modes fulfill $\psi_N^A \equiv 0$ and $D\psi_N^B = 0$, thus, for a multi-vacancy configuration, Index = # of zero modes = $N_A - N_B$.

We now dwell on cases which illustrate the underlying topological features of many-vacancy configurations, starting from a single A-vacancy ($N_A = 1$) (Fig. 3). A zero mode appears associated to Index $H = N_A = 1$, together with a vacuum charge $Q = -(1/2)e$ localized at the vacancy site and a broken parity symmetry. Adding a B-vacancy (Fig. 3) implies Index $H = |N_A - N_B| = 0$ so that the charge vanishes at each vacancy location and parity symmetry is restored.

Adding yet another A-vacancy remarkably changes the situation since Index $H = |N_A - N_B| = 1$ and parity symmetry is again broken. Each A-vacancy now holds a finite charge $Q_{\blacktriangle}$ smaller than $(1/2)e$ which depends on the exact spatial configuration. The B-vacancy carries no charge, $Q_{\triangledown} = 0$, a direct consequence of the vanishing of $\boldsymbol{q}_B$ in (23). These results, displayed in Fig. 4, have a surprising generalisation. Consider a $N_A - N_B = 1$ configuration where all the A-vacancies are charged ($Q_{\blacktriangle}$) and the B-vacancies necessarily uncharged ($Q_{\triangledown}$). Adding a B-vacancy wherever in the plane markedly changes this picture by switching off all the charges in the plane

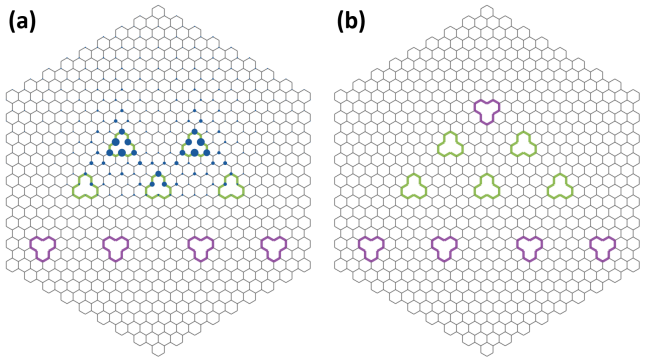

Figure 5. **Topological switch. (a)** $N_A = 5$, $N_B = 4$. In that initial configuration, Index $H = |N_A - N_B| = 1$ so that all A-vacancies are switched on with charges $Q_{\blacktriangle}$ (green upward outline) and B-vacancies are switched off, $Q_{\triangledown} \equiv 0$ (purple downward outline). **(b)** $N_A = 5$, $N_B = 5$. Adding a single B vacancy at a remote place switches off all the charges of the A-vacancies since Index $H = |N_A - N_B| = 0$. This multi-charge switching on and off is of topological nature. The spatial charge density $|\rho(\boldsymbol{r})|$ is obtained from tight binding calculations and depicted by the blue spots. The finite charges are $Q_{\blacktriangle} \approx 10^{-1} - 10^{-2}$ (in units of $e/2$) on each A-vacancy and $Q_{\triangledown} \approx 10^{-8}$ on each B-vacancy in **(a)**, and $Q_{\triangle}$, $Q_{\triangledown} \approx 10^{-8}$ in **(b)**. A small positive mass term $M \approx +10^{-9}$ has been used together with armchair boundary conditions which suppress charge accumulation on the boundary (Supplementary Note 5).

$(Q_{\triangle}, Q_{\triangledown})$. This feature, illustrated in Fig. 5, can be viewed as a topological switch, where the creation of one remote vacancy of the right kind switches off, at once, all the finite charges $Q_{\blacktriangle}$ on the graphene lattice. This effect, of topological origin, is independent of the relative position of the vacancies and results only from the vanishing of the overall Index.

V. DISCUSSION

The physics of a charged vacancy presented here, bears essential similarities with $2+1$ quantum electrodynamics (QED), such as fermion number fractionalisation and parity anomaly[26–42]. In the latter case, a dynamical external gauge field induces zero modes of massless planar fermions and vacuum charge with abnormal parity. The Index of the corresponding Dirac operator follows (10) and acquires non-zero values proportional to the strength of the gauge field. Hence, the present results provide, for graphene, a measurable realization of these QED effects with the topological content of the gauge field now replaced by vacancies with properly chosen boundary conditions. Furthermore, our findings display a coherent description of existing measurements[6,8] and provide additional predictions that can be tested with an appropriate experimental control on vacancy configurations. Including spin degrees of freedom in the Dirac picture and using Lieb's theorem[2] may enrich the picture presented here by associating to a vacancy the quantum dynamics of a localized vacuum spin which is proportional to the Dirac Index. Possible connections to recent observations of vacancy magnetic moments[11–15] should be investigated together with a generalisation to other bipartite lattices and to non-isolated vacancies. The notion of topological switch involves different and somehow unusual algebraic rules, e.g., $3Q_{\blacktriangle} + 2Q_{\triangledown} = 3Q_{\blacktriangle}$ but $Q_{\triangledown} + (3Q_{\blacktriangle} + 2Q_{\triangledown}) = 0$, which may have applications in logic circuit.

Acknowledgements. This work was supported by the Israel Science Foundation Grant No. 924/09.

* eric@physics.technion.ac.il

1. B. Sutherland, Phys. Rev. B **34**, 5208 (1986).
2. E. H. Lieb, Phys. Rev. Lett. **62**, 1201 (1989).
3. V. M. Pereira, F. Guinea, J. M. B. Lopes dos Santos, N. M. R. Peres, and A. H. Castro Neto, Phys. Rev. Lett. **96**, 036801 (2006).
4. V. M. Pereira, J. M. B. Lopes dos Santos, and A. H. Castro Neto, Phys. Rev. B **77**, 115109 (2008).
5. B. R. K. Nanda, M. Sherafati, Z. S. Popovi, and S. Satpathy, New J. Phys. **14**, 083004 (2012).
6. J. Mao, Y. Jiang, D. Moldovan, G. Li, K. Watanabe, T. Taniguchi, M. R. Masir, F. M. Peeters, and E. Y. Andrei, Nat. Phys. **12**, 545 (2016).
7. Y. Liu, M. Weinert, and L. Li, Nanotechnology **26**, 035702 (2015).
8. O. Ovdat, J. Mao, Y. Jiang, E. Y. Andrei, and E. Akkermans, Nat. Commun. **8**, 507 (2017).
9. M. Inui, S. A. Trugman, and E. Abrahams, Phys. Rev. B **49**, 3190 (1994).
10. J. J. Palacios, J. Fernández-Rossier, and L. Brey, Phys. Rev. B **77**, 195428 (2008).
11. H. Padmanabhan and B. R. K. Nanda, Phys. Rev. B **93**, 165403 (2016).
12. Y. Jiang, P.-W. Lo, D. May, G. Li, G.-Y. Guo, F. B. Anders, T. Taniguchi, K. Watanabe, J. Mao, and E. Y. Andrei, Nature communications **9**, 2349 (2018).
13. M. V. Ulybyshev and M. I. Katsnelson, Phys. Rev. Lett. **114**, 246801 (2015).
14. M. M. Ugeda, I. Brihuega, F. Guinea, and J. M. Gómez-Rodríguez, Phys. Rev. Lett. **104**, 096804 (2010).
15. A. M. Valencia and M. J. Caldas, Phys. Rev. B **96**, 125431 (2017).
16. V. Häfner, J. Schindler, N. Weik, T. Mayer, S. Balakrishnan, R. Narayanan, S. Bera, and F. Evers, Phys. Rev. Lett. **113**, 186802 (2014).
17. N. M. R. Peres, F. Guinea, and A. H. Castro Neto, Phys. Rev. B **73**, 125411 (2006).
18. N. Weik, J. Schindler, S. Bera, G. C. Solomon, and F. Evers, Phys. Rev. B **94**, 064204 (2016).
19. A. V. Shytov, M. I. Katsnelson, and L. S. Levitov, Phys. Rev. Lett. **99**, 236801 (2007).

[20] A. V. Shytov, M. I. Katsnelson, and L. S. Levitov, Phys. Rev. Lett. **99**, 246802 (2007).
[21] V. M. Pereira, J. Nilsson, and A. H. Castro Neto, Phys. Rev. Lett. **99**, 166802 (2007).
[22] M. M. Fogler, D. S. Novikov, and B. I. Shklovskii, Phys. Rev. B **76**, 233402 (2007).
[23] R. R. Biswas, S. Sachdev, and D. T. Son, Phys. Rev. B **76**, 205122 (2007).
[24] E. B. Kolomeisky, J. P. Straley, and H. Zaidi, Phys. Rev. B **88**, 165428 (2013).
[25] D. P. DiVincenzo and E. J. Mele, Phys. Rev. B **29**, 1685 (1984).
[26] R. Jackiw and C. Rebbi, Phys. Rev. D **13**, 3398 (1976).
[27] A. J. Heeger, S. Kivelson, J. R. Schrieffer, and W. P. Su, Rev. Mod. Phys. **60**, 781 (1988).
[28] R. Jackiw and J. Schrieffer, Nuclear Physics B **190**, 253 (1981).
[29] A. N. Redlich, Phys. Rev. Lett. **52**, 18 (1984).
[30] A. J. Niemi and G. W. Semenoff, Phys. Rev. Lett. **51**, 2077 (1983).
[31] A. J. Niemi and G. W. Semenoff, Phys. Rev. D **32**, 471 (1985).
[32] D. Boyanovsky and R. Blankenbecler, Phys. Rev. D **31**, 3234 (1985).
[33] R. Blankenbecler and D. Boyanovsky, Phys. Rev. D **31**, 2089 (1985).
[34] R. Blankenbecler and D. Boyanovsky, Phys. Rev. D **34**, 612 (1986).
[35] R. Jackiw, Phys. Rev. D **29**, 2375 (1984).
[36] T. Jaroszewicz, Phys. Rev. D **34**, 3128 (1986).
[37] C. R. Hagen, Phys. Rev. Lett. **64**, 503 (1990).
[38] G. W. Semenoff, Phys. Rev. Lett. **53**, 2449 (1984).
[39] F. D. M. Haldane, Phys. Rev. Lett. **61**, 2015 (1988).
[40] E. Fradkin, E. Dagotto, and D. Boyanovsky, Phys. Rev. Lett. **57**, 2967 (1986).
[41] C. Chamon, C.-Y. Hou, R. Jackiw, C. Mudry, S.-Y. Pi, and G. Semenoff, Phys. Rev. B **77**, 235431 (2008).
[42] R. Jackiw and G. Semenoff, Phys. Rev. Lett. **50**, 439 (1983).
[43] V. N. Kotov, B. Uchoa, V. M. Pereira, F. Guinea, and A. H. Castro Neto, Rev. Mod. Phys. **84**, 1067 (2012).
[44] D. C. Elias, R. V. Gorbachev, A. S. Mayorov, S. V. Morozov, A. A. Zhukov, P. Blake, L. A. Ponomarenko, I. V. Grigorieva, K. S. Novoselov, F. Guinea, and A. K. Geim, Nature Physics **7**, 701 (2011).
[45] M. Stone, Phys. Rev. B **31**, 6112 (1985).
[46] A. J. Niemi and G. W. Semenoff, Phys. Rev. D **30**, 809 (1984).
[47] C. Callias, Commun. Math. Phys. **62**, 213 (1978).
[48] In the presence of a defect, the Dirac points K and K' may be coupled, which is inconsistent with the continuum Dirac equation. Nevertheless, for the case of a vacancy, we neglect this coupling, an assumption justified a posteriori both numerically and from the long range behaviour of the resulting vacancy potential[58].
[49] M. V. Berry and R. J. Mondragon, Proc. Royal Soc. A **412**, 53 (1987).
[50] M. F. Atiyah, V. K. Patodi, and I. Singer, in *Mathematical Proceedings of the Cambridge Philosophical Society*, Vol. 77 (Cambridge University Press, 1975) pp. 43–69.
[51] E. Akkermans and R. Narevich, Philos. Mag. B **77**, 1097 (1998).
[52] E. Akkermans, J. Avron, R. Narevich, and R. Seiler, Eur. Phys. J. B **1**, 117 (1998).
[53] There exists alternative choices of chiral boundary conditions e.g., by projecting the zero modes onto a different angular momentum subspace. However, this would yield a zero mode decaying faster than $1/r$ and with a dimension-full strength.
[54] Note that it is not allowed to move the $\lim_{z\to 0}$ through the integral in (16).
[55] The sign of the Coulomb potential depends on sign M and whether the vacancy is from sublattice T_A or T_B. The resulting spectrum remains unchanged in either case but will represent particle or hole states accordingly.
[56] Y. N. Demkov and V. N. Ostrovskii, *Zero-range potentials and their applications in atomic physics* (Springer Science & Business Media, 2013).
[57] P. J. Davis, "Interpolation and approximation," (Dover publications, 1975) pp. 268–269.
[58] T. Ando and T. Nakanishi, Journal of the Physical Society of Japan **67**, 1704 (1998).

Supplementary Material

Vacancies in Graphene: Dirac Physics and Fractional Vacuum Charges

Omrie Ovdat, Yaroslav Don, and Eric Akkermans*

Department of Physics, Technion – Israel Institute of Technology, Haifa 3200003, Israel

Supplementary Note 1: Validity of the model with respect to electron electron interactions

Close to the Dirac point, namely $|Ea| \ll 1$ where a is the lattice spacing, electron-electron interactions lead to logarithmic corrections to the effective Fermi velocity which render the effective Coulomb coupling marginally irrelevant $\alpha\left(ka \to 0\right) \sim 1/\ln\left(1/ka\right)$ [1, 2]. As a result, low energy quasi-particle excitations in graphene are well approximated by non-interacting 2D massless Dirac fermions with a renormalized Fermi velocity.

We describe vacancies as scattering objects with a range $R \sim a$. Any significant spectral signal of these defects will thus appear for $|E| \lesssim 1/a$ consistent with the effective low energy regime of graphene. Hence, the physics of vacancies is well described within this regime by low E Dirac particle scattering. Most importantly, since $\alpha\left(ka \to 0\right) \ll 1$, electron-electron interactions will have an approximate effect at low energy so that both the vacuum vacancy charge and the zero modes are not affected by interactions.

The effect of interactions would be to re-shuffle the distribution of charge around the vacancies to reduce the energy of the system. Without interactions and for a vacancy configuration with $|N_{\mathrm{A}} - N_{\mathrm{B}}|$ zero modes, the ground state is $4^{|N_{\mathrm{A}} - N_{\mathrm{B}}|}$ degenerate (including spin). As proven by E. Lieb in [3] for the case of a repulsive Hubbard model, interactions will remove this degeneracy and single-out specific superpositions of these modes characterizing the energetically favourable states.

Experimental observation provide further support of these assertions. Evidence for the robustness of the Dirac point and the renormalization of the Fermi velocity was found in [2]. In an earlier work [4], we provide evidence for the existence of a single vacancy charge and the associated zero mode. The measured

*eric@physics.technion.ac.il

low energy spectra at the vacancy site is in excellent agreement with the predictions based on a free massless Dirac field in the presence of an external $1/r$ Coulomb potential. The appearance of a vacancy zero mode and its $|\psi|^2 \sim 1/r^2$ spatial profile have also been confirmed in [5].

For the case of multiple vacancies, in may suggested that Coulomb repulsion between charge lumps around vacancies would invalidate the possibility for them to mutually exist. However, if each charge lump surrounding a vacancy exerts a potential which decays as $1/r$ away from it, the strength of the electrostatic interaction diminishes by an order of magnitude at a distance of 10 lattice spacings from the vacancy. Experimental evidence support this argument (see Fig. 4a in [6] and also [5]) where it is observed that the DOS resonances associated with a single vacancy Coulomb potential vanish at a distance of $\approx$ 10nm. Therefore, in any case, the effect of mutually repulsive electrostatic interaction between the vacancy charges would be insignificant in all but a limited set of tight vacancy configurations.

Supplementary Note 2: Relation between vacuum charge and Index H

In what follows we show the relation, presented in the main text, between the vacuum charge density $\rho(\boldsymbol{r})$ and the divergence of the vector matrix element $\boldsymbol{\Delta}(\boldsymbol{r}) \equiv \frac{1}{2}\left\langle \boldsymbol{r} \right| \mathrm{tr}\left(i\boldsymbol{\sigma}\sigma_z \frac{1}{H-i0}\right) \left| \boldsymbol{r} \right\rangle$.

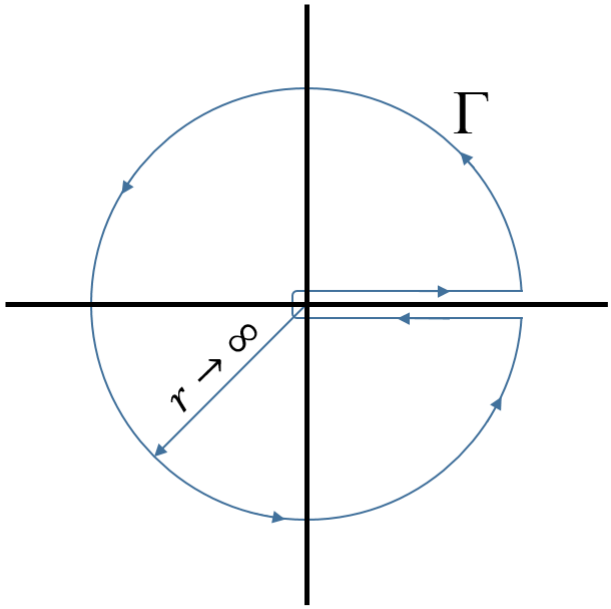

Figure 1: **Integration contour.** Contour of integration performed in (4)

As shown in [7, 8]

$$\begin{aligned}\rho(\boldsymbol{r}) &= \frac{e}{2}\sum_n \operatorname{sign}(E_n)\,\psi_n^\dagger(\boldsymbol{r})\,\psi_n(\boldsymbol{r}) \\ &= M\frac{e}{\pi}\lim_{s\to 0^+}\cos\left(\frac{\pi s}{2}\right)\int_0^\infty d\omega\omega^{-s}\frac{1}{M^2+\omega^2}\Omega\left(\boldsymbol{r},\sqrt{M^2+\omega^2}\right)\end{aligned} \tag{1}$$

where $e>0$,

$$\Omega(\boldsymbol{r},z) \equiv -iz\left\langle \boldsymbol{r}\left|\operatorname{tr}\left(\sigma_z\left(H-iz\right)^{-1}\right)\right|\boldsymbol{r}\right\rangle, \tag{2}$$

$H=-i\boldsymbol{\sigma}\cdot\boldsymbol{\nabla}$ and M is a regularising mass parameter. Using contour integration we can calculate the above integral. Since $\sqrt{M^2+\omega^2}>0$, $f(\omega)\equiv\Omega\left(\boldsymbol{r},\sqrt{M^2+\omega^2}\right)$ is exponentially decaying for $\omega\to\infty$, has no poles and obeys $f(-\omega)=f(\omega)$. Consider the integral

$$I=\int_0^\infty d\omega\,\omega^{-s}\frac{1}{M^2+\omega^2}f(\omega). \tag{3}$$

The function $z^{-s}=e^{-s\log z}\equiv re^{i\theta}$ has a branch cut that can be defined on the positive real line with $0<\theta<2\pi$. The poles of $\left(M^2+\omega^2\right)$ are at $\omega=\pm i|M|$. Integrating over the contour Γ shown in supplementary Fig. 1 and using the residue theorem

$$\begin{aligned}\oint_\Gamma dz\,z^{-s}\frac{1}{M^2+z^2}f(z) &= \frac{\pi}{|M|}\left(i|M|\right)^{-s}f\left(i|M|\right)\left(1-e^{-i\pi s}\right) \\ &= \left(1-e^{-2\pi i s}\right)I\end{aligned} \tag{4}$$

thus

$$I=\frac{\pi}{2|M|^{s+1}\cos\frac{\pi s}{2}}\lim_{z\to 0}\Omega(\boldsymbol{r},z) \tag{5}$$

and

$$\begin{aligned}\rho(\boldsymbol{r}) &= M\frac{e}{\pi}\lim_{s\to 0^+}\cos\left(\frac{\pi s}{2}\right)\left(\frac{\pi}{2|M|^{s+1}\cos\frac{\pi s}{2}}\lim_{z\to 0}\Omega(\boldsymbol{r},z)\right) \\ &= \frac{e}{2}\operatorname{sign}M\lim_{z\to 0}\Omega(\boldsymbol{r},z).\end{aligned} \tag{6}$$

Using the identity [7, 9]

$$\Omega(\boldsymbol{r},z)=\frac{1}{2}\boldsymbol{\nabla}\cdot\left\langle\boldsymbol{r}\left|\operatorname{tr}\left(i\boldsymbol{\sigma}\sigma_z\frac{1}{H-iz}\right)\right|\boldsymbol{r}\right\rangle \tag{7}$$

we obtain the alternative form

$$\rho(\boldsymbol{r})=\frac{e}{2}\operatorname{sign}(M)\,\boldsymbol{\nabla}\cdot\boldsymbol{\Delta}(\boldsymbol{r}). \tag{8}$$

Supplementary Note 3: Most general boundary condition of an non-penetrable circular wall

In what follows we derive the analogue of the 'mixed boundary condition' for the case of the Dirac Hamiltonian.

Consider the free Dirac Hamiltonian $H = \boldsymbol{\sigma} \cdot \boldsymbol{p}$. The matrix element of the difference $H - H^\dagger$ is a boundary term

$$\begin{aligned}\langle g| \left(H - H^\dagger\right) |f\rangle &= \int d\boldsymbol{r}\, g\left(\boldsymbol{r}\right)^\dagger \left(-i\boldsymbol{\sigma} \cdot \boldsymbol{\nabla} f\left(\boldsymbol{r}\right)\right) - \int d\boldsymbol{r}\, \left(-i\boldsymbol{\sigma} \cdot \boldsymbol{\nabla} g\left(\boldsymbol{r}\right)\right)^\dagger f\left(\boldsymbol{r}\right) \\ &= -i \int d\boldsymbol{S} \cdot \left(g\left(\boldsymbol{r}\right)^\dagger \boldsymbol{\sigma} f\left(\boldsymbol{r}\right)\right). \end{aligned} \tag{9}$$

In terms of Dirac gamma matrices, $H = \boldsymbol{\sigma} \cdot \boldsymbol{p} = \gamma^0 \gamma^i p^i$, thus

$$\left\langle \psi \,\middle|\, \left(H - H^\dagger\right) \,\middle|\, \psi \right\rangle = -i \int dS^i \left(\bar{\psi}\left(\boldsymbol{r}\right) \gamma^i \psi\left(\boldsymbol{r}\right)\right) \tag{10}$$

which is proportional to the current density. To impose $H = H^\dagger$ we a require a boundary condition on all eigenfunctions of H such that (9) vanishes. The corresponding boundary thus represents a perfect reflector of probability current density. For the case of a circular boundary of radius R around the origin

$$\begin{aligned}\left\langle g \,\middle|\, \left(H - H^\dagger\right) \,\middle|\, f \right\rangle &= R \int d\theta\, g\left(\boldsymbol{r}\right)^\dagger \begin{pmatrix} 0 & e^{-i\theta} \\ e^{i\theta} & 0 \end{pmatrix} f\left(\boldsymbol{r}\right) \\ &= R \int d\theta\, \left(g^{A*}\left(\boldsymbol{r}\right) f^B\left(\boldsymbol{r}\right) e^{-i\theta} + g^{B*}\left(\boldsymbol{r}\right) f^A\left(\boldsymbol{r}\right) e^{i\theta}\right) \end{aligned} \tag{11}$$

where we used the identity $\hat{r} \cdot \boldsymbol{\sigma} = \left(\begin{smallmatrix} 0 & e^{-i\theta} \\ e^{i\theta} & 0 \end{smallmatrix}\right)$ and defined $f\left(\boldsymbol{r}\right) = \left(\begin{smallmatrix} f^A & f^B \end{smallmatrix}\right)^T$, $g\left(\boldsymbol{r}\right) = \left(\begin{smallmatrix} g^A & g^B \end{smallmatrix}\right)^T$. The general set of solutions to $H\psi = E\psi$, given in terms of polar coordinates, is spanned by the basis

$$\psi_{k,m,\lambda}\left(\boldsymbol{r}\right) = e^{im\theta} \begin{pmatrix} \psi^A_{k,m,\lambda}\left(r\right) \\ \lambda i \psi^B_{k,m,\lambda}\left(r\right) e^{i\theta} \end{pmatrix} \tag{12}$$

where $k \equiv |E|$, $\lambda \equiv \operatorname{sign} E$ and $m \in \mathbb{Z}$, $j \equiv m + 1/2$ are the orbital and total angular momentum numbers respectively. Consider the eigenfunctions $f_{k,m,\lambda}\left(\boldsymbol{r}\right), g_{k',m',\lambda'}\left(\boldsymbol{r}\right)$. The corresponding boundary term reduces to

$$\begin{aligned}\langle g| \left(H - H^\dagger\right) |f\rangle &= iR \left(\lambda g^{A*}_{k',m',\lambda'}\left(R\right) f^B_{k,m,\lambda}\left(R\right) - \lambda' g^{B*}_{k',m',\lambda'}\left(R\right) f^A_{k,m,\lambda}\left(R\right)\right) \int_0^{2\pi} d\theta\, e^{i\left(m-m'\right)\theta} \\ &= 2\pi i R \delta_{mm'} \left(\lambda g^{A*}_{k',m',\lambda'}\left(R\right) f^B_{k,m,\lambda}\left(R\right) - \lambda' g^{B*}_{k',m',\lambda'}\left(R\right) f^A_{k,m,\lambda}\left(R\right)\right). \end{aligned} \tag{13}$$

For all eigenfunctions, we take the boundary conditions $\psi^A_{k,m,\lambda}/\psi^B_{k,m,\lambda} = \lambda h_m$ where h_m is some real, energy independent number, then

$$\left\langle g \left| \left(H - H^\dagger\right) \right| f \right\rangle = 2\pi i R \lambda \lambda' \delta_{mm'} \left(h_{m'} - h_m\right) g^{B*}_{k',m',\lambda'}(R) f^B_{k,m,\lambda}(R) = 0. \tag{14}$$

Supplementary Note 4: The charge density in the presence of a single vacancy

In what follows, we obtain the explicit expression for the vacuum charge density in the case of a single vacancy.

As explained in the main text, the charge density is given by ($\operatorname{sign} M \equiv 1$)

$$Q = \int d\boldsymbol{r}\, \rho(\boldsymbol{r}) = -\frac{e}{2} \operatorname{Index} H. \tag{15}$$

where,

$$\operatorname{Index} H = \lim_{z\to 0} \operatorname{Tr}\left(\frac{z}{H^B + z} - \frac{z}{H^A + z}\right) \tag{16}$$

with $H^B = D^\dagger D$, $H^A = DD^\dagger$. In what follows, we use relation (16) to obtain $\operatorname{Index} H$ and consequently $\rho(\boldsymbol{r})$.

Assuming $E > 0$, $H\psi = E\psi$ is given in terms of polar coordinates by

$$-\psi^{A\prime}_m(r) + \frac{m}{r}\psi^A_m(r) = E\psi^B_m \tag{17a}$$

$$\psi^{B\prime}_m(r) + \frac{(m+1)}{r}\psi^B_m(r) = E\psi^A_m. \tag{17b}$$

where

$$\psi(\boldsymbol{r}) = \sum_{m=-\infty}^{\infty} e^{im\theta} \begin{pmatrix} \psi^A_m(r) \\ i\psi^B_m(r) e^{i\theta} \end{pmatrix}. \tag{18}$$

The set of first order equations (17) can be decoupled into two independent second order equations

$$H^A \psi^A = E^2 \psi^A \tag{19a}$$

$$H^B \psi^B = E^2 \psi^B \tag{19b}$$

where both H^A, H^B formally equal to $-\nabla^2$. Assuming the boundary conditions corresponding to an

A-vacancy (see main text), supplementary Eqs. (19) read

$$\left(-\partial_r^2-\frac{1}{r}\partial_r+\frac{m^2}{r^2}\right)\psi_m^A(r)=E^2\psi_m^A(r)\,,\quad \begin{cases}\psi_m^A(R)=0 & m\leq 0\\ \psi_m^{A\prime}(R)/\psi_m^A(R)=\frac{m}{R} & m>0\end{cases} \tag{20a}$$

$$\left(-\partial_r^2-\frac{1}{r}\partial_r+\frac{(m+1)^2}{r^2}\right)\psi_m^B(r)=E^2\psi_m^B(r)\,,\quad \begin{cases}\psi_m^{B\prime}(R)/\psi_m^B(R)=-\frac{m+1}{R} & m\leq 0\\ \psi_m^B=0 & m>0\,.\end{cases} \tag{20b}$$

The Dirichlet conditions on ψ_m^A,ψ_m^B correspond to the chiral boundary conditions proposed in the main text to describe the physics of the vacancy. Combined with the Dirac equation (17), these constrain the additional mixed boundary conditions appearing in (20). To make (20) more symmetrical we transform $m\to -m-1$ in the second equation and redefine $\psi_{-m-1}^B\to\psi_m^B$ such that

$$\left(-\partial_r^2-\frac{1}{r}\partial_r+\frac{m^2}{r^2}\right)\psi_m^A(r)=E^2\psi_m^A(r)\,,\quad \begin{cases}\psi_m^A(R)=0 & m\leq 0\\ \psi_m^{A\prime}(R)/\psi_m^A(R)=\frac{m}{R} & m>0\end{cases} \tag{21a}$$

$$\left(-\partial_r^2-\frac{1}{r}\partial_r+\frac{m^2}{r^2}\right)\psi_m^B(r)=E^2\psi_m^B(r)\,,\quad \begin{cases}\psi_m^B=0 & m<-1\\ \psi_m^{B\prime}(R)/\psi_m^B(R)=\frac{m}{R} & m\geq -1.\end{cases} \tag{21b}$$

Define $G^{A/B}(z)\equiv\frac{1}{H^{A/B}+z}$. In position space,

$$\int d\boldsymbol{r}''\,\langle\boldsymbol{r}|\,H^{A/B}+z\,|\boldsymbol{r}''\rangle\,\langle\boldsymbol{r}''|\,G^{A/B}\,|\boldsymbol{r}'\rangle=\frac{1}{r}\delta(r-r')\,\delta(\theta-\theta')\,, \tag{22}$$

or, equivalently,

$$\left(-\partial_r^2-\frac{1}{r}\partial_r-\frac{1}{r^2}\partial_\theta^2+z\right)G^{A/B}(\boldsymbol{r},\boldsymbol{r}')=\frac{1}{r}\delta(r-r')\,\frac{1}{2\pi}\sum_{m=-\infty}^{\infty}e^{im(\theta-\theta')}, \tag{23}$$

where we used the identity

$$\delta(\theta-\theta')=\frac{1}{2\pi}\sum_{m=-\infty}^{\infty}e^{im(\theta-\theta')}. \tag{24}$$

After insertion of the following expansion

$$G^{A/B}(\boldsymbol{r},\boldsymbol{r}')=\frac{1}{2\pi}\sum_{m=-\infty}^{\infty}G_m^{A/B}(r,r')\,e^{im(\theta-\theta')}, \tag{25}$$

Table 1: **Boundary condition A-vacancy.** Boundary conditions for an A-vacancy imposed on the radial components of the resolvent operators G^A, G^B. The conditions are symmetrical $\forall m \neq 0, -1$ ($\forall j \neq \pm 1/2$).

m	G^A_m	G^B_m
≤ -2	Dirichlet	Dirichlet
-1	Dirichlet	Mixed
0	Dirichlet	Mixed
≥ 1	Mixed	Mixed

supplementary Eq. (23) reduces to the set

$$\left(-\partial_r^2 - \frac{1}{r}\partial_r + \frac{m^2}{r^2} + z\right) G_m^{A/B}(r, r') = \frac{1}{r}\delta(r - r'). \tag{26}$$

Although $G_m^{A/B}(r, r')$ obey the same (trivial) equation, they are constrained to different sets of boundary conditions corresponding to (21)

$$\left(-\partial_r^2 - \frac{1}{r}\partial_r + \frac{m^2}{r^2} + z\right) G_m^A(r, r') = \frac{1}{r}\delta(r - r'), \quad \begin{cases} G_m^A(R, r') = 0 & m \leq 0 \\ \partial_r G_m^A(R, r') / G_m^A(R, r') = \frac{m}{R} & m > 0 \end{cases} \tag{27a}$$

$$\left(-\partial_r^2 - \frac{1}{r}\partial_r + \frac{m^2}{r^2} + z\right) G_m^B(r, r') = \frac{1}{r}\delta(r - r'), \quad \begin{cases} G_m^B(R, r') = 0 & m < -1 \\ \partial_r G_m^B(R, r') / G_m^B(R, r') = \frac{m}{R} & m \geq -1. \end{cases} \tag{27b}$$

The boundary conditions in (27) are symmetrical with respect to the label A, B for all $m \neq 0, -1$ ($j \neq \pm 1/2$) as shown in Tab. 1. We further require that $G_m^{A/B}(r, r')$ decay for $r, r' \to \infty$.

The solutions of (27) are given by

$$G_m^{A/B} = I_m\left(\sqrt{z} r_<\right) K_m\left(\sqrt{z} r_>\right) + \Gamma_m^{A/B} K_m\left(\sqrt{z} r\right) K_m\left(\sqrt{z} r'\right) \tag{28}$$

where $I_n(x), K_n(x)$ are the modified Bessel functions of the first and second kind, $r_< \equiv \min(r, r')$, $r_> \equiv \max(r, r')$ and $\Gamma_m^{A/B}$ are coefficients to be determined by boundary conditions. The first term in (28) is a particular solution of the non-homogeneous differential equation in (27) [10]. The second term is a solution of the corresponding homogeneous equation and is required so that (28) obeys the necessary boundary conditions. Imposing these conditions and utilizing the symmetry expressed in Tab. 1 gives

$$\Gamma_m^A = \Gamma_m^B \quad \forall m \neq 0, -1. \tag{29}$$

In addition,

$$\Gamma_0^A = -\Gamma_{-1}^B = -I_0\left(\sqrt{z}R\right)/K_0\left(\sqrt{z}R\right) \tag{30a}$$

$$\Gamma_0^B = -\Gamma_{-1}^A = I_1\left(\sqrt{z}R\right)/K_1\left(\sqrt{z}R\right), \tag{30b}$$

and

$$\Gamma_0^B - \Gamma_0^A = \Gamma_{-1}^B - \Gamma_{-1}^A = \frac{1}{\sqrt{z}RK_0(\sqrt{z}R)K_1(\sqrt{z}R)}. \tag{31}$$

Finally we arrive to

$$\begin{aligned}
\text{Index}\, H &= \lim_{z\to 0} z\ \text{Tr}\left(\frac{1}{H^B+z} - \frac{1}{H^A+z}\right) \\
&= \lim_{z\to 0} z\ \text{tr}\left(G^B - G^A\right) \\
&= \frac{z}{2\pi}\int d\boldsymbol{r}\sum_m \left(G_m^B(r,r) - G_m^A(r,r)\right) \\
&= \frac{z}{2\pi}\lim_{z\to 0}\int d\boldsymbol{r}\ \left[\left(\Gamma_0^B - \Gamma_0^A\right)K_0\left(\sqrt{z}r\right)^2 + \left(\Gamma_{-1}^B - \Gamma_{-1}^A\right)K_{-1}\left(\sqrt{z}r\right)^2\right] \\
&= \frac{z}{2\pi}\lim_{z\to 0}\left(\Gamma_0^B - \Gamma_0^A\right)\int d\boldsymbol{r}\ \left(K_0\left(\sqrt{z}r\right)^2 + K_{-1}\left(\sqrt{z}r\right)^2\right).
\end{aligned} \tag{32}$$

Inserting (31) and using the identity

$$K_0\left(\sqrt{z}r\right)^2 + K_1\left(\sqrt{z}r\right)^2 = -\frac{1}{\sqrt{z}}\boldsymbol{\nabla}\cdot\left(K_0(\sqrt{z}r)K_1(\sqrt{z}r)\hat{r}\right), \tag{33}$$

we obtain

$$\text{Index}\, H = -\frac{1}{2\pi R}\lim_{z\to 0}\int d\boldsymbol{r}\ \boldsymbol{\nabla}\cdot\left(\frac{K_0(\sqrt{z}r)K_1(\sqrt{z}r)}{K_0(\sqrt{z}R)K_1(\sqrt{z}R)}\hat{r}\right). \tag{34}$$

In the case of a B-vacancy, corresponding to the boundary conditions provided by the table in the main text, the analogue equations of $G_m^{A/B}(r,r')$ are

$$\left(-\partial_r^2 - \frac{1}{r}\partial_r + \frac{m^2}{r^2} + z\right)G_m^A(r,r') = \frac{1}{r}\delta(r-r'), \qquad \begin{cases} G_m^A(R,r') = 0 & m < -1 \\ G_m^{A\prime}(R)/G_m^A(R) = \frac{m}{R} & m \geq -1 \end{cases} \tag{35a}$$

$$\left(-\partial_r^2 - \frac{1}{r}\partial_r + \frac{m^2}{r^2} + z\right)G_m^B(r,r') = \frac{1}{r}\delta(r-r'), \qquad \begin{cases} G_m^B(R,r') = 0 & m \leq 0 \\ G_m^{B\prime}(R,r')/G_m^B(R,r') = \frac{m}{R} & m > 0\,. \end{cases} \tag{35b}$$

The boundary conditions in (35), can be summarized in Tab. 2 which is identical to Tab. 1 up to the exchange of columns $A \leftrightarrow B$. Thus, from (16) it is apparent that the calculation of the charge density will follow as in the case of the A-vacancy but with an opposite sign.

Table 2: **Boundary condition A-vacancy.** Boundary conditions for a B-vacancy imposed on the radial components of the resolvent operators G^A, G^B. The conditions are symmetrical $\forall m \neq 0, -1$ ($\forall j \neq \pm 1/2$) and are the same those presented in Tab. 1 up to the exchange of columns $A \leftrightarrow B$.

m	G^A_m	G^B_m
≤ -2	Dirichlet	Dirichlet
-1	Mixed	Dirichlet
0	Mixed	Dirichlet
≥ 1	Mixed	Mixed

Supplementary Note 5: Armchair, zigzag and periodic boundary conditions

Fig. 1a, Fig. 2a and Fig 3 in the main text are obtained from diagonalizing the matrix elements of the tight binding Hamiltonian

$$H_{\text{TB}} = -t \sum_{\langle i,j \rangle} \left(c_i^\dagger c_j + \text{H.c.} \right) + M \sum_i s_i c_i^\dagger c_i \tag{36}$$

in the one particle subspace and position space basis. In (36), the label i represents the lattice sites and $c_i^\dagger, c_j$ are creation and annihilation operators. The first term contains a sum over nearest neighbour sites and in the second term $s_i = \pm 1$ when i corresponds to a site from sublattice A, B respectively. Parameters t, M are kinetic energy and mass terms. Our lattice consists of 1302 sites with $M/t = 10^{-9}$. The presence of the mass term shifts the zero modes to sign $(N_A - N_B)$. The role of this term is to remove the ambiguity of sign E_n when $E_n = 0$ in equation 3 of the main text. Since $M/t \ll 1$, the mass term has negligible effect on the charge density compared to the $M \to 0$ limit.

We present in supplementary Fig. 2 the effects of using a zigzag edge as opposed to an armchair edge in the numerical diagonalisation of the (finite) tight binding Hamiltonian. In the presence of an open zigzag edge (supplementary Fig. 2a) some of the charge accumulates at the corresponding boundary. This effect can be removed by imposing periodic boundary conditions on this direction (supplementary Fig. 2b) or using armchair boundary conditions in all directions (as in main text).

Supplementary Note 6: The charge density in the presence of a multiple vacancies

In what follows we present the formalism of low energy scattering theory in which we obtain a closed form expression of the charge density for the case of a multi-vacancy configuration. Using this expression we were able to generate Figs. 2b, 3b of the main text.

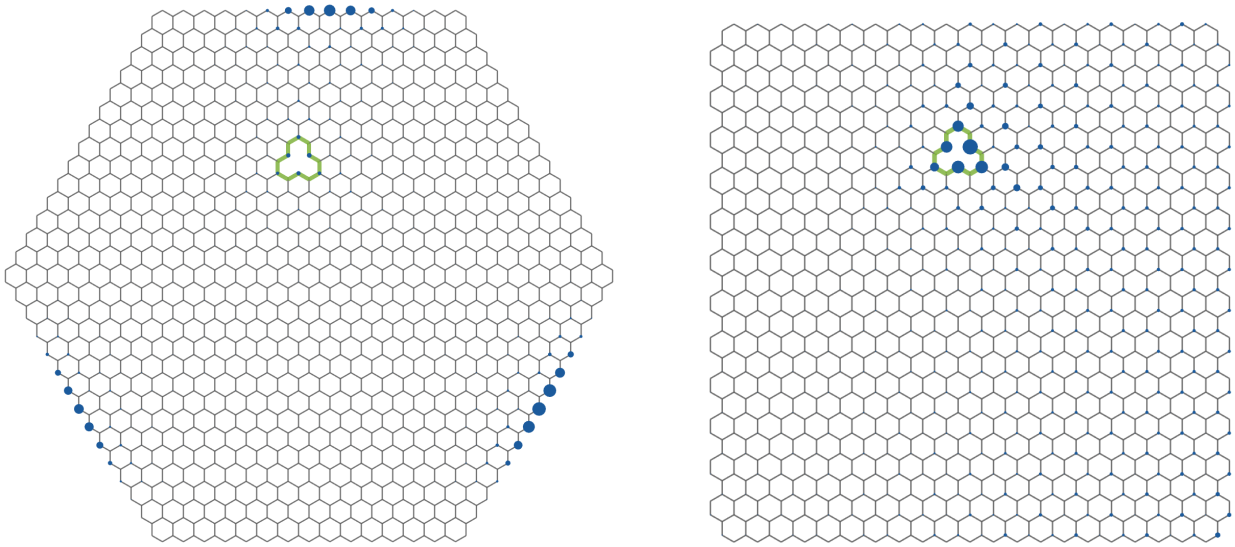

Figure 2: **Boundary effects on charge distribution. a.** Zig-zag boundary on a hexagonal sheet. A large portion of the charge is distributed on the edges corresponding to the majority sublattice. **b.** Periodic (cylindrical) boundary conditions on a square sheet. The periodic boundary is on the horizontal (zig-zag) edges. As a result, there is no accumulation of charge on the 'zigzag edge' in this case.

General scattering theory

Consider a Dirac particle in a $2+1$ dimensional plane with one puncture at the origin. The Hamiltonian is $H = \boldsymbol{\sigma} \cdot \boldsymbol{p}$. The general $E > 0$ solution, written in terms of polar coordinates is

$$\psi(\boldsymbol{r}) = \sum_{m\in\mathbb{Z}} \frac{i^m}{2} e^{im\theta} e^{-im\theta_k} \left(\begin{pmatrix} H_m^{(2)}(kr) \\ ie^{i\theta} H_{m+1}^{(2)}(kr) \end{pmatrix} + e^{2i\delta_m} \begin{pmatrix} H_m^{(1)}(kr) \\ ie^{i\theta} H_{m+1}^{(1)}(kr) \end{pmatrix} \right) \tag{37}$$

where $\boldsymbol{k} = |E|(\cos\theta_k, \sin\theta_k)$, $j = m + 1/2$ is the total angular momentum, $\delta_m(k)$ is the scattering phase shift and $H_m^{(1)}(x), H_m^{(2)}(x)$ are the Hankel functions of the first and second kind. We can expand ψ to the form of an incoming plane wave and outgoing scattered radial wave

$$\begin{aligned} \psi(\boldsymbol{r}) &= \sum_{m\in\mathbb{Z}} \frac{i^m}{2} e^{im\theta} e^{-im\theta_k} \left(\begin{pmatrix} H_m^{(2)}(kr) \\ ie^{i\theta} H_{m+1}^{(2)}(kr) \end{pmatrix} + \begin{pmatrix} H_m^{(1)}(kr) \\ ie^{i\theta} H_{m+1}^{(1)}(kr) \end{pmatrix} \right) \\ &\quad + \sum_{m\in\mathbb{Z}} \frac{i^m}{2} e^{im\theta} e^{-im\theta_k} \left(e^{2i\delta_m} - 1\right) \begin{pmatrix} H_m^{(1)}(kr) \\ ie^{i\theta} H_{m+1}^{(1)}(kr) \end{pmatrix} \\ &= e^{i\boldsymbol{k}\cdot\boldsymbol{r}} \begin{pmatrix} 1 \\ e^{i\theta_k} \end{pmatrix} + \sum_{m\in\mathbb{Z}} i^m e^{im(\theta-\theta_k)} f_m(k) k^{1/2} \begin{pmatrix} H_m^{(1)}(kr) \\ ie^{i\theta} H_{m+1}^{(1)}(kr) \end{pmatrix}, \end{aligned} \tag{38}$$

such that,

$$\psi(\boldsymbol{r}) \overset{r\to\infty}{\approx} e^{i\boldsymbol{k}\cdot\boldsymbol{r}}\begin{pmatrix}1\\ e^{i\theta_k}\end{pmatrix} + f(\boldsymbol{k},\theta)\begin{pmatrix}1\\ e^{i\theta}\end{pmatrix}\frac{e^{ikr}}{\sqrt{r}}, \tag{39}$$

where we used the identities

$$e^{i\boldsymbol{k}\cdot\boldsymbol{r}} = \sum_{m\in\mathbb{Z}} \frac{i^m}{2} e^{im(\theta-\theta_k)}\left(H_m^{(2)}(kr) + H_m^{(1)}(kr)\right) \tag{40a}$$

$$H_m^{(1)}(kr) = \frac{(1-i)i^{-m}}{\sqrt{\pi kr}} e^{ikr} + \mathcal{O}\left(r^{-3/2}\right), \tag{40b}$$

and defined,

$$f_m(k) \equiv \left(e^{2i\delta_m} - 1\right)/2\sqrt{k} \tag{41a}$$

$$f(\boldsymbol{k},\theta) \equiv \sqrt{\frac{1}{\pi}}(1-i)\sum_{m\in\mathbb{Z}} e^{im(\theta-\theta_k)} f_m(k), \tag{41b}$$

f_m being the scattering amplitude of the partial wave associated with angular momentum m. For a reason that will become clear later, we would like to rearrange the sum (38) into pairs of $m, -m-1$ modes (equivalent to $j = \pm(m+1/2)$)

$$\begin{aligned}\psi &= e^{i\boldsymbol{k}\cdot\boldsymbol{r}}\begin{pmatrix}1\\ e^{i\theta_k}\end{pmatrix} + \sum_{m\in\mathbb{Z}} i^m e^{im(\theta-\theta_k)} f_m(k)\, k^{1/2}\begin{pmatrix}H_m^{(1)}(kr)\\ ie^{i\theta}H_{m+1}^{(1)}(kr)\end{pmatrix}\\ &= \left(e^{i\boldsymbol{k}\cdot\boldsymbol{r}} + \frac{4}{ik^{1/2}}\sum_{m\geq 0} G_m^f(\boldsymbol{r};k)\, F_m(k)\, U^m\right)\begin{pmatrix}1\\ e^{i\theta_k}\end{pmatrix}\end{aligned} \tag{42}$$

where we used the identity $H_{-m}^{(1)}(x) = e^{i\pi m}H_m^{(1)}(x)$, and

$$G_m^f(\boldsymbol{r};k) \equiv \frac{i^{m+1}k}{4}\begin{pmatrix}H_m^{(1)}(kr) & ie^{-i\theta}H_{m+1}^{(1)}(kr)\\ ie^{i\theta}H_{m+1}^{(1)}(kr) & H_m^{(1)}(kr)\end{pmatrix}, \tag{43a}$$

$$U \equiv \begin{pmatrix}e^{i(\theta-\theta_k)} & 0\\ 0 & e^{-i(\theta-\theta_k)}\end{pmatrix}, \tag{43b}$$

$$F_m(k) \equiv \begin{pmatrix}f_m(k) & 0\\ 0 & f_{-m-1}(k)\end{pmatrix}. \tag{43c}$$

The form presented in (42) shows that the amplitude of ψ is a sum of two contributions: an incoming plane wave and a scattered wave given by a sum over angular momentum contributions $G_m^f F_m U^m$. The physics of the scatterer is completely encoded in $F_m(k)$. The amplitudes G_m^f are intrinsic characteristics of the free system.

In the low energy regime, $kR \ll 1$, R being the range of the potential or vacancy in our case, the scattering amplitude in the lowest angular momentum channels are generally the most dominant and all higher partial waves can be neglected giving

$$\psi = \left(e^{i\boldsymbol{k}\cdot\boldsymbol{r}} + \frac{4}{ik^{1/2}} G_0^f\left(\boldsymbol{r};k\right) F_0\left(k\right) \right) \begin{pmatrix} 1 \\ e^{i\theta_k} \end{pmatrix}. \tag{44}$$

Hereafter, we refer strictly to G_0^f, F_0 and neglect their subscript for brevity. In the case of an arbitrary incoming wave packet

$$\Phi\left(\boldsymbol{r}\right) = \int d\theta_k \Phi\left(\theta_k\right) \begin{pmatrix} 1 \\ e^{i\theta_k} \end{pmatrix} e^{i\boldsymbol{k}\cdot\boldsymbol{r}}, \tag{45}$$

composed out of plane waves with $|k| = E$, an immediate generalization of (44) gives

$$\psi = \Phi\left(\boldsymbol{r}\right) + \frac{4}{ik^{1/2}} G^f\left(\boldsymbol{r};k\right) F\left(k\right) \Phi\left(0\right). \tag{46}$$

Note that

$$G^f\left(\boldsymbol{r};k\right) = \left(-i\boldsymbol{\sigma}\cdot\boldsymbol{\nabla} + k\right) \left(\frac{i}{4} H_0^{(1)}\left(kr\right) \right) \tag{47}$$

is the outgoing Green's function of $H - k$ on the free plane (i.e. no scatterers),

$$\begin{aligned} \left(H-k\right) G^f\left(\boldsymbol{r};k\right) &= \left(-i\boldsymbol{\sigma}\cdot\boldsymbol{\nabla} - k\right)\left(-i\boldsymbol{\sigma}\cdot\boldsymbol{\nabla} + k\right) \left(\frac{i}{4} H_0^{(1)}\left(k\boldsymbol{r}\right) \right) \\ &= -\left(\nabla^2 + k^2\right) \left(\frac{i}{4} H_0^{(1)}\left(k\boldsymbol{r}\right) \right) \\ &= \delta\left(\boldsymbol{r}\right) \mathbf{1}_{2\times 2}. \end{aligned} \tag{48}$$

This relation reflects the fact that, in the limit $kR \ll 1$, the scattered wave corresponds a wave radiated by a point source with an amplitude given by $F_0\left(k\right)\Phi\left(0\right)$.

In what follows we show explicitly that indeed only the $m = 0, -1$ (s-wave) scattering amplitudes are important for $kR \ll 1$, R being that range of the vacancy.

The scattering amplitudes f_m

The boundary conditions corresponding to a vacancy from sublattice A, B given in the main text are

$$\psi^A_{m\leq 0}\left(R\right) = \psi^B_{m>0}\left(R\right) = 0 \tag{49a}$$

and

$$\psi^A_{m<-1}\left(R\right) = \psi^B_{m\geq -1}\left(R\right) = 0 \tag{49b}$$

respectively. Applying (49a) to the general wave function solution (37) gives

$$e^{2i\delta_m^A} = \begin{cases} -\frac{H_{m+1}^{(2)}(kR)}{H_{m+1}^{(1)}(kR)} & m > 0 \\ -\frac{H_m^{(2)}(kR)}{H_m^{(1)}(kR)} & m \leq 0 \end{cases} \tag{50}$$

which, from (41a), corresponds to

$$f_m^A(k) = -\frac{1}{\sqrt{k}} \begin{cases} \frac{J_{m+1}(kR)}{H_{m+1}^{(1)}(kR)} & m > 0 \\ \frac{J_m(kR)}{H_m^{(1)}(kR)} & m \leq 0 \end{cases} \tag{51a}$$

$$\overset{kR \ll 1}{\sim} \frac{1}{\sqrt{k}} \begin{cases} (kR)^{2(m+1)} & m > 0 \\ \frac{1}{\log(kR)} & m = 0 \\ (kR)^{-2m} & m < 0 \end{cases} \tag{51b}$$

where $J_m(x)$ is the Bessel function. Note that

$$f_m^A = f_{-m-1}^A \quad , \forall m \neq 0, -1. \tag{52}$$

Applying (49b) to (37) gives

$$e^{2i\delta_m^B} = \begin{cases} -\frac{H_{m+1}^{(2)}(kR)}{H_{m+1}^{(1)}(kR)} & m \geq -1 \\ -\frac{H_m^{(2)}(kR)}{H_m^{(1)}(kR)} & m < -1 \end{cases} \tag{53}$$

which corresponds to

$$f_m^B(k) = -\frac{1}{\sqrt{k}} \begin{cases} \frac{J_{m+1}(kR)}{H_{m+1}^{(1)}(kR)} & m \geq -1 \\ \frac{J_m(kR)}{H_m^{(1)}(kR)} & m < -1 \end{cases} \tag{54}$$

Note that $f_m^B = f_m^A \ \forall m \neq 0, -1$ and that

$$f_0^B = f_{-1}^A, \ f_{-1}^B = f_0^A. \tag{55}$$

From (51b) and (55), it is apparent that for $kR \ll 1$, all the partial wave scattering amplitudes vanish except $f_0^A = f_{-1}^B$ which diverge. Thus, the most dominant contributions to the scattering amplitude arrives from the $j = \pm 1/2$ (s-wave) channel.

Vacuum charge density for a general configuration of multiple vacancies

Utilizing the formalism above, we obtain a closed form expression for the charge density $\rho(\boldsymbol{r})$ in the framework of the continuous Dirac model. Although not illuminating at first sight, this expression allows

to plot figures 2b, 3b of the main text.

The charge density can be written in the form (6) ($\operatorname{sign} M \equiv 1$)

$$\rho(\boldsymbol{r}) = \frac{e}{2} \lim_{z\to 0} \Omega(\boldsymbol{r}, z) \tag{56}$$

where $\Omega(\boldsymbol{r}, z) = -iz \langle \boldsymbol{r}| \operatorname{tr}\left(\sigma_z (H - iz)^{-1}\right) |\boldsymbol{r}\rangle$. We would like to obtain the matrix element $\Omega(\boldsymbol{r}, z)$ for a general vacancy configuration. In the low energy regime, $kR \ll 1$, and in the presence of a single vacancy the solution of the Dirac equation is given by

$$\psi(\boldsymbol{r}) = \Phi(\boldsymbol{r}) + \frac{4}{ik^{1/2}} G^f(\boldsymbol{r}; k) F(k) \Phi(0) \tag{57}$$

as shown in supplementary Eq. (46). The physical meaning of this expression is that an incoming wave packet $\Phi(\boldsymbol{r})$ is scattered as a point source radial wave with amplitude $F(k)\Phi(0)$. In the case of a general vacancy configuration $\boldsymbol{r}_{iA}$, $\boldsymbol{r}_{iB}$ expression (57) can be generalised to [11]

$$\psi(\boldsymbol{r}) = \Phi(\boldsymbol{r}) + \frac{4}{ik^{1/2}} \sum_{i=1}^{N_A} G^f(\boldsymbol{r} - \boldsymbol{r}_{iA}; k) F_A(k) \psi_{i,A} + \frac{4}{ik^{1/2}} \sum_{i=1}^{N_B} G^f(\boldsymbol{r} - \boldsymbol{r}_{iB}; k) F_B(k) \psi_{i,B} \tag{58}$$

where $F_{A,B}$ correspond to the scattering amplitudes of vacancies A, B respectively and

$$\begin{aligned}
\psi_{i,A} = \Phi(\boldsymbol{r}_{iA}) &+ \frac{4}{ik^{1/2}} \sum_{\substack{j=1 \\ j\neq i}}^{N_A} G^f(\boldsymbol{r}_{iA} - \boldsymbol{r}_{jA}; k) F_A(k) \psi_{j,A} \\
&+ \frac{4}{ik^{1/2}} \sum_{j=1}^{N_B} G^f(\boldsymbol{r}_{iA} - \boldsymbol{r}_{jB}; k) F_B(k) \psi_{j,B} \qquad (59a) \\
\psi_{i,B} = \Phi(\boldsymbol{r}_{iB}) &+ \frac{4}{ik^{1/2}} \sum_{j=1}^{N_A} G^f(\boldsymbol{r}_{iB} - \boldsymbol{r}_{jA}; k) F_A(k) \psi_{j,A} \\
&+ \frac{4}{ik^{1/2}} \sum_{\substack{j=1 \\ j\neq i}}^{N_B} G^f(\boldsymbol{r}_{iB} - \boldsymbol{r}_{jB}; k) F_{0,B}(k) \psi_{j,B}. \qquad (59b)
\end{aligned}$$

Supplementary Eqs. (58), (59) simply reflect the fact that the amplitude of ψ is the amplitude of the incoming wave and the amplitude of point source radial waves scattered from each vacancy with scattering amplitudes $F_A(k)$, $F_B(k)$. Coefficients $\psi_{i,A}$, $\psi_{i,B}$, as given in (59), represent the amplitude at each vacancy point corresponding to the contributions of the incoming wave and all the scattered waves from the other vacancies.

Consider the matrix element $G(\boldsymbol{r}, \boldsymbol{r'}; iz) = \left\langle \boldsymbol{r} \middle| (H - iz)^{-1} \middle| \boldsymbol{r'} \right\rangle$. It is the Green's function of $H - iz$,

that is, it is the response of the system at $\boldsymbol{r}$ to a point source of wave function located at $\boldsymbol{r'}$. Since in (56) we are only interested in the low energy limit $z \to 0$ limit, the expression for $G(\boldsymbol{r}, \boldsymbol{r'}; iz)$ can be obtained from setting $\Phi = G^f(\boldsymbol{r} - \boldsymbol{r'}; k)$ in (58), (59), with $G^f(\boldsymbol{r} - \boldsymbol{r'}; k)$ given in (43a) and $k = iz$

$$G(\boldsymbol{r}, \boldsymbol{r'}; k) = G^f(\boldsymbol{r} - \boldsymbol{r'}; k) + \frac{4}{ik^{1/2}} \sum_{i=1}^{N_A} G^f(\boldsymbol{r} - \boldsymbol{r}_{iA}; k) F_A(k) G_{i,A} + \frac{4}{ik^{1/2}} \sum_{i=1}^{N_B} G^f(\boldsymbol{r} - \boldsymbol{r}_{iB}; k) F_B(k) G_{i,B} \tag{60}$$

and

$$G_{i,A} = G^f(\boldsymbol{r}_{iA} - \boldsymbol{r'}; k) + \frac{4}{ik^{1/2}} \sum_{j=1,\, j\neq i}^{N_A} G^f(\boldsymbol{r}_{iA} - \boldsymbol{r}_{jA}; k) F_A(k) G_{j,A} + \frac{4}{ik^{1/2}} \sum_{j=1}^{N_B} G^f(\boldsymbol{r}_{iB} - \boldsymbol{r}_{jB}; k) F_B(k) G_{j,B} \tag{61a}$$

$$G_{i,B} = G^f(\boldsymbol{r}_{iB} - \boldsymbol{r'}; k) + \frac{4}{ik^{1/2}} \sum_{j=1}^{N_A} G^f(\boldsymbol{r}_{iA} - \boldsymbol{r}_{jA}; k) F_A(k) G_{j,A} + \frac{4}{ik^{1/2}} \sum_{j=1,\, j\neq i}^{N_B} G^f(\boldsymbol{r}_{iB} - \boldsymbol{r}_{jB}; k) F_B(k) G_{j,B}. \tag{61b}$$

By solving the linear system (61) we can directly obtain

$$\Omega(\boldsymbol{r}, z) = -iz \lim_{\boldsymbol{r'} \to \boldsymbol{r}} \operatorname{tr}\left(\sigma_z G(\boldsymbol{r}, \boldsymbol{r'}; iz)\right) \tag{62}$$

and consequently (56). In Figs. 2b and 3b of the main text, we chose $zR = 0.4 \times 10^{-6}$.

Vacuum charge density for a single A-vacancy using scattering theory

Utilizing the formalism above, we would like to obtain the vacuum charge density in the presence of a single vacancy. To that purpose we use identity (6) ($\operatorname{sign} M \equiv 1$)

$$\rho(\boldsymbol{r}) = \frac{e}{2} \lim_{z \to 0} \Omega(\boldsymbol{r}, z) \tag{63}$$

and obtain an explicit expression for the matrix element $\Omega(\boldsymbol{r}, z) = -iz \left\langle \boldsymbol{r} \middle| \operatorname{tr}\left(\sigma_z (H - iz)^{-1}\right) \middle| \boldsymbol{r} \right\rangle$.

Consider the matrix element $G(\boldsymbol{r}, \boldsymbol{r'}; iz) = \left\langle \boldsymbol{r} \middle| (H - iz)^{-1} \middle| \boldsymbol{r'} \right\rangle$. It is the Green's function of $H - iz$, that is, it is the response of the system at $\boldsymbol{r}$ to a point source of wave function located at $\boldsymbol{r'}$. Since in (63) we are only interested in the low energy limit $z \to 0$ the expression for $G(\boldsymbol{r}, \boldsymbol{r'}; iz)$ can be obtained from

setting $\Phi = G^f\left(\boldsymbol{r}-\boldsymbol{r'};k\right)$ in (46), with $G^f\left(\boldsymbol{r}-\boldsymbol{r'};k\right)$ given in (43a) and $k=iz$

$$G\left(\boldsymbol{r},\boldsymbol{r'};k\right)=G^f\left(\boldsymbol{r}-\boldsymbol{r'};k\right)+G^f\left(\boldsymbol{r};k\right)F\left(k\right)G^f\left(-\boldsymbol{r'};k\right) \tag{64}$$

and thus

$$\Omega\left(\boldsymbol{r},z\right)=-iz\lim_{\boldsymbol{r'}\to\boldsymbol{r}}\operatorname{tr}\left(\sigma_z G\left(\boldsymbol{r},\boldsymbol{r'};iz\right)\right). \tag{65}$$

Using properties of Bessel functions [12], expressions (47) and (51a) can be written as

$$G^f\left(\boldsymbol{r};iz\right)=\left(-i\boldsymbol{\sigma}\cdot\boldsymbol{\nabla}+iz\right)\left(\frac{1}{2\pi}K_0\left(zr\right)\right) \tag{66}$$

and

$$f_{B,-1}=f_{A,0}=\frac{2\pi i}{z}\frac{I_0(zR)}{K_0(zR)} \tag{67a}$$

$$f_{B,0}=f_{A,-1}=-\frac{2\pi i}{z}\frac{I_1(zR)}{K_1(zR)} \tag{67b}$$

where $I_n\left(x\right),K_n\left(x\right)$ are the modified Bessel functions of the first and second kind. Using (43c), (66), (67) we can directly obtain (65). Note that the first term in (64) is trivial and vanishes over the trace. The second term gives

$$\Omega\left(\boldsymbol{r},z\right)=-\frac{iz^3}{4\pi^2}\left(f_{A,0}-f_{A,-1}\right)\left(K_0\left(zr\right)^2+K_1\left(zr\right)^2\right). \tag{68}$$

Using the Bessel function identities

$$I_1(x)K_0(x)+I_0(x)K_1(x)=\frac{1}{x} \tag{69a}$$

$$\boldsymbol{\nabla}\cdot\left(\hat{r}K_0\left(zr\right)K_1\left(zr\right)\right)=-z\left(K_0\left(zr\right)^2+K_1\left(zr\right)^2\right) \tag{69b}$$

we obtain

$$f_{A,0}-f_{A,-1}=\frac{2\pi i}{z}\left(\frac{1}{zRK_0\left(zR\right)K_1\left(zR\right)}\right) \tag{70}$$

and consequently

$$\Omega\left(\boldsymbol{r},z\right)=-\frac{1}{2\pi R}\boldsymbol{\nabla}\cdot\left(\frac{K_0\left(zr\right)K_1\left(zr\right)}{K_0\left(zR\right)K_1\left(zR\right)}\hat{r}\right). \tag{71}$$

Note that this result is identical to the one obtained in (34) and exhibits a second equivalent way to calculate Q and $\rho\left(\boldsymbol{r}\right)$ using (63) instead of (15) and (16).

For a vacancy of type B we only need to change $A\to B$ in (68). From (55) the only difference will be an overall sign.

References

[1] V. N. Kotov, B. Uchoa, V. M. Pereira, F. Guinea, and A. H. Castro Neto, Rev. Mod. Phys. **84**, 1067 (2012).

[2] D. C. Elias, R. V. Gorbachev, A. S. Mayorov, S. V. Morozov, A. A. Zhukov, P. Blake, L. A. Ponomarenko, I. V. Grigorieva, K. S. Novoselov, F. Guinea, and A. K. Geim, Nature Physics **7**, 701 (2011).

[3] E. H. Lieb, Phys. Rev. Lett. **62**, 1201 (1989).

[4] O. Ovdat, J. Mao, Y. Jiang, E. Y. Andrei, and E. Akkermans, Nat. Commun. **8**, 507 (2017).

[5] M. M. Ugeda, I. Brihuega, F. Guinea, and J. M. Gómez-Rodríguez, Phys. Rev. Lett. **104**, 096804 (2010).

[6] J. Mao, Y. Jiang, D. Moldovan, G. Li, K. Watanabe, T. Taniguchi, M. R. Masir, F. M. Peeters, and E. Y. Andrei, Nat. Phys. **12**, 545 (2016).

[7] A. J. Niemi and G. W. Semenoff, Phys. Rev. D **30**, 809 (1984).

[8] M. Stone, Phys. Rev. B **31**, 6112 (1985).

[9] C. Callias, Commun. Math. Phys. **62**, 213 (1978).

[10] G. B. Arfken and H. J. Weber, *Mathematical methods for physicists* (Elsevier Academic Press, 2005).

[11] S. Li and E. J. Heller, Phys. Rev. A **67**, 032712 (2003).

[12] M. Abramowitz and I. A. Stegun, eds., *Handbook of Mathematical Functions: With Formulas, Graphs, and Mathematical Tables* (Dover Publications, Inc., New York, 1965).

5 Discussion

Broadly described, the research in this thesis focuses on the interface between anomalies and quantum condensed matter. Our results originate from two projects, the first one described in [27–29] and the second in [84]. Both studies are characterized by a quantum breaking of scale and parity symmetry respectively. Utilizing numerical and analytic tools of quantum mechanics, quantum field theory (QFT) as well as experimental data, the systems we have studied enabled us to deepen our understanding and observe this phenomenon combined with a rich set of other features such as quantum phase transitions, universality, discrete scale invariance, limit cycles and fractional vacuum charge .

The first project studies, from a general perspective, the occurrence of a CSI to DSI transition in quantum systems with relation to the prototype case of the Schrödinger $1/r^2$ potential (1.1). As described in [27], we analytically demonstrated the existence of a universal QPT (Figs. 2, 3) in H_D for arbitrary space dimension $d \geq 2$ and independently of the short distance regularization. In accordance with H_S in (1.1), the transition is characterized by a CSI under critical phase and a DSI over-critical phase. We obtained an explicit formula for the low energy fractal quasi-bound spectrum in the over-critical regime (Fig. 3 lower panel). In contrast to H_S, H_D displays an additional parity symmetry which may be broken by the regularization. In that case, the degeneracy of the overcritical fractal spectrum is removed and two intertwined geometric ladders of quasi bound states appear in the lowest angular momentum channel ($j = \pm 1/2$) as exhibited by Fig. 2-5.

On the experimental side, we observed the CSI to DSI transition around a single

charged vacancy in graphene. By tuning the amount of charge around the vacancy we were able to measure and analyze three geometric ladder resonances for a broad range of β values. In particular, we observe the overcritical spectrum and we obtain an experimental value for the universal geometric ladder factor in full agreement with the theoretical prediction (Figs 5,6).

A further argument in support of the universality of this QPT is achieved by comparing the experimental results obtained in graphene with those deduced from a completely different physical problem. To that purpose, we dwell for a short while recalling the basics underlying Efimov physics [13]. Back in 1970, Efimov [11, 12] studied the quantum problem of three identical nucleons of mass m interacting through a short range (r_0) potential. He pointed out that when the scattering length a of the two-body interaction becomes very large, $a \gg r_0$, there exists a scale free regime for the low energy spectrum, $\hbar^2/ma^2 \ll E \ll \hbar^2/mr_0^2$, where the corresponding bound states energies follow the geometric series ($\sqrt{-E_n} = -\tilde{\epsilon}_0 e^{-\pi n/s_0}$) where $s_0 \simeq 1.00624$ is a dimensionless number and $\tilde{\epsilon}_0$ a problem-dependent energy scale. Efimov deduced these results from an effective Schrödinger equation in $d = 3$ with the radial $(l = 0)$ attractive potential $V(r) = -(s_0^2 + 1/4)/r^2$. Using equations (1.1), (1.4) and the critical value $\zeta_c = (d-2)^2/4 = 1/4$ for this Schrödinger problem, we deduce the ζ value for the Efimov effect to be $s_0^2 + 1/4 > \zeta_c$ corresponding to the overcritical regime of the QPT. The value of β matching to the Efimov geometric series factor e^{π/s_0} is $\beta_E = \sqrt{s_0^2 + 1/4} = 1.1236$, referred to as the fixed Efimov value. Despite being initially controversial, Efimov physics has turned into an active field especially in atomic and molecular physics where the universal spectrum has been studied experi-

mentally [89–97] and theoretically [13]. The first two Efimov states E_n $(n = 1, 2)$ have been recently determined using an ultra-cold gas of caesium atoms [90]. Although the Efimov spectrum always lies at a fixed and overcritical value of the coupling, unlike the case of graphene where β can be tuned, the universal character of the overcritical regime allows nevertheless for a direct comparison of these two extremely remote physical systems. To that purpose, we included in Fig. 5 the Efimov value β_{E} in the expression obtained for the massless Dirac fermion in a Coulomb potential and insert the corresponding data points obtained for cold atomic caesium in the graphene plot up to an appropriate scaling of $\tilde{\epsilon}_0$. The results are fully consistent thus emphasizing in another way the universality presented.

There are other remote examples of systems displaying this universal QPT, e.g., flavored QED3 [98], and roughening transitions [24]. Our results provide a useful and original probe of characteristic features of this universal QPT and motivate a more thorough study of it.

In order to gain further understanding of the elements inducing this QPT we studied in [28] the system H_L given in (1.6), using a direct analytic approach, and found, in accordance with the $N = 1$ case, that there is a quantum phase transition at $\lambda_{N,c} \equiv (2N-1)!!^2/2^{2N}$ for all $N > 1$ from a CSI phase to a DSI phase in the low energy regime $|E|^{1/2N} L \ll 1$, where $L > 0$ is a short distance cutoff. The CSI phase contains no bound states and the DSI phase is characterized by an infinite set of bound states forming a geometric series similar to (1.4) (Fig. 2,3). The transition and $\lambda_{N,c}$ value are independent of the short distance physics and for $(\lambda_N - \lambda_{N,c}) \to 0^+$, the analytic behavior of the spectrum is characteristic of the BKT scaling in analogy

with $N = 1$.

In [29] we formulated a RG description for systems described by H_N given in (1.7) and studied its solutions numerically. We show that departure from scale invariance characterized by fixed point annihilation (Fig. 1), and subsequently universal DSI, is a generic feature in the landscape of Hamiltonians (1.7). Depending on the values of λ_i, we find additional possibilities including: isolated periodic flow (non-linear limit cycle see Fig. 2) and quasi-periodic flow (limit tori, see Fig. 4). In addition, we showed that these types of RG flows can be simply determined from the characteristic power laws of the $E = 0$ wave function (Table 1).

The second project focused on the physics of vacancies in graphene and its relation, if any, to fundamental Dirac phenomena. As described in [84] we present a continuous Dirac model of graphene, valid at low energy and applicable to an arbitrary configuration of isolated vacancies, which accounts for local charge, zero modes and parity symmetry breaking and shows their direct relation. The localized, fractional and pseudo-scalar nature of the vacancy charge is a consequence of the asymmetry between positive and negative parts of the spectrum as expressed by the occurrence of zero energy modes. This fractional charge does not display Friedel-like density oscillations which are expected to arise from localized perturbations in a metallic or semiconductor system [99] and essentially differs from the screening resulting from the insertion of external charge defects [45, 46, 100, 101]. We show that the amount of charge associated with $N_A + N_B$ vacancies is proportional to $|N_A - N_B|$. The vacuum charge density and its corresponding total charge are obtained by solving the scattering problem of massless Dirac fermions by one vacancy while imposing on their

wave function a new type of 'chiral' boundary conditions. This choice unveils the topological nature of the charge and its relation to zero modes under the form of an Index theorem (Fig. 1). We generalize these results to multi-vacancy configurations and we demonstrate the interest of topological features to achieve remote charge switching (Figs. 1-3).

The physics of a charged vacancy bears essential similarities with $2+1$ quantum electrodynamics (QED), such as fermion number fractionalization and parity anomaly [67–83]. In the latter case, a dynamical external gauge field induces zero modes of massless planar fermions and vacuum charge with abnormal parity. As a result, the Index of the corresponding Dirac operator acquires non-zero values proportional to the strength of the gauge field. Hence, the present results provide, for graphene, a measurable realization of these QED effects with the topological content of the gauge field now replaced by vacancies with properly tailored boundary conditions. Furthermore, our findings display a coherent description of existing measurements [27, 44] and provide additional predictions that can be tested with an appropriate experimental control on vacancy configurations. Including spin degrees of freedom in the Dirac picture and using Lieb's theorem [52] may enrich the picture presented here by associating to a vacancy the quantum dynamics of a localized vacuum spin proportional to the Dirac Index. Possible connections to recent observations of vacancy magnetic moments [58–60, 62] should be investigated together with a generalization to other bipartite lattices and to non-isolated vacancies.

The notion of topological switch (Fig. 3) involves different and somehow unusual algebraic rules, e.g., $3Q_{\blacktriangle} + 2Q_{\triangledown} = 3Q_{\blacktriangle}$ but $Q_{\triangledown} + (3Q_{\blacktriangle} + 2Q_{\triangledown}) = 0$, which may

have applications in logic circuit. The induced potential, arising from electron-electron interactions, can be obtained from the charge density in the Hartree approximation

$$V(\boldsymbol{r}) = \int d\boldsymbol{r}' \, \frac{\rho(\boldsymbol{r}')}{|\boldsymbol{r} - \boldsymbol{r}'|} \tag{5.1}$$

with $\rho(\boldsymbol{r})$ in the formula taken to be the density in the non interacting case. Such an approach was considered, for example, in [102] to calculate the induced potential of an external charge defect.The robustness of the Dirac picture in graphene [103], the short range properties of the vacancy and the consistency with observation give further validity to the results which provide a benchmark to incorporate other interactions schemes.

References

[1] Eric Akkermans, "Statistical mechanics and quantum fields on fractals," in *Fractal Geometry and Dynamical Systems in Pure and Applied Mathematics II: Fractals in Applied Mathematics*, Vol. 601, edited by David Carfí, Michel L. Lapidus, Erin P. J. Pearse, and Machiel van Frankenhuijsen (American Mathematical Society (AMS), 2013) pp. 1–21.

[2] Stephen L. Adler, "Axial-vector vertex in spinor electrodynamics," Phys. Rev. **177**, 2426–2438 (1969).

[3] J. S. Bell and R. Jackiw, "A PCAC puzzle: $\pi^0 \to \gamma\gamma$ in the σ-model," Il Nuovo Cimento A (1965-1970) **60**, 47–61 (1969).

[4] Sidney Coleman and Roman Jackiw, "Why dilatation generators do not generate dilatations," Annals of Physics **67**, 552 – 598 (1971).

[5] K M Case, "Singular Potentials," Phys. Rev. **80**, 797–806 (1950).

[6] L. D. Landau, *Quantum mechanics : non-relativistic theory* (Butterworth-Heinemann, Oxford Boston, 1991).

[7] Jean-Marc Lévy-Leblond, "Electron capture by polar molecules," Phys. Rev. **153**, 1–4 (1967).

[8] Horacio E. Camblong, Luis N. Epele, Huner Fanchiotti, and Carlos A. García Canal, "Quantum anomaly in molecular physics," Phys. Rev. Lett. **87**, 220402 (2001).

[9] David B. Kaplan, Jong-Wan Lee, Dam T. Son, and Mikhail A. Stephanov, "Conformality lost," Phys. Rev. D **80**, 125005 (2009).

[10] Cristiano Nisoli and A. R. Bishop, "Attractive inverse square potential, $u(1)$ gauge, and winding transitions," Phys. Rev. Lett. **112**, 070401 (2014).

[11] V. Efimov, "Energy levels arising from resonant two-body forces in a three-body system," Physics Letters B **33**, 563–564 (1970).

[12] V Efimov, "Weakly-bound states of three resonantly-interacting particles," Sov. J. Nucl. Phys **12**, 589–595 (1971).

[13] Eric Braaten and H.-W. Hammer, "Universality in few-body systems with large scattering length," Physics Reports **428**, 259 – 390 (2006).

[14] Roman W Jackiw, *Diverse topics in theoretical and mathematical physics* (World Scientific, 1995).

[15] K. Meetz, "Singular potentials in nonrelativistic quantum mechanics," Il Nuovo Cimento (1955-1965) **34**, 690–708 (1964).

[16] Dmitrij Maksimovič Gitman, IV Tyutin, and Boris Leonidovich Voronov, *Self-adjoint Extensions in Quantum Mechanics: General Theory and Applications to Schrödinger and Dirac Equations with Singular Potentials*, Vol. 62 (Springer, 2012).

[17] Sergio Albeverio, Raphael Høegh-Krohn, and Tai Tsun Wu, "A class of exactly solvable three-body quantum mechanical problems and the universal low energy behavior," Phys. Lett. A **83**, 105–109 (1981).

[18] S. R. Beane, P. F. Bedaque, L. Childress, A. Kryjevski, J. McGuire, and U. van Kolck, "Singular potentials and limit cycles," Phys. Rev. A **64**, 042103 (2001).

[19] Erich J Mueller and Tin-Lun Ho, "Renormalization group limit cycles in quantum mechanical problems," arXiv preprint cond-mat/0403283 (2004).

[20] Eric Braaten and Demian Phillips, "Renormalization-group limit cycle for the $1/r^2$ potential," Phys. Rev. A **70**, 052111 (2004).

[21] H-W Hammer and Brian G Swingle, "On the limit cycle for the $1/r^2$ potential in momentum space," Annals of Physics **321**, 306–317 (2006).

[22] Sergej Moroz and Richard Schmidt, "Nonrelativistic inverse square potential, scale anomaly, and complex extension," Annals of Physics **325**, 491–513 (2010).

[23] Alessandro De Martino, Denis Klöpfer, Davron Matrasulov, and Reinhold Egger, "Electric-dipole-induced universality for Dirac fermions in graphene," Phys. Rev. Lett. **112**, 186603 (2014).

[24] Eugene B. Kolomeisky and Joseph P. Straley, "Universality classes for line-depinning transitions," Phys. Rev. B **46**, 12664–12674 (1992).

[25] Kristan Jensen, "Semi-Holographic Quantum Criticality," Phys. Rev. Lett. **107**, 231601 (2011), arXiv:1108.0421 [hep-th] .

[26] Kristan Jensen, Andreas Karch, Dam T. Son, and Ethan G. Thompson, "Holographic Berezinskii-Kosterlitz-Thouless transitions," Phys. Rev. Lett. **105**, 041601 (2010), arXiv:1002.3159 [hep-th] .

[27] O. Ovdat, Jinhai Mao, Yuhang Jiang, E. Y. Andrei, and E. Akkermans, "Observing a scale anomaly and a universal quantum phase transition in graphene," Nature Communications **8**, 507 (2017).

[28] Daniel K. Brattan, Omrie Ovdat, and Eric Akkermans, "Scale anomaly of a lifshitz scalar: A universal quantum phase transition to discrete scale invariance," Phys. Rev. D **97**, 061701 (2018).

[29] Daniel K Brattan, Omrie Ovdat, and Eric Akkermans, "On the landscape of scale invariance in quantum mechanics," Journal of Physics A: Mathematical and Theoretical **51**, 435401 (2018).

[30] Jean Alexandre, "Lifshitz-type quantum field theories in particle physics," Int. J. Mod. Phys. **A26**, 4523–4541 (2011).

[31] R. M. Hornreich, Marshall Luban, and S. Shtrikman, "Critical behavior at the onset of $\vec{\mathrm{k}}$-space instability on the λ line," Phys. Rev. Lett. **35**, 1678–1681 (1975).

[32] G. Grinstein, "Anisotropic sine-gordon model and infinite-order phase transitions in three dimensions," Phys. Rev. B **23**, 4615–4630 (1981).

[33] Eduardo Fradkin, David A. Huse, R. Moessner, V. Oganesyan, and S. L. Sondhi, "Bipartite Rokhsar–Kivelson points and Cantor deconfinement," Phys. Rev. B **69**, 224415 (2004).

[34] Ashvin Vishwanath, L. Balents, and T. Senthil, "Quantum criticality and de-

confinement in phase transitions between valence bond solids," Phys. Rev. B **69**, 224416 (2004).

[35] Eddy Ardonne, Paul Fendley, and Eduardo Fradkin, "Topological order and conformal quantum critical points," Annals Phys. **310**, 493–551 (2004).

[36] Shinji Mukohyama, "Horava-Lifshitz cosmology: A review," Class. Quant. Grav. **27**, 223101 (2010).

[37] Shamit Kachru, Xiao Liu, and Michael Mulligan, "Gravity duals of Lifshitz-like fixed points," Phys. Rev. **D78**, 106005 (2008).

[38] Petr Horava, "Quantum Gravity at a Lifshitz Point," Phys. Rev. **D79**, 084008 (2009).

[39] Petr Horava, "Spectral dimension of the universe in quantum gravity at a Lifshitz point," Phys. Rev. Lett. **102**, 161301 (2009).

[40] Tomas Brauner, "Spontaneous symmetry breaking and Nambu-Goldstone bosons in quantum many-body systems," Symmetry **2**, 609–657 (2010).

[41] A.B. Cambel, *Applied Chaos Theory: A Paradigm for Complexity* (Elsevier Science, 1993).

[42] A. Gorsky and F. Popov, "Atomic collapse in graphene and cyclic renormalization group flow," Phys. Rev. D **89**, 061702 (2014).

[43] Yusuke Nishida, "Renormalization group analysis of graphene with a supercritical Coulomb impurity," Phys. Rev. B **94**, 085430 (2016).

[44] Jinhai Mao, Yuhang Jiang, Dean Moldovan, Guohong Li, Kenji Watanabe, Takashi Taniguchi, Massoud Ramezani Masir, Francois M. Peeters, and Eva Y. Andrei, "Realization of a tunable artificial atom at a supercritically charged vacancy in graphene," Nat. Phys. **12**, 545–549 (2016).

[45] A. V. Shytov, M. I. Katsnelson, and L. S. Levitov, "Vacuum polarization and screening of supercritical impurities in graphene," Phys. Rev. Lett. **99**, 236801 (2007).

[46] A. V. Shytov, M. I. Katsnelson, and L. S. Levitov, "Atomic Collapse and Quasi-Rydberg States in Graphene," Phys. Rev. Lett. **99**, 246802 (2007).

[47] Vitor M. Pereira, Valeri N. Kotov, and A. H. Castro Neto, "Supercritical Coulomb impurities in gapped graphene," Phys. Rev. B **78**, 085101 (2008).

[48] Vitor M. Pereira, Johan Nilsson, and A. H. Castro Neto, "Coulomb impurity problem in graphene," Phys. Rev. Lett. **99**, 166802 (2007).

[49] Y Liu, M Weinert, and L Li, "Determining charge state of graphene vacancy by noncontact atomic force microscopy and first-principles calculations," Nanotechnology **26**, 035702 (2015).

[50] O. Lehtinen, J. Kotakoski, A. V. Krasheninnikov, A. Tolvanen, K. Nordlund, and J. Keinonen, "Effects of ion bombardment on a two-dimensional target: Atomistic simulations of graphene irradiation," Phys. Rev. B **81**, 153401 (2010).

[51] Jian-Hao Chen, Liang Li, William G. Cullen, Ellen D. Williams, and Michael S.

Fuhrer, "Tunable Kondo effect in graphene with defects," Nat. Phys. **7**, 535–538 (2011).

[52] Elliott H. Lieb, "Two theorems on the Hubbard model," Phys. Rev. Lett. **62**, 1201–1204 (1989).

[53] Vitor M. Pereira, F. Guinea, J. M. B. Lopes dos Santos, N. M. R. Peres, and A. H. Castro Neto, "Disorder induced localized states in graphene," Phys. Rev. Lett. **96**, 036801 (2006).

[54] Vitor M. Pereira, J. M. B. Lopes dos Santos, and A. H. Castro Neto, "Modeling disorder in graphene," Phys. Rev. B **77**, 115109 (2008).

[55] BRK Nanda, M Sherafati, ZS Popović, and S Satpathy, "Electronic structure of the substitutional vacancy in graphene: density-functional and green's function studies," New Journal of Physics **14**, 083004 (2012).

[56] M. Inui, S. A. Trugman, and Elihu Abrahams, "Unusual properties of mid-band states in systems with off-diagonal disorder," Phys. Rev. B **49**, 3190–3196 (1994).

[57] J. J. Palacios, J. Fernández-Rossier, and L. Brey, "Vacancy-induced magnetism in graphene and graphene ribbons," Phys. Rev. B **77**, 195428 (2008).

[58] Haricharan Padmanabhan and B. R. K. Nanda, "Intertwined lattice deformation and magnetism in monovacancy graphene," Phys. Rev. B **93**, 165403 (2016).

[59] Yuhang Jiang, Po-Wei Lo, Daniel May, Guohong Li, Guang-Yu Guo, Frithjof B. Anders, Takashi Taniguchi, Kenji Watanabe, Jinhai Mao, and Eva Y. Andrei,

"Inducing kondo screening of vacancy magnetic moments in graphene with gating and local curvature," Nature Communications **9**, 2349 (2018).

[60] M. V. Ulybyshev and M. I. Katsnelson, "Magnetism and interaction-induced gap opening in graphene with vacancies or hydrogen adatoms: Quantum Monte Carlo study," Phys. Rev. Lett. **114**, 246801 (2015).

[61] M. M. Ugeda, I. Brihuega, F. Guinea, and J. M. Gómez-Rodríguez, "Missing atom as a source of carbon magnetism," Phys. Rev. Lett. **104**, 096804 (2010).

[62] A. M. Valencia and M. J. Caldas, "Single vacancy defect in graphene: Insights into its magnetic properties from theoretical modeling," Phys. Rev. B **96**, 125431 (2017).

[63] V. Häfner, J. Schindler, N. Weik, T. Mayer, S. Balakrishnan, R. Narayanan, S. Bera, and F. Evers, "Density of states in graphene with vacancies: Midgap power law and frozen multifractality," Phys. Rev. Lett. **113**, 186802 (2014).

[64] N. M. R. Peres, F. Guinea, and A. H. Castro Neto, "Electronic properties of disordered two-dimensional carbon," Phys. Rev. B **73**, 125411 (2006).

[65] Norman Weik, Johannes Schindler, Soumya Bera, Gemma C. Solomon, and Ferdinand Evers, "Graphene with vacancies: Supernumerary zero modes," Phys. Rev. B **94**, 064204 (2016).

[66] Bill Sutherland, "Localization of electronic wave functions due to local topology," Phys. Rev. B **34**, 5208–5211 (1986).

[67] R. Jackiw and C. Rebbi, "Solitons with fermion number $1/2$," Phys. Rev. D **13**, 3398–3409 (1976).

[68] A. J. Heeger, S. Kivelson, J. R. Schrieffer, and W. P. Su, "Solitons in conducting polymers," Rev. Mod. Phys. **60**, 781–850 (1988).

[69] R. Jackiw and J.R. Schrieffer, "Solitons with fermion number $1/2$ in condensed matter and relativistic field theories," Nuclear Physics B **190**, 253 – 265 (1981).

[70] A. N. Redlich, "Gauge noninvariance and parity nonconservation of three-dimensional fermions," Phys. Rev. Lett. **52**, 18–21 (1984).

[71] A. J. Niemi and G. W. Semenoff, "Axial-anomaly-induced fermion fractionization and effective gauge-theory actions in odd-dimensional space-times," Phys. Rev. Lett. **51**, 2077–2080 (1983).

[72] A. J. Niemi and G. W. Semenoff, "Anomalies, Levinson's theorem, and fermion determinants," Phys. Rev. D **32**, 471–475 (1985).

[73] D. Boyanovsky and R. Blankenbecler, "Axial and parity anomalies and vacuum charge: A direct approach," Phys. Rev. D **31**, 3234–3250 (1985).

[74] Richard Blankenbecler and Daniel Boyanovsky, "Fractional charge and spectral asymmetry in one dimension: A closer look," Phys. Rev. D **31**, 2089–2099 (1985).

[75] Richard Blankenbecler and Daniel Boyanovsky, "Induced quantum numbers in (2+1)-dimensional QED," Phys. Rev. D **34**, 612–618 (1986).

[76] R. Jackiw, "Fractional charge and zero modes for planar systems in a magnetic field," Phys. Rev. D **29**, 2375–2377 (1984).

[77] T. Jaroszewicz, "Fermion-solenoid interactions: Vacuum charge and scattering theory," Phys. Rev. D **34**, 3128–3140 (1986).

[78] C. R. Hagen, "Aharonov-Bohm scattering of particles with spin," Phys. Rev. Lett. **64**, 503–506 (1990).

[79] Gordon W. Semenoff, "Condensed-matter simulation of a three-dimensional anomaly," Phys. Rev. Lett. **53**, 2449–2452 (1984).

[80] F. D. M. Haldane, "Model for a quantum Hall effect without landau levels: Condensed-matter realization of the "parity anomaly"," Phys. Rev. Lett. **61**, 2015–2018 (1988).

[81] Eduardo Fradkin, Elbio Dagotto, and Daniel Boyanovsky, "Physical realization of the parity anomaly in condensed matter physics," Phys. Rev. Lett. **57**, 2967–2970 (1986).

[82] Claudio Chamon, Chang-Yu Hou, Roman Jackiw, Christopher Mudry, So-Young Pi, and Gordon Semenoff, "Electron fractionalization for two-dimensional Dirac fermions," Phys. Rev. B **77**, 235431 (2008).

[83] R. Jackiw and G. Semenoff, "Continuum quantum field theory for a linearly conjugated diatomic polymer with fermion fractionization," Phys. Rev. Lett. **50**, 439–442 (1983).

[84] Omrie Ovdat, Yaroslav Don, and Eric Akkermans, "Vacancies in graphene: Dirac physics and fractional vacuum charges," arXiv preprint arXiv:1807.10297 (2018).

[85] Harald Friedrich, "Scattering theory," (2013).

[86] Wolfram Research, Inc., "Mathematica, Version 11.2," Champaign, IL, 2017.

[87] P. Lancaster and L. Rodman, *Algebraic Riccati Equations*, Oxford science publications (Clarendon Press, 1995).

[88] Yu N Demkov and Valentin Nikolaevich Ostrovskii, *Zero-range potentials and their applications in atomic physics* (Springer Science & Business Media, 2013).

[89] T Kraemer, M Mark, P Waldburger, JG Danzl, C Chin, B Engeser, AD Lange, K Pilch, A Jaakkola, H-C Nägerl, *et al.*, "Evidence for Efimov quantum states in an ultracold gas of Caesium atoms," Nature **440**, 315–318 (2006).

[90] Bo Huang, Leonid A. Sidorenkov, Rudolf Grimm, and Jeremy M. Hutson, "Observation of the second triatomic resonance in Efimov's scenario," Phys. Rev. Lett. **112**, 190401 (2014).

[91] Scott E Pollack, Daniel Dries, and Randall G Hulet, "Universality in three-and four-body bound states of ultracold atoms," Science **326**, 1683–1685 (2009).

[92] Noam Gross, Zav Shotan, Servaas Kokkelmans, and Lev Khaykovich, "Observation of universality in ultracold ^{7}Li three-body recombination," Phys. Rev. Lett. **103**, 163202 (2009).

[93] Thomas Lompe, Timo B. Ottenstein, Friedhelm Serwane, Andre N. Wenz, Gerhard Zürn, and Selim Jochim, "Radio-frequency association of Efimov trimers," Science **330**, 940–944 (2010).

[94] Shuta Nakajima, Munekazu Horikoshi, Takashi Mukaiyama, Pascal Naidon, and Masahito Ueda, "Measurement of an Efimov trimer binding energy in a three-component mixture of ^{6}Li," Phys. Rev. Lett. **106**, 143201 (2011).

[95] Shih-Kuang Tung, Karina Jiménez-García, Jacob Johansen, Colin V. Parker, and Cheng Chin, "Geometric scaling of Efimov states in a ^{6}Li-^{133}Cs mixture," Phys. Rev. Lett. **113**, 240402 (2014).

[96] R. Pires, J. Ulmanis, S. Häfner, M. Repp, A. Arias, E. D. Kuhnle, and M. Weidemüller, "Observation of Efimov resonances in a mixture with extreme mass imbalance," Phys. Rev. Lett. **112**, 250404 (2014).

[97] Maksim Kunitski, Stefan Zeller, Jörg Voigtsberger, Anton Kalinin, Lothar Ph. H. Schmidt, Markus Schöffler, Achim Czasch, Wieland Schöllkopf, Robert E. Grisenti, Till Jahnke, Dörte Blume, and Reinhard Dörner, "Observation of the Efimov state of the Helium trimer," Science **348**, 551–555 (2015).

[98] Thomas Appelquist, Daniel Nash, and L. C. R. Wijewardhana, "Critical behavior in (2+1)-dimensional QED," Phys. Rev. Lett. **60**, 2575–2578 (1988).

[99] J. Friedel, "Metallic alloys," Il Nuovo Cimento (1955-1965) **7**, 287–311 (1958).

[100] M. M. Fogler, D. S. Novikov, and B. I. Shklovskii, "Screening of a hypercritical charge in graphene," Phys. Rev. B **76**, 233402 (2007).

[101] Eugene B. Kolomeisky, Joseph P. Straley, and Hussain Zaidi, "Fermion space charge in narrow band-gap semiconductors, Weyl semimetals, and around highly charged nuclei," Phys. Rev. B **88**, 165428 (2013).

[102] Mikhail I Katsnelson, *Graphene: carbon in two dimensions* (Cambridge University Press, New York, 2012).

[103] Valeri N. Kotov, Bruno Uchoa, Vitor M. Pereira, F. Guinea, and A. H. Castro Neto, "Electron-electron interactions in graphene: Current status and perspectives," Rev. Mod. Phys. **84**, 1067–1125 (2012).

שבירה של סימטריית סקלה וזוגיות

בגראפן: אוניברסליות, סימטריית

סקלה דיסקרטית ומטען של הואקום

עמרי עבדת

שבירה של סימטריית סקלה וזוגיות

בגראפן: אוניברסליות, סימטריית

סקלה דיסקרטית ומטען של הואקום

חיבור על מחקר

לשם מילוי חלקי של הדרישות לקבלת התואר דוקטור

לפילוסופיה

עמרי עבדת

הוגש לסנט הטכניון - מכון טכנולוגי לישראל

שבט, תשע"ט, חיפה, ינואר, 2019

המחקר נעשה בהנחיית פרופסור אריק אקרמן בפקולטה לפיסיקה

אני מודה לטכניון על התמיכה הכספית הנדיבה בהשתלמותי

תקציר

התיאור של התנהגות החומר ביקום במסגרת תיאוריה קוונטית מניב שלל תופעות מפתיעות אשר לעיתים אינן עולות בקנה אחד עם התחזיות של התיאוריה הקלאסית. בהקשר זה, אחת תופעות המעניינות ביותר היא התכנות 'אנומליות' המתארות סימטריה הקיימת בתיאור הקלאסי אך נשברת בתמונה הקוואנטית. קבוצה מעניינת במיוחד של אנומליות מתרחשת כאשר סימטריית סקאלה רציפה של מערכת קוונטית נשברת לסימטריית סקאלה דיסקרטית כאשר פרמטר של המערכת גדול מערך קריטי מסויים. מעבר כזה הוא דוגמה למעבר פאזה קוונטי בטמפרטורה אפס. אנומליה זו מתרחשת עבור חלקיק תחת השפעת פוטנציאל הדועך ריבועית ביחס למרחק ומתארת תופעה הנקראת 'אפקט אפימוב'. במערכת זו, כאשר עוצמת הפוטנציאל גדלה מערך קריטי מסויים, מבנה רמות האנרגיה משתנה מפאזה אשר אין בה רמות כלל לפאזה בה יש מספר אינסופי של רמות אנרגיה הנערמות קרוב לאנרגיה אפס ומסודרות במבנה של טור גאומטרי. מבנה זה, מבטא את הסימטריה של המערכת למתיחה של ציר האנרגיה במכפיל המתאים לטור הגיאומטרי ואת חוסר הסימטריה למתיחה בכל מכפיל אחר.

חלקה הראשון של התזה מוקדש לחקר התכנות מעבר פאזה זה במסגרת כללית של מערכות אשר מכילות סימטריית סקאלה רציפה בתיאור הקלאסי. בחלק זה אנו חוקרים את המאפיינים האוניברסליים של המעבר ואת מרכיביו בתוך מערכות נוספות בהן הוא מתרחש. התמקדות מיוחדת ניתנת למערכת המתארת חלקיק דיראק (ספין $1/2$) ללא מסה הנע תחת השפעת פוטנציאל קולון, כלומר, מערכת המקבילה לאטום המימן עם אלקטרון חסר מסה. במערכת זו, הראנו את קיומו של מעבר מסימטריית סקאלה רציפה לדיסקרטית ואת האוניברסליות של מעבר זה ביחס לפוטנציאל הדועך ריבועית במרחק. כמו כן, אנו מציגים ראיות ניסיוניות משכנעות להימצאותו של המעבר סביב חור טעון בשריג של גראפן. חור זה נוצר על ידי ניתוק של אטום פחמן אחד מן השריג. בנוסף למערכת דיראק־קולון חקרנו קבוצה נפרדת של מערכות אשר להן סימטריית סקאלה רציפה ויחס דיספרציה לא איזוטרופי בין אנרגיה לתנע. הראנו כי המעבר מסימטריית סקאלה רציפה לדיסקטרית הוא מאפיין גנרי של מערכות אלו. במסגרת תיאור של חבורת הרנורמליזציה, סימטריית סקלה דיסטרית מתאפיינת, קרוב לנקודת המעבר הקריטית, על ידי מסלול סגור ומושך (מעגל

גבול). שינויים במרחב הפרמטרים משנים תמונה זו לתמונה הנשלטת על ידי מסלול קוואזי מחזורי (טורוס גבול) או נקודת שבת. ישנו קשר ישיר בין הנקודה הקריטית, תמונת חבורת הרנורמלציה והמעריכים המתארים את פונקציות הגל באנרגיה 0.

דוגמא נוספת לאנומליה מתרחשת כאשר סימטריית זוגיות של מצב היסוד של חלקיק דיראק חסר מסה נשברת בנוכחות שטף מגנטי. במקרה זה, השטף גורם ליצירת רמות חלקיקיות עם אנרגיה 0 ומטען של מצב היסוד העובר תחת זוגיות באופן אבנורמלי (פסאודו סקלר). כתוצאה מכך, האינדקס של אופרטור דיראק המתאר את המערכת שווה לערך שונה מאפס הפרופרציוני לשטף המגנטי וגם למטען.

חלקה השני של התזה מוקדש לחקר הפיסיקה של חורים בגראפן הנוצרים על ידי ניתוק אטומי פחמן מן השריג. בנוכחות חור בודד, נוצר מטען מקומי מסדר גודל יחידה המשרה פוטנציאל קולון ללא מיסוך. כמו כן, הסימטריה בין שני תתי השריגים המשולשים נשברת ונוצרים רמות חלקיקיות עם אנרגיה 0. במסגרת העבודה שלנו נציג מודל דיראק רציף המתאר את הפיסיקה של גראפן בנוכחות מערך חורים כללי. נקשר בין קיום רמות חלקיקיות עם אנרגיה 0, מטען של הואקום עם ערך חצי שלם ושבירה של סימטריית זוגיות. קשר זה מבסס את קיומו של משפט אינדקס במערכת והוא מושג על ידי בחירה של תנאי שפה מסויימים סביב החורים המתאימים לפיסיקה של גראפן. כתוצאה מכן, חורים בגראפן מאפשרים לממש מאפיינים בסיסיים של אלקטרודינמיקה קוואנטית ב $2+1$ מימדים כאשר נוכחות שדה כיול מוחלפת בחורים במישור.